Evolutionary implication of mechanotransduction in development

Adrien Bouclet

Université Paris Descartes
École Doctorale Frontières Du Vivant

Evolutionary implication of mechanotransduction in development

Par **Adrien Bouclet**

Thèse de doctorat d'Interface Physique-Biologie

Dirigée par **Emmanuel Farge**

Présentée le 17 juin 2014

Devant un jury composé de :

Jean-Antoine Lepesant	Président du jury
Detlev Arendt	Rapporteur
Suzannah Rutherford	Rapporteur
Michael Koepf	Examinateur
Stephane Ronsseray	Examinateur
Emmanuel Farge	Directeur de Thèse

“Ils ne savaient pas que c’était impossible,

alors ils l’ont fait. ”

“They didn’t know it was impossible,

So they did it.”

Mark Twain

Remerciements

En tout premier lieu je tiens à remercier **Emmanuel** pour ces 5 années passées dans son laboratoire, en stage, puis en thèse. Merci de m'avoir accepté, encouragé et m'avoir tant appris. Merci pour ton encadrement si parfait au cours de ces années où tu as su me guider, m'inspirer mais aussi me pousser à me surpasser. Je n'aurais pu rêver d'un meilleur mentor et les mots me manquent pour exprimer pleinement toute ma reconnaissance.

Un grand merci à **Thibaut** pour tout. Ton implication, ton aide précieuse et constamment sollicitée au cours de ces années. Je n'aurais jamais pu réaliser autant de choses sans toi, ce fut toujours un immense plaisir de travailler à tes cotés lors de tes venues au labo.

I would like to thank the members of the jury. Detlev Arendt for having accepted to by a reviewer of this work, Suzannah Rutherford for having accepted to be a reviewer of this work and for your support and enthusiasm, when I first presented this PhD project. I am not sure I would have been able to realize this PhD without your positive feedback. I would like to thank Michael Koepf for being part of my jury as a member specialist in in silico simulations, and Stéphane Ronsseray for having accepted to be a member of the jury and for all your precious interactions and the feedbacks on the epigenetic project of the PhD. I would like to thank Jean Antoine Lepesant who honours me in being president of the jury.

Merci à Tatiana pour ton aide au cours de ces derniers mois qui m'a permis d'écrire sereinement tout en sachant les expériences entre de bonnes mains. J'espère que tu pourras prendre la relève. Je tenais aussi à remercier tous les membres de l'équipe Maria-Elena Fernandez-Sanchez, Sandrine Barbier, Anne-Christine Brunet, Démosthène Mitrossilis, Jens Roeper ainsi que les anciens membres de l'équipe Fanny Serman et Padra Ahmadi, pour votre temps vos interactions et la vie que l'on a partagé ces trois dernières années.

Merci enfin à tous ceux qui ont contribué même indirectement dans cette thèse par leurs discussions, leur bonne humeur, les projets fous développés à l'école doctorale ou simplement leur amitié : Alix, Camille, Guillaume, Marie, Maeva …

Merci à mes parents pour leur support pendant toutes ces années d'études, et d'avoir cru en moi.

Merci enfin à Chloé pour avoir su me supporter et m'encourager. Merci aussi de m'accompagner et d'écrire avec moi les prochains chapitres à venir.

Merci à vous

Sommaire

Introduction

Mechanotransduction is a branch of biology having emerged in the 80's. Mechanotransduction consists in the conversion of a mechanical stimulus into the activation of a biochemical activity. This field has first developed based on the response of endothelial tissues to blood flows, as well as on the reaction of tumorous cells to the rigidity of their fibrotic environment (1 Gospodarowicz 1978, 2 Resnick 1993, 3 Ghajar 2008). Nowadays, this field develops in a high variety of fields, involving bone remodelling, cell differentiation in response to substrate rigidity or the impact of mechanical constraints associated to morphogenetic movements on gene expression during development, *in vivo* (4 Farge, 2011, 5 Mammoto 2010). One of the specificities of mechanotransduction consists in its interdisciplinary nature, which requires a strong coupling between distinct disciplines, involving physics, biology, and computational sciences.

In this thesis, I first focused on the testing of the hypothesis of the mechanotransductive activation of the apical accumulation of Myosin-II (Myo-II) that leads to *Drosophila* embryos mesoderm invagination, in response to the active cell apex pulsations preceding gastrulation in the mesoderm. This hypothesis was proposed on the basis of previous experiments realized in my host lab, having consisted in the rescue of mesoderm invagination in pulsation and invagination defective mutants, in response to a simple mechanical indent of the mesoderm. Here I tested quantitatively the plausibility of such mechanical trigger of the active apical accumulation of Myo-II leading to subsequent mesoderm invagination, in response to the mechanical strains developed by the endogenous pulsative movements of mesoderm cell apexes*, in silico.*

In a second part, I tested experimentally the role of the mechanical strains developed by the very first morphogenetic movements of zebrafish (*Danio rerio*) and *Drosophila* embryos, in the early specification of mesoderm cells identity. Specifically, to test this hypothesis, I developed magnetic biophysical tools to mimic the epiboly morphogenetic movements in epiboly defective zebrafish embryos. The finding of beta-catenin (β-cat) as the common mechanosensitive pathway involved in earliest mesoderm genes expression, in response to the very first morphogenetic movements of embryogenesis in both species, allowed us to suggest such mechanotransduction pathway as conserved from the last common ancestor of both species, namely the last common ancestor of bilaterians, therefore possibly involved in the origins of mesoderm emergence in the ancestor, which represents a currently important opened question of evo-devo.

In a third part, I developed experiments of mechanical indent of *Drosophila* embryos germ cells, and demonstrated the production of generational heritable developmental defects induced on at least 3 generations. These experiments suggest accidental mechanical perturbation of germ cells as a putative new motor mode of heritable modulations in the genetic developmental program of embryogenesis, with the molecular mechanism underlying such transmission being currently in progress.

1- Mechanics in development

a- Forces in biology

To understand the way mechanics is actively involved in organism's physiology regulation, one has to evaluate the major forces and mechanical stresses at work in living systems. Here we will thus begin by reviewing the main different forces known to be involved in biological systems.

i- Forces generation at the intra-cellular scale:

The 3 major biological structures involved in forces generation are microtubules, actin, and myosin.

- Microtubules are polymers constitutive of the cytoskeleton. They are constituted by the polymerization of dimeric globular proteins. Polymerization, for example against plasma membranes, can act as an active force of cell deformation.

- Actin is a protein that polymerizes into micro-filaments, which are also constitutive of the cytoskeleton. Actin is involved in many cellular processes. It combines with Myosin in muscle contraction, as well as in the regulation of cell shape change and cell motility, for instance.

- Myosin is an ATP motor protein playing a key role with actin in muscle contraction, cell shape change and motility processes.

ii- Type of deformation in biological systems:

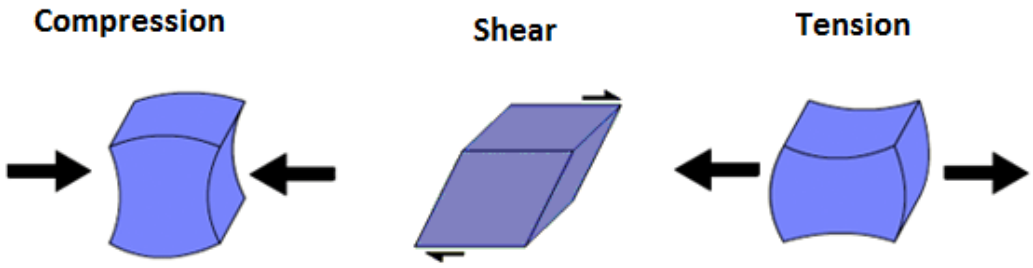

Figure 1 Deformation of a solid under compression, shear and tension.

Tension: Tension is generated by the pulling of a given materials (Figure 1). For instance, during cell division in anaphase, the microtubules pull the chromatid sisters of each chromosome, resulting into splitting. The chromatin sisters thus become separate chromosomes, and are pulled along microtubules toward their centrosomes (6 Zhou J et al 2002).

Compression: Compression is generated by the application of pushing forces on a given materials (Figure 1). This compression usually increases the internal pressure of the object. For instance, in tumours, uncontrolled growth in a confined domain generates a mechanically induced compressive stress that changes the biological behaviour of cancer cells (7 Janet M. Tse et al 2012).

Shear stress Shear stress involves a tissue movement limited by a given surface of the tissue compared to the opposite one (Figure 1). It does not involve tension or compression. For instance, the frictional force of fluid flow on the surface of cells leads to shear deformation of the cell. The shear stress generated by the heart pumping blood flow on vascular endothelial cells plays a key role in endothelial cell and hematopoietic cell fate determination (8 le Noble et al. 2004, 9 Adamo et al. 2009).

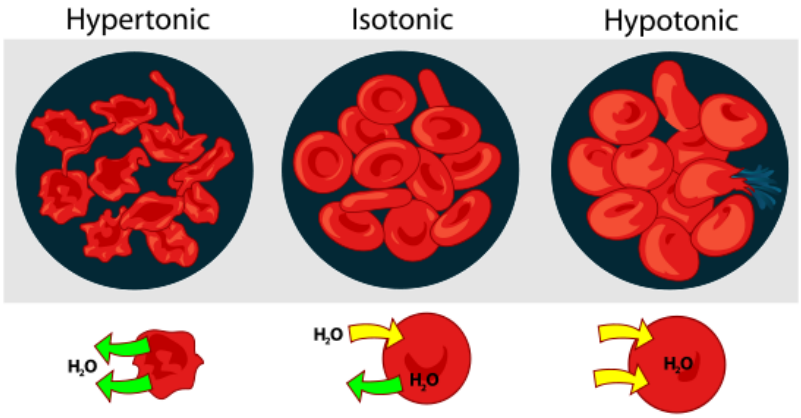

Figure 2 Effect of osmotic pressure on red blood cells. In hypertonic cases the water of blood cells has a smaller concentration of solutes compared to external water so the water leave the cells and goes in the solution to equilibrate concentrations. In isotonic there is a no net flow between the blood cells and the solution. When the blood cells are hypotonic there is a flow from outside the cells to inside.

Osmotic pressure: Osmotic pressure is generated by a flow of a solvent moving through a semi permeable membrane into a containing solute. The flow is directed from the less concentrated solution toward the more concentrated (Figure 2). For instance, cells become more hydrated as they move from the ovary to the uterus, and associated changes in osmotic pressure activate egg cells mechanically by altering cell shape, membrane tension and mechanosensitive ion channel activity (10 Horner and Wolfner 2008).

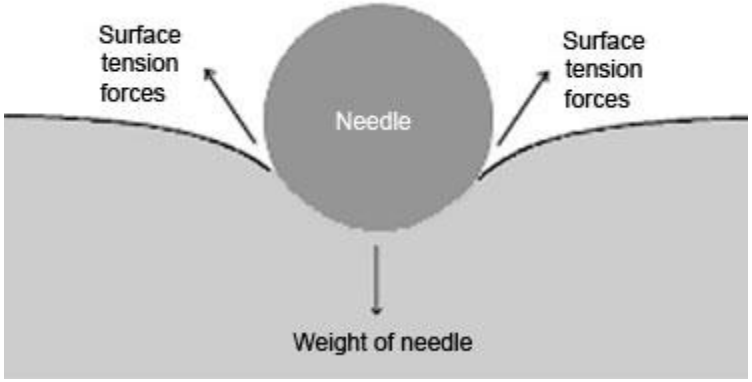

Figure 3: The surface tension creates an opposite force to compensate the needle weight. The needle is not inside the water but remain outside so the surface does not break

Surface tension: Surface tension is generated by a liquid that has a tendency to minimize the surface area interface with external medium by contraction (Figure 3). Prior to tissue stabilisation by extracellular matrix (ECM) secretion, embryonic tissues can be considered at long time scales as liquids governed by an effective surface tension, which is determined by intercellular adhesion and cytoskeletal stress governed by Cadherins and acto-myosin-based contractility (11 Foty and Steinberg 2005, 12 Krieg et al., 2008).

Spring forces: Elastic forces are generated when an elastic materials is compressed or stretched, and act to come back to its unstrained rest length. The force associated to the elastic deformation can either be a compression or a tension, depending on the difference between the resting length and the actual length of the object. In the modelling part of the manuscript, adherent apexes of epithelial cells will be submitted to elastic forces having a tendency to recover their initial length after deformation.

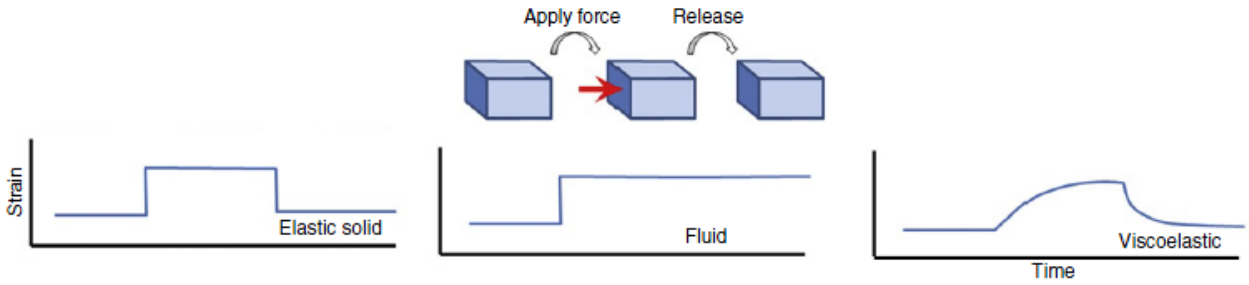

Figure 4: After application of the force a fluid and a solid are deformed. When the force is released the elastic solid comes back immediately to its shape, the fluid keeps its shape. The viscoelastic system will take a certain characteristic time to respond to external force modification.

Viscous forces: A materials can be deformed or move in response to applied forces, but the dynamics of its response can be very different depending on the viscous property of its surrounding medium. An elastic solid without viscosity will immediately recover its original shape after deformation forces vanishing. In contrast, an

elastic structure characterized by a non zero viscosity will take a certain characteristic time to recover its initial shape after the deforming force is removed. Living cells are generally visco-elastic (Figure 4).

b- Forces in embryonic development

Spermatozoid propulsion force

Embryonic development starts with the fecundation of the egg by the spermatozoid. The first mechanical force here processing is the adenosine triphosphate fuelled motor protein, which allows the spermatozoid to swim towards the egg (13 Allen et al 2010, 14 Brokaw 1989). Interestingly, the spermatozoid rotating filament exploits hydrodynamic viscous forces associated to its movement by leaning on water by friction, thereby generating its propulsive force (15 Acheson, D.J., Elementary Fluid Dynamics, book).

First asymmetric division

Once fertilized, a biochemical process hardens the outer layer of the egg in mammalians, to physically block the penetration of other spermatozoids inside (16 Boccaccio et al. 2012). After fertilization, the oocyte starts dividing. First division is asymmetric or symmetric depending on the organism, an asymmetric division producing a smaller cell at the posterior pole and a bigger one at the anterior. The mitotic spindle, which controls the division position, is pushed and pulled by mechanical interactions associated to microtubule and actin filaments polymerization, until it reaches a given position (17 Reinsh et al 1998, 18 Desai 1997, 19 Papalopulu 2012), in C. elegans (20 Kozlowski et al 2007).

Egg-chamber mechanical stability

In Drosophila embryos, the egg chamber shape is maintained by a mechanical balance between germ line cysts growing into the volume, and epithelial follicle surface cells tension, with cell divisions adapting to the follicle epithelial surface to volume increase. During this phase, Myo-II activity in the apex of the epithelium leads to the tension that resists to volume increase, which ensures the mechanical equilibrium between the internal volume and the epithelial surface, therefore maintening the mechanical stability of the overall structure (21 Wang and Riechmann, 2007).

Left right asymmetry breaking

In mouse embryos, rotation of node cells in clockwise direction produces a directed flow (22 Nonaka et al. 2002). This flow generates a left/right morphogen gradient with a calcium concentration asymmetry. This primary asymmetry creates a patterning at the origin of the body left/right symmetry breaking (23 Tanaka et al 2005).

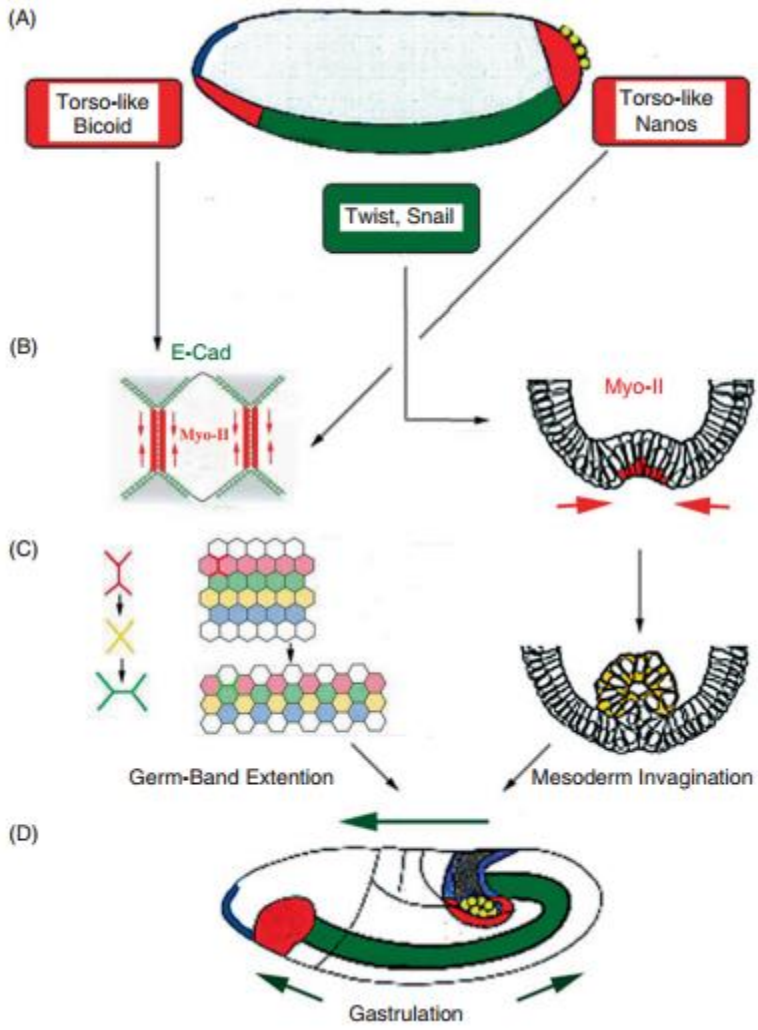

Figure 5: Control of multicellular morphogenetic movements in gastrulation of Drosophila embryos, via genetically controlled intracellular polarities in Myo-II concentration. Adapted from Fernandez-Sanchez et al., 2010. Germ-band extension (A) Before gastrulation, the pattern of expression of developmental genes determining the anteroposterior polarity of the embryo is controlled by the expression of the maternal gene products Bicoid in the anterior and Nanos in the posterior (in red). (B) This combines to the expression of the terminal patterning genes controlled by the maternal gene Torso-like product, to establish the planar polarity of Myo-II submembranar concentration (in red, left). The origin of the underlying molecular mechanism linking anteroposterior patterning gene expression to planar polarity remains to be fully understood. (C) The consequence of the polarity is an increase of tension in membranes perpendicular to the anteroposterior axis, leading to a decrease of these surface areas, then to the dorsoventral cell intercalation (adapted from Bertet et al., 2004) extending the anteroposterior length of the tissue at gastrulation (D, green arrows). Mesoderm invagination. (A) Before gastrulation, the pattern of expression of developmental genes determining the dorsoventral polarity of the embryo is controlled by the expression of the maternally induced nuclear translocation of the transcription factor Dorsal, which activates the expression of the ventral mesodermal genes twist and snail (in green). (B) These genes are necessarily together to induce the submembrane apical accumulation of Myo-II (in red, right) that increases the apical surface tension. (C, D) This leads to the decrease of apical surface area compared to basal surface areas, triggering the inward curvature and invagination of the mesoderm at gastrulation. The understanding of the underlying molecular mechanisms linking the expression of the patterning genes twist and snail to apical attraction of Myo-II are better and better understood.

Tissue folding

After determination of axes, and in addition proliferation forces, cells develop specific forces that shape the 3D structure of the embryo. Indeed, changes in cell shapes can drive such shaping and are involved at many steps of embryogenesis. These shape changes require the generation of intra-cellular mechanical forces. In the epithelium, there exists a mechanical E-cadherin-E-cadherin junctions between neighboring cells. In the apical adherent junctions, E-cadherins are linked to Actin by β-cat. This linkage couples cells apexes, such that apical constriction due to apical accumulation of contractile Myos-II creates a mechanical curvature that deforms the cells and generates an invagination during morphogenesis (Figure 5). This process underlies the mesoderm invagination of *Drosophila* embryos, and is controlled by the transcription factors Twist and Snail (24 Costa wieschauss, 1993). An equivalent process is involved in neural tube formation, through the folding of the initially planar neural plate into a hollow tube (25 Colas et al 2001).

Not only cell shape changes, but also cell movements are involved multicellular morphogenetic movements. A well-known example consists in cell intercalation leading to tissue elongation, in many morphogenetic embryonic processes. In *Drosophila* embryos, the planar polarity of apical accumulation Myo-II in junctions, specific of the cell-cell contacts parallel to the dorso-ventral axis of the embryo, leads to a contractile decrease of the size these junctions, thereby triggering a dorso-ventral cell intercalation, which elongates the embryo along the antero-posterior axis (Figure 5).

Tissue closure

In *Drosophila*, dorsal closure is another well-studied major morphogenetic movement. This process is similar to wound healing, for which a gap in the epithelium is closed through the mechanical action of different cell types. It starts with accumulation of Actin and Myo-II at the edge of lateral epidermis, which increases cell traction forces that pull the edges to the midline and case the cell apices to constrict. In epithelial cells, microtubules seal the gap with a zippering (Figure 6). This process represents an example in which cells transie*ntl*y reorganize their microtubules to fulfil a specialized morphogenetic task (26 A.Jacinto 2002).

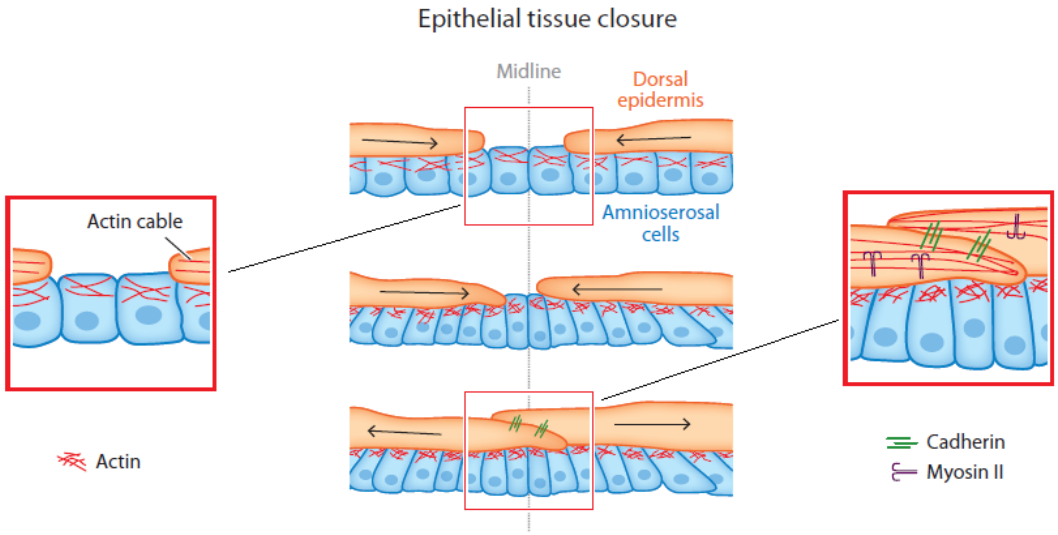

Figure 6: Epithelial dorsal closure in drosophila (adapted from Mammoto 2010)

Many mechanical processes are involved during development, as well as are acting during the life on organism. These forces can be involved in very different ways. Many of them are physical responses to biochemical reactions and are used to shape the organism, but do not activate other biochemical reactions. In contrast, several mechanical strains trigger biochemical reactions, thereby initiating mechanotransduction events that will regulate physiological processes, such as major embryonic developmental event.

2- Mechanotransduction: from cultured cells to embryogenesis

Mechanotransduction is a specific process that involves the conversion of an applied mechanical stimulus into the activation of a biochemical activity (phosphorylation, activation of transduction pathways, transcription…). As we saw at the beginning of the introduction, the initiation of this field of research initiated on the morphologic response of endothelial tissues to hydrodynamics blood flows, and of tumorous cells to the fibrotic rigidity of their environment (27 Gospodarowicz et al. 1978, 28 Nakache et al 1988). Precisely, mechanotransduction was first studied in cell culture, with the study of several mechanically regulated phenomena, including induction of apoptosis, cell division regulation, junction reorganization, mechanical cell interaction modulation, cell contractility and cell motility regulation, cytoskeleton architecture reorganization (29 Bershadsky et al., 2003; 30 Dike et al., 1999; 31 Ghajar and Bissell, 2008, 32 Mitrossilis et al, 2010, 33 Saez A. et al, 2007,34 Fink et al, 2011,35 Tseng Q et al, 2012). The outcome of these processes was initially structural in nature (i.e associated to mechanical cell or tissue propertiess).

More recently was proposed another aspect of mechanotransduction: the cellular differentiation induced by mechanical cues. In 2002, Rauch et al (36) identified BMP2 signalling as a transduction pathway involved in the trigger of mechanically controlled cellular myoblast-osteoblast trans-differentiation, in cell culture. The existence of mechanical induction processes was subsequently observed *in vivo*, during *Drosophila* embryos gastrulation, in which early endoderm differentiation was demonstrated to require a beta-catenin dependent mechanical cue generated by convergent extension (Farge 2003), as well as in cell culture in stem cells in which the rigidity of the substrate orientated cell differentiation (37 Engler et al., 2006; 38 McBeath et al., 2004).

In the past few years, mechanotransduction *in vivo* constituted an increasingly investigated axis of research area of biology. For instance, experiments demonstrated that intra-cellular mechanical constrains generated from the inside or the outside the nucleus could directly influence gene expression (39 Buxboim et al., 2010; 40 Shivashankar 2011; 41 Simon and Wilson, 2011; 42 Wang et al., 2009).

In *Drosophila* oogenesis and cysts formation, the tension increase of follicle epithelial cells due to internal volume cysts increase was proposed to be a mechanical cue leading to cell proliferation and thus to an epithelial follicle surface growth adapting to the volume. Indeed, blocking cysts growth suppressed epithelial cells Myo-II activity and cell division, indicating that tension stress activates proliferation (43 Wang and Riechmann, 2007). Such behaviour is in line with Nelson et al. (44) observations of high stress induced proliferation in epithelial monolayers, *in vitro*.

Forces are also used in organ formation, for example in zebrafish heart and blood vessel formation. In zebrafish, the heart starts beating in the zebrafish embryos before being used, as well as before being fully formed (45 Kimmel 1995). The associated blood flow generates a pressure that participates to the development of the cardiac loop, chamber and valve (46 Hove et al 2003, 47 Voronov et al 2004). Such hydrodynamic shear stress is also required for the development of hematopoietic system, as well as required to maturate the vascular network of the brain, since blood flow also regulates vasculature's pruning (48 Chen et al. 2012). Another example consists in bone joints formation during late mice development, which is ensured by keeping joint cells in a pluripotent state instead of an osteoblastic state, in response to mechanical cues due to bone

chocks generated by spontaneous muscle contractions of the embryo, in a beta-catenin dependent mechanotransductive process (49 Khan et al 2009).

During embryo morphogenesis, sub-membranar apical stabilisation of Myo-II (50 Pouille, Ahmadi et al, 2009), as well as junctional apical stabilisation of Myo-II (51 Fernandez-Gonzales, Dev Cell 2009), were found to be mechano-sensitive, and to be involved in the trigger of mesoderm invagination and in the reinforcement of junctions, respectively, in response to morphogenetic movements involved at gastrulation.

I - Mechanotransduction in *Drosophila* embryo mesoderm invagination: transition from individual pulsating to collective constriction apex behaviour

1- Introduction

a- *Drosophila* embryo mesoderm invagination

The first part of my PhD aims at evaluating the plausibility of the involvement of a mechanotransductive pathway having been rece*ntl*y suggested to be required for the generation of the first morphogenetic movement of *Drosophila* gastrulation: mesoderm invagination. This pathway is known to control the apical constriction of the ventral cells of the *Drosophila* embryo that triggers mesoderm invagination. My work asks the question of the activation of stable apical constriction by a mechanotransduction process in response to unstable actively fluctuating apical pulsations. It was published in Physical Biology "Mechanotransduction in mechanically coupled pulsating cells: transition to collective constriction and mesoderm invagination simulation" (52 Bouclet, Driquez, Farge 2011).

In *Drosophila* embryos, gastrulation begins with apical accumulation of Myo-II in mesodermal ventral cells. Mesoderm invagination is induced by the subsequent acto-myosin contractile forces of apical cell surfaces, that generate inward mesoderm curvature (Figure 7).

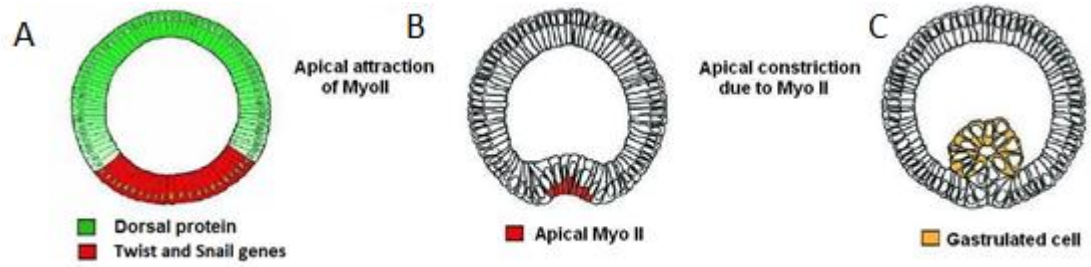

Figure 7: (A) Before gastrulation, the dorso-ventral patterning of the embryo is controlled by the maternally induced nuclear translocation of the transcription factor Dorsal (in green), which activates the expression of the ventral mesodermal genes twist and snail (in red). (B)These genes are necessary together to induce the submembrane apical accumulation of Myosin-II (in red) which contractile interaction with activ increases the apical surface tension.(C) This leads to the decrease of apical surface area compared to basal surface area, triggering the inward curvature and invagination of the mesoderm at gastrulation (in yellow).

Such redistribution of Myo-II requires the expression of different factors. Indeed, apical stabilization of Myo-II requires the expression of the transcription factor Snail, and of the secreted factor Fog, which is a signalling molecule expressed under the control of Twist and upstream of a Rho pathway (53 Costa et al 1994, 54 Seher et al 2007).

Interestingly, apical constriction is characterized by two phases of apical constriction (Figure 8A). The first one, spatially stochastic and pulsating, under the control of Snail, is followed by the second one which is coordinated and dependent on the expression of Fog, wich trigger mesoderm folding. Normal mesoderm invagination does not exist without any of these two factors. Effectively because mutants of *fog* show only the stochastic phase, the collective phase can be considered as Fog dependent (55 Sweeton et al 1991). *snail* mutants are defective in both the stochastic and collective phases (Sweeton et al 1991, 56 Martin et al 2009), indicating that the stochastic phase is indeed Snail dependent, but also that Snail is also required for the Fog-dependent collective phase, thereby requiring the coupling the Snail and Fog pathways (Figure 8 A).

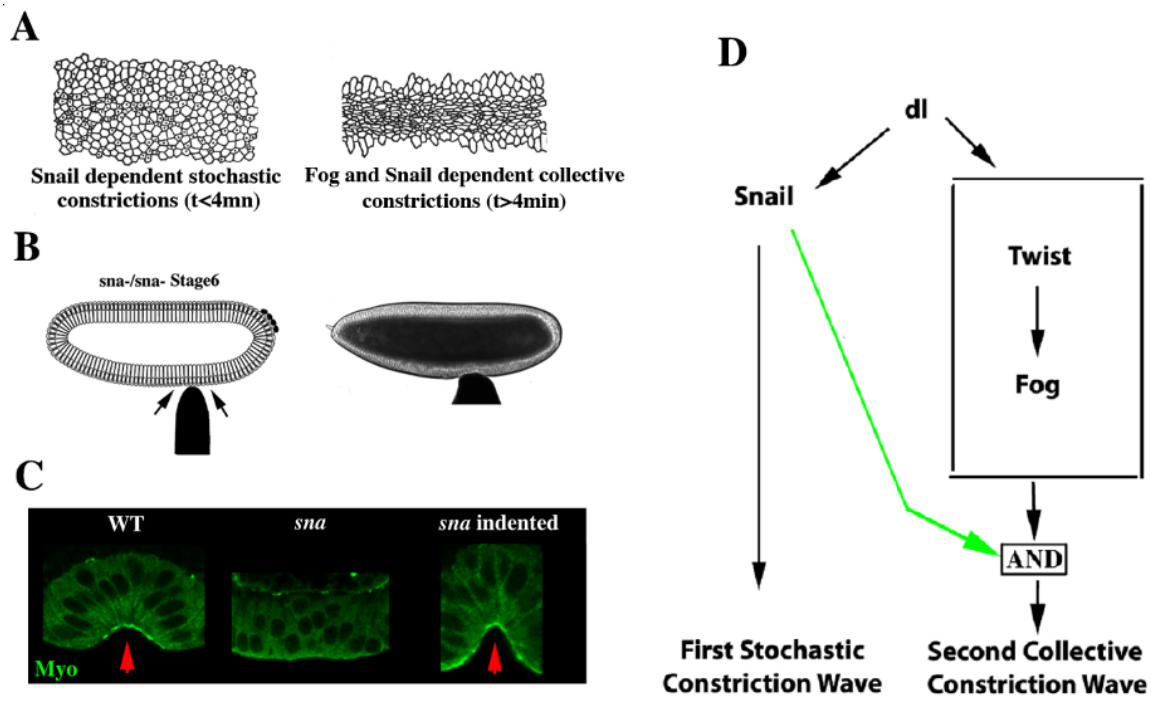

Figure 8: (A) Stochastic and collective constrictions in Drosophila. (B) Mesoderm indent of Drosophila at stage 5 (C) Myosin is expressed after mechanical constraint (D) genetic pathway of mesoderm cell's invagination

It was suggested (57 Pouille et al 2009) that the first stochastic constriction wave, which is Snail dependent, is required to mechanically activate the second phase, through a mechanotransduction process involving the Fog signalling pathway (Figure 8 B,D).

Effectively, it has been shown that applying a local indent on the mesodermal epithelium, to qualitatively replace the mechanical strains lacking in non-pulsating *sna*$^{-}$ embryos, can rescue the apical stabilization of Myo-II, the stable apical constriction and the invagination of mesoderm cells, all missing in *sna* mutants. The deformation consisted in a 5µm indent made with a 50µm needle controlled by a micromanipulator, to precisely control the deformation. In other words, one can rescue a wild type phenotype from a *snail* phenotype by indenting it. Pouille et al. demonstrated that the underlying mechanotransduction process consisted in mechanical inhibition of Fog endocytosis by membrane tension, which enhanced the downstream of Fog signalling pathway, thereby triggering the activation of the Rho dependent apical accumulation of Myo-II.

These experiments thus suggested a Fog-dependent mechanotransduction effect of apical accumulation of Myo-II in response to the *snail* mechanical fluctuation of apex size. My work consisted in testing the plausibility of such hypothesis for the regulation of mesoderm invagination *in vivo*, *in silico,* in close relation to published experiments.

b- Existing models of gastrulation

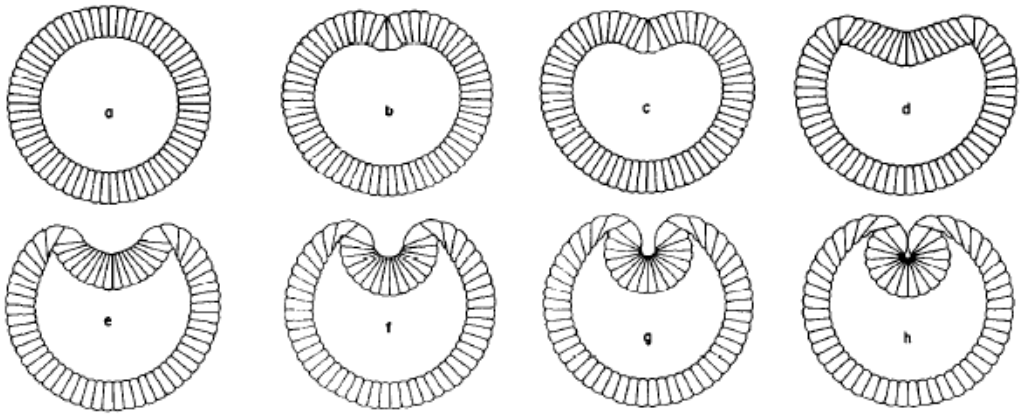

Figure 9: Computer simulation of ventral furrow formation in Drosophila (Odell 1981).

Since around 1990, the importance of computational models of embryonic morphogenesis has been more and more valued. This interest is mainly due to two characteristics: (i) the computational power has dramatically increased, (ii) the number of quantitative experimental data now allows the building of models that are more and more complex.

One of the topics of computing modelling is the study of morphogenesis mechanism related to the complex mechanics of developmental biology, to the particular point of coupling genetics with mechanical forces. Both parameters effectively shape the embryo through reciprocal interplay regulations between mechanics and genetic (58 Koehl 1990; 59 Taber, 1995, 60 Farge 2003; 61 Vogel and Sheetz, 2006; 62 Wozniak and Chen 2009; 63 Mammoto and Ingber, 2010).

One of the first model of morphogenesis was described by (64) Odell et al in 1981. It is presented as 2D model where cells are considerate as viscoelastic elements with a contractile apex. The constriction of one cell can act by stretching on the neighbouring cells, thereby inducing a wave of constriction generating a local invagination.

Subsequently to this first model, several other models were designed. Many of them described growth of embryos from different species at different stages (65 Sherrard 2010). Here we will focus on the modelling of gastrulation of *Drosophila* gastrulation, and more specifically on the formation of the ventral furrow, which is the stage of development I focused on during my PhD.

The different models of *Drosophila* mesoderm invagination belong to the following distinct assumptions:

- Mesoderm cell distinction: the epithelium can be separated in 2 types of tissues. Mesodermal cells are mechanically separated from ectodermal cells and their respective behaviours are different.

- Active or passive deformation: the cell shape is changed in a pre-descriptive way (active) or driven by forces and in a visco-elastic dynamic way (passive).

- Geometry of the system: the number of dimensions managed in the simulation can be 1D, 2D or 3D.

- Timescale behaviour: cells can be considerated as elastic on long time scale or visco-elastic in short time scale. The viscosity of the tissue can be neglected if the system is represented as a sequence of equilibrium states

- Rigidity of viteline membrane : the viteline membrane that protect the embryo from the outside can be rigid or deformable

- Cell division: there is no cell division during gastrulation the total number of cells remains constant.

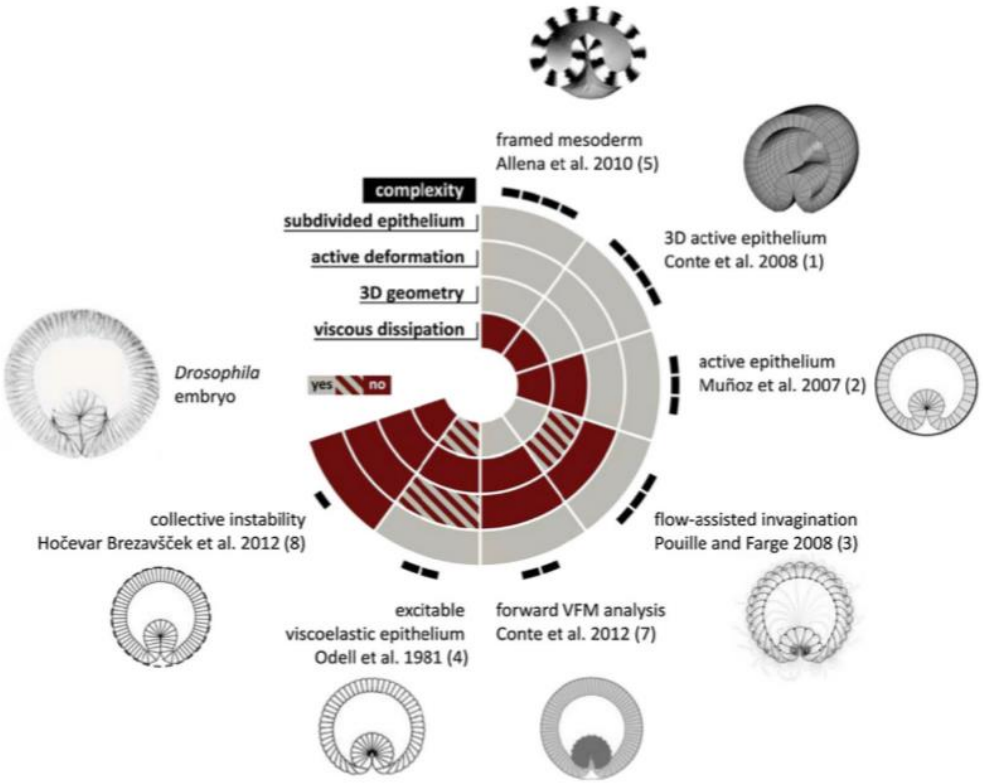

Figure 10: This figure represent some of the model represented by order of complexity. The objective of this representation is to summarize the way the embryo is represented in all the papers published in the field.

In the first model of Odell, cells behave like a viscoelastic material (Figure 10.4). In this model, if the apex deformation reaches a threshold, the cells rest area of the apex decreases, which leads to a constriction. Here, the constriction of one cell can be enough to open neighbouring cells up to the threshold such that one cell can be sufficient to make the all tissue constrict. However, the underlying equations are mathematical, a priori designed to give the wished result in advance, and were not physico-biologically relevant. Nevertheless, this first model was able to represent the initial and final conditions of sea urchin gastrulation accurately. This work was pioneer in its field, and one had to wait for 10 years (66 Davidson 1995) to see another published model of sea urchin gastrulation. Note that at this period, less experimental informations were available on the regulation of gastrulation.

In 2008, Munoz et al (67) and Conte et al (68) produced simulations based on Odell's simulation, but in 2D and in 3D instead of 1D (Figure 10.2, Figure 10.1). In these models, the mesoderm and the ectoderm do not behave the same. The global embryo was considered as a closed system, which total volume does not change. When the mesodermal epithelial cell apex constricts, the basal membrane of the cell elongates so the ectodermal basal cell membrane have to shorten. This leads to a constriction that is not tubular. The 3D model didn't bring more answer than the 2D model gives, and consisted in a confirmation on the results found in 2D.

In 2008, Pouille et al (69) produced a model in which subcellular component are taken into consideration (acto-myosin cortex, individual membranes, junction and internal viscous cytoplasm). In contrast to all other simulations, in which cells are considered with flat apical based and lateral membranes, the shape of the cell membranes can be bent, and are therefore defined by mechanical parameter of elasticity but not geometrically imposed. The cells are filled with fluid. The invagination is "constrained" by cortical membranes elasticity and viscous hydrodynamics laws, in response to active constriction due to the acto-myosin present in the apical apex surface of mesodermal cells. In this model (Figure 10.3) the furrow forms and invaginates, but does not fully close, probably due to the lower number of cells of the simulations compared to *in vivo*.

In 2009, Conte et al (70) produced another model that generated systematic patterns and deformation represented as a diagram. The objective of this model was to determine the conditions to have a successful invagination verifying that, the invagination should happen inside the embryo, cells cant fuse, and the two most far mesodermal cells must end next to the other to close the tube. In 2012 Conte (71) created a new model, closely compared to videos taken by Broadland et al (72 Brodland 2010).

In 2012, Ho cevar Brezav s ceket al (73) generated a model trying to find the minimum requirement for furrow formation, independent of apical accumulation of Myo-II patterning. In their model, they found that all cells can be identical, with no need of any pattern of constricting cells. A change in the cross-sectional area of a subgroup of cells is enough to create an invagination, if exists an apico-basal constricting membranes or apico-basal asymmetries of surface tension. Even though a cross-section gradient of thickness is observed in the *Drosophila* embryo epithelium, Drosophila embryos are indeed characterized by patterned apical accumulation of Myo-II. However, in 2010 Sherrar et all (74 Sherrad et al 2010) interestingly showed acidian endoderm gastrulation in response to apico-basal constriction.

Here one can realize that all models are characterized by many different predictions and can explain furrow formation by different ways. Indeed identic shapes predictions can be made following different approaches. In our model, we chose to develop the simplest structural description (1D description and 2D tissue description) with the simplest mechanical description (viscoelastic mechanically coupled cells) with a more complete genetic description (Snail dependent pattern of pulsating cells, considered to Fog dependent patterns of cells mechanically activable in constriction).

2 - The Snail/Fog patterned mechanosensitive model: a 1 Dimension model

To describe a multi-cellular system of mechanically connected apexes, I built a simple model on the basis of a chain of N viscoelastic cells mechanically coupled by adherent junctions (Figure 11).

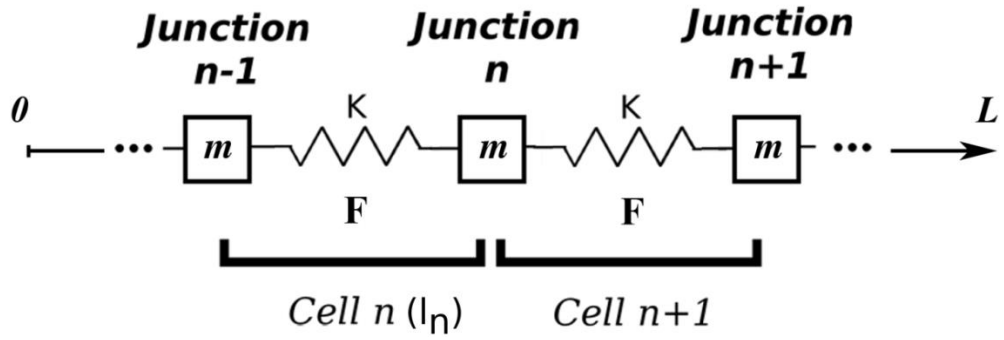

Figure 11: Representation of the simulated cellular tissue. One cell is represented by a spring of elastic modulus $K=K_{pa}$, bordered by 2 junctions of mass m. The cell environment is viscous and characterized by a modulus of friction F.

All apexes are allowed to follow a deformation along one axis. The movement of one junction associated to an apex shape change can be described by the following physical equation, which describes the movement of viscoelastic system based on the fundamental equation of dynamics:

$$\begin{aligned} m\frac{\mathrm{d}^2 L_n}{\mathrm{d}t^2} = & -K_{pa} * [(L_n - L_{n-1}) - l_{0,n}] \\ & + K_{pa} * [(L_{n+1} - L_n) - l_{0,n+1}] \\ & - F\frac{\mathrm{d}L_n}{\mathrm{d}t} \end{aligned} \qquad 1$$

With:

-m the mass of the junction

-L_n is the position of the junction n

-K_{pa} is the passive elastic constant of the cell

-l_{0n} is the size of the unconstrained cell apex n

-F is the hydrodynamic viscous friction of the medium neighboring on the moving junction

-l_n (expressed later) is the diameter of the cell n defined by $L_n - L_{n-1}$

The first term of equation (1) is corresponding to the acceleration of the junction of mass m. This inertial term can be neglected compared to the viscous term (see below) because the movement acts at low Reynolds number and is dominated by the viscosity of the tissue at the cell length and time scales of the embryo (Pouille and Farge 2008).

The second and third terms correspond to the elastic force of a spring $F=-K*(L_n-L_{0n})$. The second term corresponds to mechanical interaction of junctions n and n-1. If $L_n - L_{n-1}$ is bigger than L_{0n} of constraint cells, the length $L_n - L_{n-1}$ will have a tendency to decrease due to elastic force exerted by junction *n-1* to junction *n* , generating a negative force on L_n *(equation 1).*

The third term corresponds to mechanical interaction of junctions n+1 and n. If $L_{n+1} - L_n$ is bigger than L_{0n} of constraint cells, the length $L_{n+1} - L_n$ will have a tendency to decrease due to elastic force exerted by junction *n+1* to junction *n,* generating a positive force on L_n *(equation 1).*

The last term corresponds to the viscous hydrodynamic Stokes force that applies on junction *n,* a force that opposes proportionally to the speed, which writes: $-F\,dL_n/dt$.

Hydrodynamic interactions between junctions were neglected, because the characteristic time of viscous relaxation is on the order 1 second compared to the characteristic biological time of our system (around 80 seconds).

We thus find for junction n and for junction n-1 respectively:

$$\frac{dL_n}{dt} = -\left(\frac{K_{pa}}{F}\right) * (l_n - l_{0n}) + \left(\frac{K_{pa}}{F}\right) * (l_{n+1} - l_{0n+1}) \qquad (2a)$$

$$\frac{dL_{n-1}}{dt} = -\left(\frac{K_{pa}}{F}\right) * (l_{n-1} - l_{0n-1}) + \left(\frac{K_{pa}}{F}\right) * (l_n - l_{0n}) \qquad (2b)$$

by defining the apex size $l_n = L_n - L_{n-1}$. Subtracting (2a) and (2b) leads to :

$$\frac{dl_n}{dt} = \left(\frac{K_{pa}}{F}\right) * (l_{n+1} - l_{0n+1}) - 2\left(\frac{K_{pa}}{F}\right) * (l_n - l_{0n}) + \left(\frac{K_{pa}}{F}\right) * (l_{n-1} - l_{0n-1}) \qquad (3)$$

We additionally took into account the fact that the tissue is closed, with a constant total size constraint taken into consideration by adding a mean field constraint term, leading to:

$$\frac{dl_n}{dt} = \left(\frac{K_{pa}}{F}\right) * (l_{n+1} - l_{0n+1}) - 2\left(\frac{K_{pa}}{F}\right) * (l_n - l_{0n}) + \left(\frac{K_{pa}}{F}\right) * (l_{n-1} - l_{0n-1}) - \left(\frac{K_{pa}}{F}\right) * \frac{1}{N} * \sum_{n=1}^{N}(l_n - l_n(t=0)). \quad (4)$$

The term have effectively a tendency to decrease a given l_n, if as a mean value on all cells, <l> is higher than $l_{no}=l_n(t=0)$.

To mimic the pulsative effect of Snail, here we additionally excite the cell apexes with a sinusoidal active fluctuation, that is stopped once the critical length activating the Fog pathway, l_{act}, is reached.

$$dl_{exc}/dt = A_{exc}\sin(\omega t + \phi) \quad (5)$$

Finally, here we model the Fog-dependent mechanical activation of the constriction by a decrease of the resting cell length l_{0n} once the cell attempts the critical size l_{act} that dilates the apex such that Fog endocytosis is inhibited, thereby activating the downstream of Fog signalling pathway (Pouille et al, 2009). This is modeled by irreversibly activating the decrease of l_{0n} into the simulation, once it attempts the l_{act} critical value, as following:

$$\frac{dl_{0n}}{dt} = -\left(\frac{K_{fog}}{F}\right) * \left(\frac{l_n^{\alpha+1}}{l_n^{\alpha} + l_c^{\alpha}}\right) * \left[\left(\frac{1}{1+e^{-(t-\tau_1)}}\right) * \left(\frac{1}{1+e^{+(t-(\tau_1-\tau_0))}}\right) + \left(\frac{1}{1+e^{-(t-\tau_2)}}\right) * \left(\frac{1}{1+e^{+(t-(\tau_2-\tau_0))}}\right) + \left(\frac{1}{1+e^{-(t-\tau_3)}}\right) * \left(\frac{1}{1+e^{+(t-(\tau_3-\tau_0))}}\right)\right] \quad (6)$$

The contraction equation (5) describes a decrease of l_{0n} with time, following a sharp threshold effect around a minimum value for the size apex l_c ensured by high values of α (here taken as 10) that ensures the existence of a minimal non-negative value for l_n in the dynamical process. K_{Fog} is the contractile modulus. The ratchet-like nature of the constriction observed experimentally (Martin 2009) is here modeled by the introduction of the exponential terms modelling three temporal gates opening at times τ_1, τ_2 and τ_3 during τ_0. The succession of the three gates generates the two temporal steps mimicking the ratchet process observed *in vivo* in the process of constriction, plus the final stabilization step (see the experimental curve in black in Figure 13c). τ_0, the resilient time during which no constriction occurs after a stabilized constriction pulse, and τ 1, τ 2 and τ 3, the times at which the stabilized constriction pulses are initiated will be introduced directly from their values measured on the experimental curve (Figure 13c black curve). In addition to this equation of contractibility, a delay Ta be-

tween the activation of the pathway and the constriction of cells was introduced into the simulation to take into account the characteristic time of the activation of the Fog signalling pathway separating the blocking of endocytosis of Fog from apical stabilization of Myo-II. The delay time was numerically introduced by activating equation (5) Ta after l_n as attempted l_{act} for any single cell. The delay time was taken on Ta= 86s, the characteristic time of activation of functional stabilization of Myo-II by mechanical deformation (Fernandez et al. 2009)

The 1D simulation was patterned by 50 centre mesoderm cells expressing Snail (oscillating) and Fog (contractile under deformation) in green in the figure, by two border domains of 25 mesoderm cells expressing Fog (contractile under deformation) in red, and by two external ectoderm domains of 100 cells each (mechanically passive) in blue. This reflected the cell pattern proportions into a cross-section of the middle of the embryo, with a high arbitrary total number of cells. Based on Alberga et al (75 Alberga 1991)**,** we subsequently took 9 cells expressing Fog and Snail (red), 18 cells expressing only Fog (green) and 30 mechanically passive (blue), to model the 1D cross-section with real number of cells.

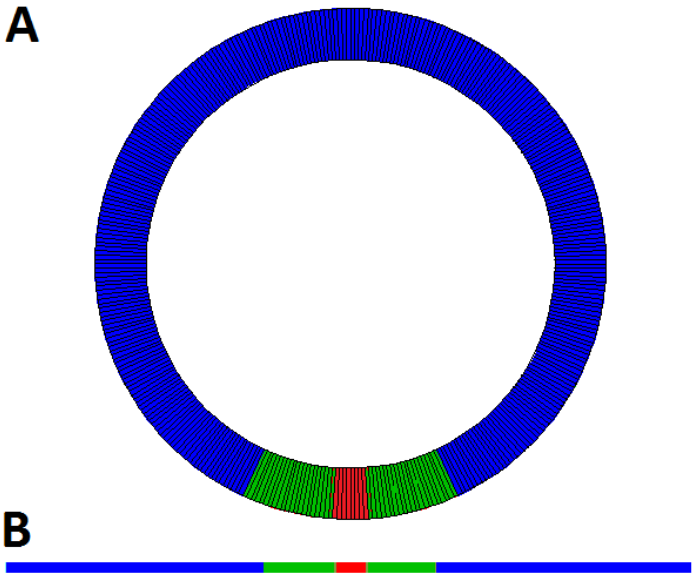

Figure 12: (A) regular cut of the embryo (B) The embryo represented in the simulation as a line of apexes. The different colors represent the different gene expression: In red cells expressing snail and fog. In green cells expressing only fog. In blue one express neither snail nor fog.

Individual cells were excited by sinusoidal active fluctuations with random phases, and with an amplitude A_{exc} leading to the collective oscillations characterized by the amplitude of apex size pulses on the order of 5% observed *in vivo* in the mesoderm of the wild-type embryo, with a period of 83s. Interestingly, this is also characteristic of the mutant of *twist* (i.e. expressing no Fog) characterized by *snail*-dependent fluctuations only (76 Martin *et al* 2009). We assumed the 5% amplitude oscillations as the critical size l_{act} activating the Fog pathway.

3- Simulation's results

a- Quantitative phenocopy of experimental constriction dynamics by *in silico* modelling

We succeeded to reproduce the constriction transition experimentally observed, characterized by a transient regime during which cells oscillate typically twice, before the emergence of a subsequent regime of collective stable constriction at 2–3 min (77 Kam et al 1991, 78 Martin et al 2009)(Figure 13).

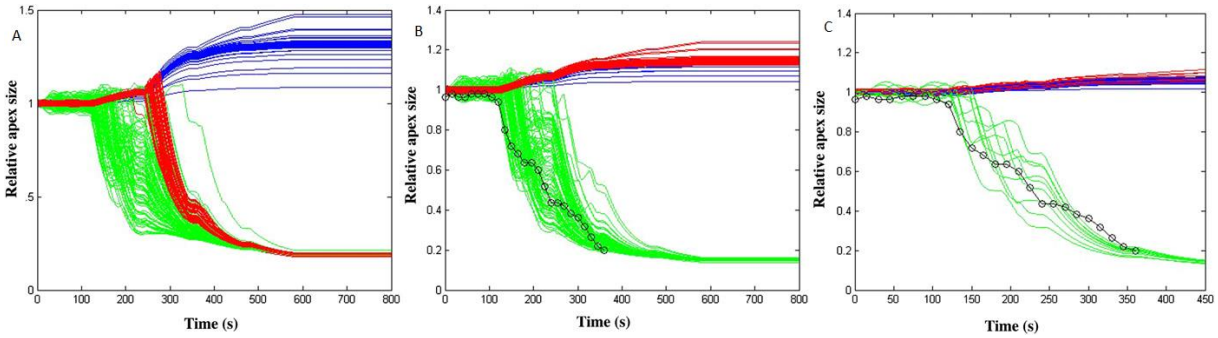

Figure 13: (A) 1D 300 cell chain patterned by 50 Snail and Fog expressing cells in the : of the mesoderm (green), two ventro-lateral mesoderm domains of 25 cells each expressing only Fog (red), and two lateral domains of 100 ectoderm cells each expressing neither Snail nor Fog (blue). Snail-dependent single cell oscillations of 0.25% of amplitude lead to collective movements characterized by pulses of apex size of 5% that activate the Fog-dependent active collective constriction after two cycles of oscillations (120 s), as observed in vivo (Martin et al 2009). Collective constriction is complete at 400 s, as observed in vivo ((8) Kam et al 1991). Note that in addition to the phase, the initial size of the cells was also randomized with an amplitude of 0.1% in the simulation, to add stochasticity in the active fluctuations. (B) Similar results were obtained taking into account the fact that contractile ventro-lateral cells are delayed in constriction compared to (A) (mostly red Fog expressing cells) because they are submitted to curvature constraints preventing them from constricting (see the text), (C) as well as with a reduced number of cells reflecting anisotropic constriction along the dorso-ventral axis (see the text). Experimental apex cell diameter length (dotted line) was calculated on the basis of lexp = 2∗(A/π)1/2 where A is the area of the cell apex from experimental data of reference (Martin et al 2009), approximating the cell as cylinders with apexes as disks. Simulation results are robust and representative of all simulations tested with the same set of parameters (at least three times for each set of parameters).

Interestingly, in Figure 13 A, we observe that the cells expressing only Fog (in red) constrict in response to Snail dependent oscillations. In a 3D geometry they should not been able to do it because of the high curvature imposed on the ventro-lateral cells by the invagination of the most central mesodermal cells expressing both Snail and Fog (in green). We then suggested that even though activated, the lateral mesodermal cell expressing Fog only cannot contract because of such curvature. This feature was thus mimicked in the simulation by preventing constriction in the lateral cells expressing Fog only. As a result, the simulation showed a dynamics of constriction that fits with the experimental curve (black circles) for an individual constricting cell (Figure 13B), for an arbitrary number of 100 cells. Figure 13C represents the same conditions with the smaller number of cells characterizing quantitatively the real number of cells of a dorso-ventral cross section. Within this condition, we

find a behaviour of constricting cells in good quantitative agreement again with the dynamics of experimental individual cell constriction.

b- Passive and active collective behaviours

Interestingly, here we find that the amplitude of the individual excitation is of 0.25%, namely significantly smaller than the 5% critical length activating the contractile Fog signalling pathway, by a factor of 20. Therefore, collective movements emerging from mechanical coupling between individual cells are in this simulation necessary to transi*ent*ly generate single cell oscillations of amplitude larger than the critical length activating the constriction.

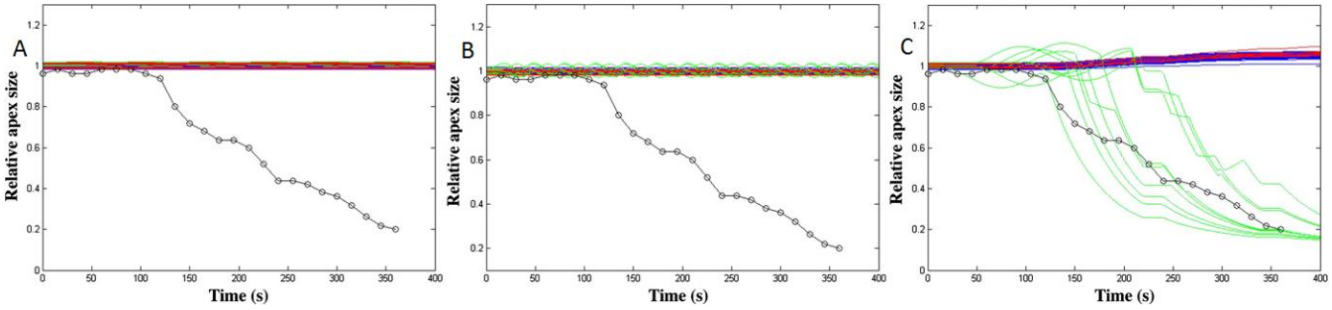

Figure 14: (A) The mechanical coupling between cells was eliminated, leaving all other parameters of the simulation of figure 2 constant. Uncoupled cell oscillations did not trigger collective constriction, showing the necessity of collective effects to trigger the active constriction transition. (B) The frequency of individual cell excitation was doubled (the oscillation period was changed from the 60 s observed in vivo to 30 s), leaving all other parameters of the simulation of figure 2 constant. Coupled cell oscillations did not trigger collective constriction, because of the decrease of the amplitude of the collective oscillations which pass under the value of constriction activation of Aexc = 1.0.5, giving limited viscoelastic time response of the cells (see the text). (C) Halving the frequency makes the transition still robustly efficient. Simulation results are robust and representative of all simulations tested with the same set of parameters (at least three times for each set of parameters).

In addition, once activated in a single cell, the Fog signalling pathway generates a stable active constriction that dilates neighbouring cells. Then, the probability for those neighbouring cell apex sizes to become larger than the critical size increases. As a consequence, neighbouring cells constrict in response to the first cell constriction, leading, in turn, to the constriction of their own neighbouring cells. The involvement of such a collective effect of active constriction was verified by impairing cell–cell mechanical interaction by introducing a coupling constant A_t in front of the first and third terms of the second member of equation (4), and putting A_t=0. In this case, no cell constricts because collective movements are missing and do not allow anymore to reach the 5% required for the active constriction to be triggered (Figure 14 A). Interestingly, full deletion of adhesive properties between cells would be required to test such prediction of the model, partial adhesion inhibition still allowing tension to be transmitted between cells and leading to membrane tension through strong membrane tethering (Martin et al 2010).

This result suggests that the collective passive response of the mechanically coupled cells to the Snail-dependent active excitation could be necessary for individual cells to attempt the critical size activating the Fog-dependent contraction, in a configuration for which individual uncoupled cell oscillation amplitudes would not be sufficient. The activation of the constriction could, in turn, propagate from cell to cell and lead to the coordinated active constriction necessary for mesoderm invagination

c- A critical role for the frequency of Snail dependent pulsations

Then, I decided to modify the excitation frequency to study the sensitivity of the system response to the dynamics of its excitation. Due to the viscoelasticity, changing the excitation frequency of individual cells should change the oscillation amplitude of the cells. This is due to the fact that high frequencies do not let the time to collective modes to explore the full amplitude it could explore without viscosity, because of to the viscosity medium. Indeed, doubling the frequency of the Snail dependent oscillations decreased the amplitude of oscillation of the connected cells in response to the solicitation, thereby leading to a loss of the collective constriction phase (Figure 14 B).

In contrast, if we half the frequency, we observe an increase of oscillation amplitude that is much bigger than in the case reflecting endogenous frequency (Figure 14C). This is because in that case we let more time to collective modes to explore the amplitude it could explore fully without viscosity, due to the lower viscosity of the medium. In this case collective constriction occurs, but do phenocopy experimental data with less quantitative accuracy

Strikingly, mutants of Snail effectively show experimentally a doubling of the frequency of excitation compared to Twist mutants or wild types, with amplitude of fluctuations significa*ntl*y reduced, and a lack of transition (13 Martin et al 2009). This result suggests that in addition to the amplitude of the excitation, the frequency of the Snail-dependent excitation might also be a critical parameter leading to the activation of the Fog-dependent constriction wave.

d- The alternative hypothesis of a mean field hydrostatic pressure

In the model just presented, the mechanical strain activating one cell is due to the constriction of the neighbouring cell. An alternative possibility would be that membrane tension leading to the inhibition of Fog endocytosis is triggered by hydrostatic pressure increase in the mesoderm due to the cells having already constricted. In this model all the cells would interact together through a mean field pressure generated by cell shape changes (Figure 15).

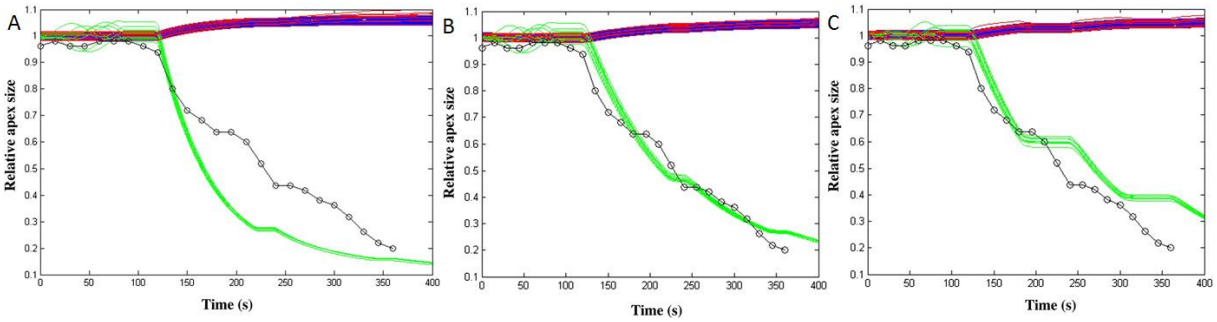

Figure 15: (A) Simulation of constriction effects associated with a mean effect of increase of hydrostatic pressure instantaneously propagating along mesoderm cells, leading to membrane tension increase and activation of Fog-dependent constriction, with all other parameters of figure 2(C) constant. (B) Decrease of Kfog by a factor of 2 compared to (A). (C) Tuning of Kfog and τ parameters to fit the initiation of constriction and levels of the constriction steps never fits the observed dynamics of the steps. In the specific case of the figure, Kfog was divided by 2 and τ 0 fixed at 70 s. Simulation results are robust and representative of all simulations tested with the same set of parameters (at least three times for a set of parameters).

During the Snail-dependent apex oscillations, individual cells transiently take trapezoidal shapes due to the decrease of the apex surface. Such shape change decreases the total surface of the apex at constant volume, possibly leading to an increase of hydrostatic pressure inside the cell. Hydrostatic pressure should propagate immediately along the mesoderm through lateral cell plasma membrane deformations, and increase the mean internal pressure in all mesodermal cells. As a consequence, membrane tension should increase in all cells. In response to the increase of membrane tension, Fog endocytosis would be inhibited, thereby activating the downstream pathway leading to Myo-II apical attraction. We have added in this simulation a mean field pressure proportional to the number of cells constricted and critical pressure activation to activate the constriction. Within these conditions, the transition was found to be much more sudden than the transition predicted by cell–cell local interactions, with all cells following the same dynamics of constriction at the same time (Figure 15 A). The same result was obtained in the absence or in the presence of adherens junctions (A_t = 1) with immediate activation of all contractile cells. By decreasing K_{fog} by a factor of 2, the simulation dynamics better fits the observations, except that the ratchet steps were delayed in amplitude and time (Figure 15 B). By playing with the characteristic time scale of the ratchet, the ratchet events could be located at correct characteristic amplitude, but not at correct characteristic time, and diverged from the experimental curve after one step (Figure 15 C). It was not possible to find a set of parameters correctly fitting both the long mean and short ratchet dynamics of the constriction using the hydrodynamics model. This suggested that cell–cell mechanical interactions leading to active constriction could be viscoelastic and local through apex–apex interactions, rather than hydrostatic and non-local through cell–cell pressure interactions across the mesoderm.

4- Conclusion

a- The mechanosensitive model quantitatively phenocopies experimental apex constriction dynamics

Mesoderm invagination is associated with apical constrictions of mesoderm cells leading to trapezoidal cell shape change. This process is driven by apical coalescence of Myo-II, with an initial 2–3 min unstable stochastic phase of coalescence followed by a collective phase of stabilized apical accumulation leading to coordinated constriction (Martin et al 2009, Sweeton et al 1991). The mechanical strains developed by the Snail-dependent stochastic phase were proposed to activate the Fog signalling pathway through the mechanical blocking of endocytic degradation of Fog, in response to endocytic vesicle flattening responding to an increase in membrane tension. This proposal was supported by experiments of mechanical indent of snail mutants which rescued both apical redistribution of Myo-II and mesoderm invagination (Pouille et al 2009).

Here we simulate the response of the Fog expressing cells of the mesoderm to the Snail-dependent constriction pulsations, within a collection of 80 mechanically coupled cells. In this model, the origins of the Snail-dependent pulsations are not discussed and are modelled as forced oscillations, in contrast to the development of models of spontaneous cell oscillations of aminosera cells during dorsal closure (79 Solon et al 2009). The result of our simulation suggests that the mechanical perturbations leading to collective constriction propagate locally through cell–cell mechanical interactions between cells. The model predicts a modulus of constriction initiating the collective effects four times higher than the passive modulus of cell deformation. In the initial Odell model constriction (Odell et al 1981), active constriction was reversible depending on the value of ln compared to l_{act}. The present model describes individual constrictions as irreversible, even though a cell may cross back l_{act}, due to the influence of its neighbouring cells. In Odell's previous model a single cell in the centre of the future invaginated domain was forced to constrict such that neighbouring cells would activate constriction (Odell et al 1981). Here we find that collective effects generated by mechanical coupling between cells can activate cell constriction even though the amplitude of excitation of individual uncoupled cells would be smaller than the critical apex size activating constriction. This could suggest that collective effects allow smaller fluctuations of size to trigger collective active constrictions as compared to a single cell constriction process. Furthermore, the simulations indicate that in addition to the amplitude of the fluctuations, their frequency could be a critical control parameter of the activation of the constriction phase transition. Note that In comparison to figure (Figure 15 A) model prediction, mutant tissues characterized by defects of adherens junctions still show stable myosin contractibility (80 Dawes-Hoang et al 2005, Martin et al 2010, 81 Sawyer et al 2009). However, even though adherens junction defects appeared to be sufficient to lead to the separation of acto-myosin networks in individual cells under stress, membrane connections are still present in between the cells of the armadillo most pronounced mutant, which are characterized by membrane tethers connecting the cells separated at the onset of gastrulation (Martin et al 2010).

In the mesoderm, membrane tension leading to the inhibition of Fog endocytosis is thought to be the mechanical factor that triggers the mechanotransduction process that generates apical myosin stabilization (Pouille et al 2009). The residual adherens points that form the membrane tethers between the still connected cells

should thus lead to a membrane tension possibly able to activate the inhibition of Fog endocytosis and to activate its downstream pathway. Alternatively, the oscillations of the onset of gastrulation could irreversibly trigger the activation of the Fog pathway just before the mechanical separation of cells, leading to separation of cells and apical stabilization of myosin and constriction.

Interestingly the generalization of the simulation to a 2D simulation of the surfaces epithelium, realized by Benjamin Driquez, robustly let the same result (see perspectives, Bouclet, Driquez 2011).

b- Physiological function of collective constriction transition

What would be the physiological function of a collective phase of apex constriction mechanically activated by a stochastic phase of constriction? Cells of the mesoderm must constrict in a coordinated way in order to trigger a dynamically efficient locally regular invagination. In the *Drosophila* embryo, stabilized constriction initiates at 2.5 min, with mesoderm invagination initiated at 5 min, realized at 10 min, and closed at 20 min (Martin et al 2010). If a substantial number of cells would still be actively oscillating with a time scale of 1 min during the first 5 to 10 min and even during the full 20 min of invagination, the invagination of the 700 cell mesoderm would be locally perturbed by such movement and by the non-closing of their apexes and would be irregular. This would be the case even though a global constraint of bending would have had the time to propagate along the mesoderm and to tend to curve the elastic tissue on the 20 min time scale (Conte et al 2009). A good way for this collective system of individual cells to behave identically and rapidly in a coordinated way in stopping oscillations and initiating constriction collectively is that individuals interact in such a way that the behaviour of individuals triggers the same behaviour in neighbouring individuals. Thus, a good way for a collective set of cells to constrict in a coordinated way is to interact together such that the constriction of individual cells triggers a constriction of the other neighbouring cells. Because individual cell behaviour is in this case mechanical in nature, the most direct way to mediate this interaction is the mechanical strain generated by individual cells on neighbouring cells, and mechanical activation of a signal transduction pathway leading to the active constriction in neighbouring cells. Indeed, such a mechanical signal has the advantage of propagating rapidly along the 250 µm tissue of 700 cells on the time scale of minutes. Thus, mechanical activation of constriction could be required for efficient coordination of constrictions for regular invagination formation on the observed highly dynamical 10 min time scale of Drosophila embryo gastrulation. In addition, the existence of Snail dependent oscillating cells disseminated throughout the mesoderm necessarily homogenizes and accelerates the process of collective constriction, as compared to a model in which the constriction of one cell would initiate a directional propagation across the mesoderm (Odell 1981). Furthermore, as we saw, collective oscillations also make mesoderm invagination more sensitive to individual cell oscillations that are significa*ntl*y smaller than the critical size activating constriction.

c- Constriction transition leading to mesoderm invagination as emerging from 'mechano-genetic' coupling in development

Mechanical activation of collective constriction is a supracellular mechanism that belongs to physical mechanical interactions between cells interacting with genetically controlled active fluctuations (Snail dependent) coupled to the expression of mechanosensitive pathways (Fog-dependent) in individual cells. It can be described in analogy with phase transitions, with unusual features compared to classical physical systems due to the involvement of genetic and biochemical processes on a macroscopic scale system composed of cells as individual elements. Effectively, in contrast to most classical statistical physics systems for which the thermal fluctuations oppose the energy of interaction between elements that tend to organize the collective system (i.e. to decrease entropy), in this analogy the fluctuations of the system trigger the organized coordinated constriction of individual cells, rather than oppose it. This is in this case due to the mechanotransduction and active constriction downstream effect. This shows an original transition behaviour characterized by highly active and reactive biochemical properties of living matter. Thus, new multicellular scale mechanisms of development here emerge from a transition regulated by mechanotransduction processes that trigger the rapid and large length scale coordinated constriction of cells leading to regular invagination, in response to active fluctuations. As we saw, such a mechanism regulating mesoderm invagination results from molecular scale (genetic and biochemical) to multicellular scale (tissue mechanical strain) reciprocal interplay, rather than to predominant biochemical molecular scale, or predominant physical multicellular scale mechanisms. This interplay linking the molecular to the tissue multicellular scales plays at the intermediate scale of the cell. It is ensured by the existence of a cellular mechanotransducer process coupling both the genetic and soft matter properties of the cell. Effectively, mechanotransduction is thought to be triggered by the mechanically induced flattening of soft matter plasma membranes in response to tension, which prevents the formation of endocytic vesicles. This blocks the endocytosis of the Fog secreted factor expressed by the genome, which leads to the activation of the downstream pathway triggering Myo-II apical accumulation, cell constriction and finally mesoderm invagination.

Thus, here we find macroscopic multicellular mechanical properties that couple to genetic properties to generate fine-tuned morphogenetic processes. Indeed, in the specific case of mesoderm invagination, molecular genetics without mechanical strains (expression of Fog without mechanical deformation), or mechanical strains without genetics (deformation without expression of Fog) do not trigger mesoderm invagination in *sna twi* mutants (Pouille et al 2009). Here it is the reciprocal interaction between both biological genetics (molecular products expressed in individual cells) and physical mechanics (multicellular scale mechanical properties) that generates mesoderm invagination. This reciprocal interaction is regulated by a mechanotransduction process that couples the membrane soft matter physics properties to the secreted factor Fog expressed by the genome. The mechanical physics nature of the interplay allows rapid and long-range coordination of constriction, and the biological genetic nature of Fog expression ensures a fine genetically predetermined pattern for collective constrictions, and therefore invagination.

5- Perspectives

The first perspective consisted in the extension of this model to a 2D model. Indeed, most publications represent a cross cut of the embryo allowing the monitoring of the invagination. In our case, to realize a 2D model, here we need to consider not only the cross-cut of the cell apex, but the full surface of the apexes. Instead of having a line of cells (
Figure 12 B) we modelled the 2D surface of the epithelium at apexes position (
Figure 12.

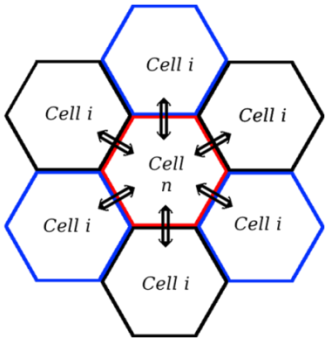

Figure 16: The cell n is link to 6 other cell every change Δa of area of n will directly influence the area of other cells with a deformation of – Δa/6.

Such development of the model was realized by Benjamin Driquez in our common publication (Bouclet, Driquez et al 2011), in which each cell is able now to interact with the 6 neighbours.

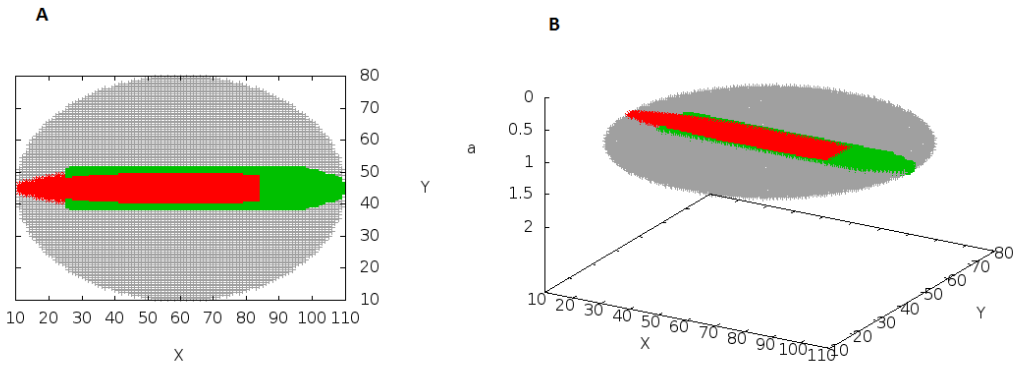

Figure 17: Superior view (A) and ¾ view representing the ventral part of the Drosophila embryo in the 2D model.

The results given by this model confirmed the one obtained in 1D. They validated the plausibility of a requirement of the coupling between gene products biochemical activity and mechanical strain in the triggering of the invagination of the *Drosophila* embryo mesoderm.

The second perspective now consists in testing *in vivo* the predictions of the model, like the possibility for the mesoderm to invaginate with based on physiologically relevant cells constrictions mimicked in a mutant of *sna*. Some of those predictions are curren*tl*y tested by Démostène Mitrosillis, post doc in the lab.

Finally, the robustness of these in silico findings could ultimately be tested in 3D, by enclosing a constant internal volume with the Figure 17, 2D patterned cells, and by additionally giving a thickness to the cells.

II- Evolutionary conservation of early mesoderm specification by mechanotransduction in Bilateria

The objective of this second part of my thesis consist in testing the conservation of the mechanical activation of the β-cat pathway, already known to be involved in the mechanical activation of the endoderm differentiation in invertebrate *Drosophila* embryos, during vertebrate zebrafish *Danio Rerio* embryos development. This work was realized in collaboration with Thibaut Brunet (a PhD biologist), with a participation involving us two as first co-author of the manuscript: "Evolutionary conservation of early mesoderm specification by mechanotransduction in Bilateria" published in Nature Communications (82 Bouclet, Brunet 2013).

In addition to the *Drosophila* arthropod (83 Farge, 2003, 84 Desprat et al, 2008), we know that there exists mechanical activation of the β-cat pathway in vertebrates, like in mice and humans bone cells (85 Norvell, 2004, Calcif Tissue Int, 86 Khan et al, 2009,) and in mouse cancer cells (87 Whitehead 2008, 88 Samuel et al). The common ancestor of these species was living around 600 million years ago. Here we ask the question of whether this ancestor already possessed a mechanically activable β-cat pathway. To investigate this, we realized a parallel study between *Drosophila* and zebrafish early embryos, at the onset of their multi-cellular morphogenetic movements. Finding a common mechanosensitive behaviour of the β-cat in both species at earliest stages of development showedl in addition en-light a putative primary function of β-cat mechanosensitivity in the common ancestor.

1- Introduction

a- Zebrafish development

The development of the zebrafish embryo consists in several steps, beginning with the fertilization of the embryo,here is taken as time 0 of development.

ZYGOTE PERIOD (0-3/4 h)

The newly fertilized egg is about 0.7 mm in diameter at fertilization. It remains at zygote stage until the first cleavage occurs, about 40 minutes after fertilization. During this period the embryo consists in one cell (Figure 18).

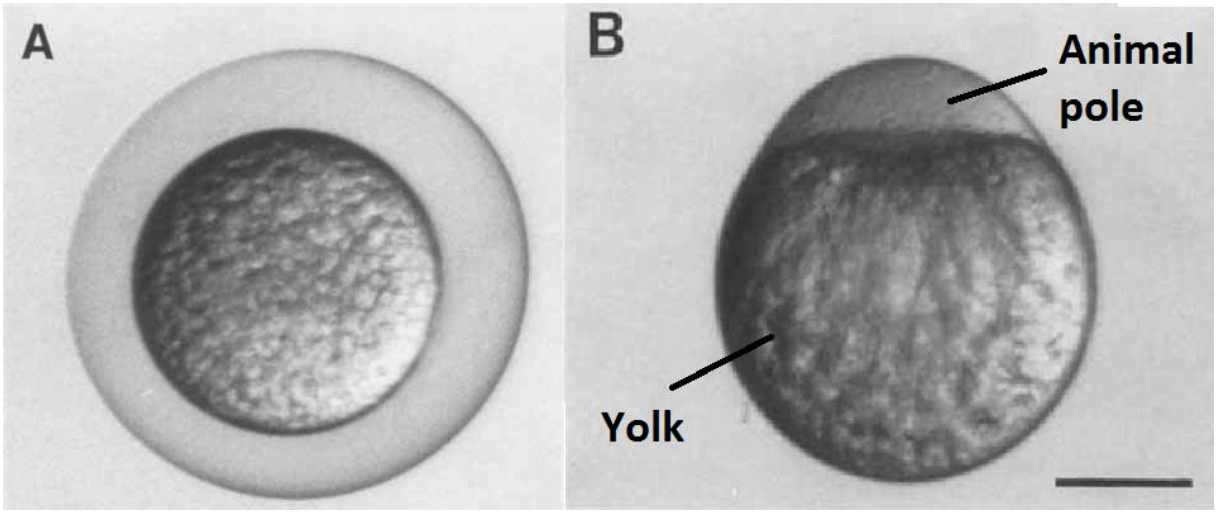

Figure 18: The zygote period. A: The zygote within its uplifted chorion, a few minutes after fertilization. B: The dechorionated zygote with the animal pole to the top single cell and the yolk down , about 10 min after fertilization. Scale bar = 250 pm (89 from Kimmel 1995).

CLEAVAGE PERIOD (3/4-2H 1/4)

After first cleavage, cells divide almost every each 15 minutes, until the embryo gets to 64 cells (90 Kimmel and Law, 1985). All cells are synchronized and their divisions occur simultaneously. The cleavage period continues until stage 64 cells. The superficial cells at the enveloping layer are called the EVL (Figure 19, Figure 20).

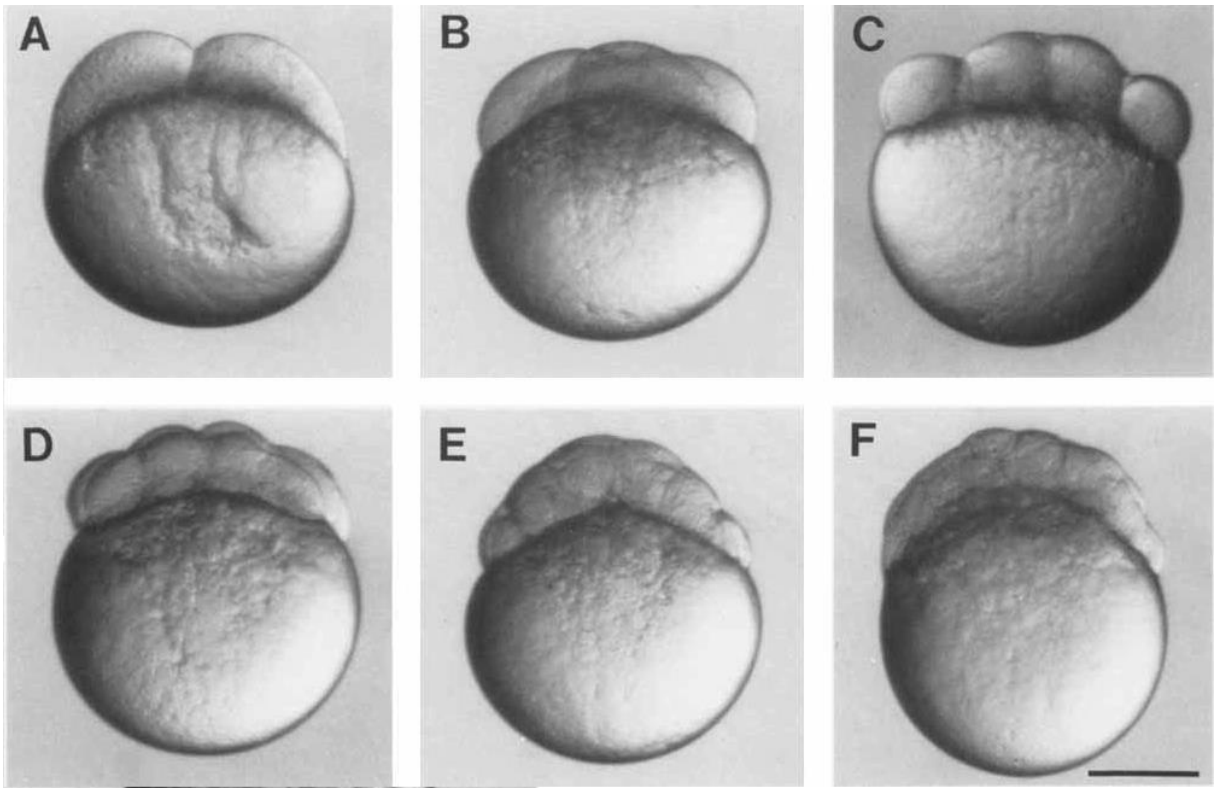

Figure 19: Embryos during the cleavage period. Face views, except for B, which shows the embryo twisted about the animal-vegetal axis, roughly 0.75h from the face view. A: Two-cell stage (0.75 h). 8: Four-cell stage (1h). C: Eight-cell stage (1.25 h). D: Sixteen-cell stage (1.5 h). E: Thirty-two cell stage (1.75 h). F: Sixty-four cell stage (2 h). Scale bar = 250 pm (from Kimmel 1995).

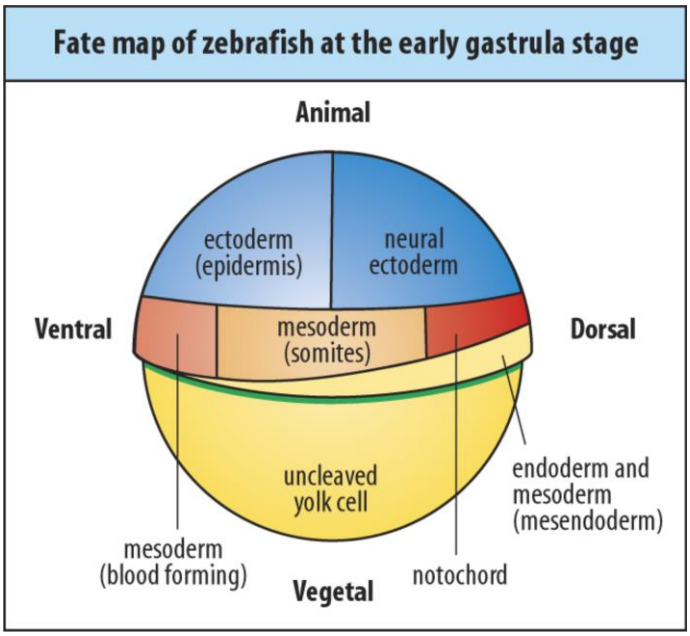

Figure 20: zebrafish embryo fate-map at 30% epiboly.

BLASTULA PERIOD (2H-5H1/4)

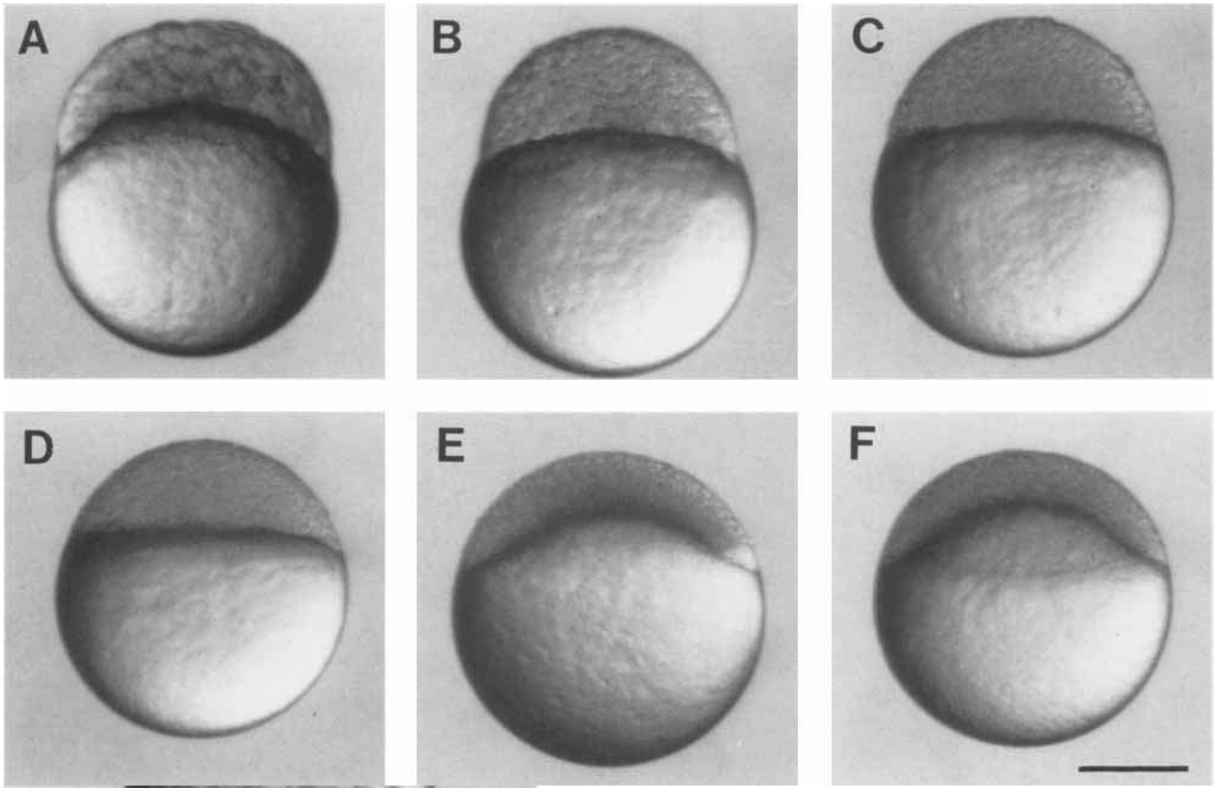

Figure 21: Face views of embryos during the blastula period. A: 256-cell stage (2.5 h). B: High stage (3.3 h). C: Transition between the high and oblong stages (3.5 h). D: Transition between the oblong and sphere stages (3.8h). E: Dome stage (4.3h). F: 30%-epiboly stage (4.7h). Scale bar = 250 pm (from Kimmel 1995).

The divisions continue at constant rate until 512 cells. At mid-512 stage (Figure 21 B) there is a morphogenetic change, the EVL cells that are near the yolk lose their lower border(not shown). This is the beginning of the yolk syncytial layer (YSL) formation, which defines the layer at the frontier between cells and the yolk (Figure 20) (91 Kane et al., 1992, 92 Trinkaus, 1992). The first sign of epiboly is the dome formation (93 Solnica-Krezel and Driever, 1994) (Figure 20, Figure 21 E). Epiboly is defined by an engulfment of the blastoderm around the yolk initiated at dome stage. One classically measures the advancement of epiboly by the percentage of yolk engulfment. The blastula period stop when the epiboly is 30% (Figure 21 F). Then start the gastrula period.

GASTRULA PERIOD (51/4-10 h)

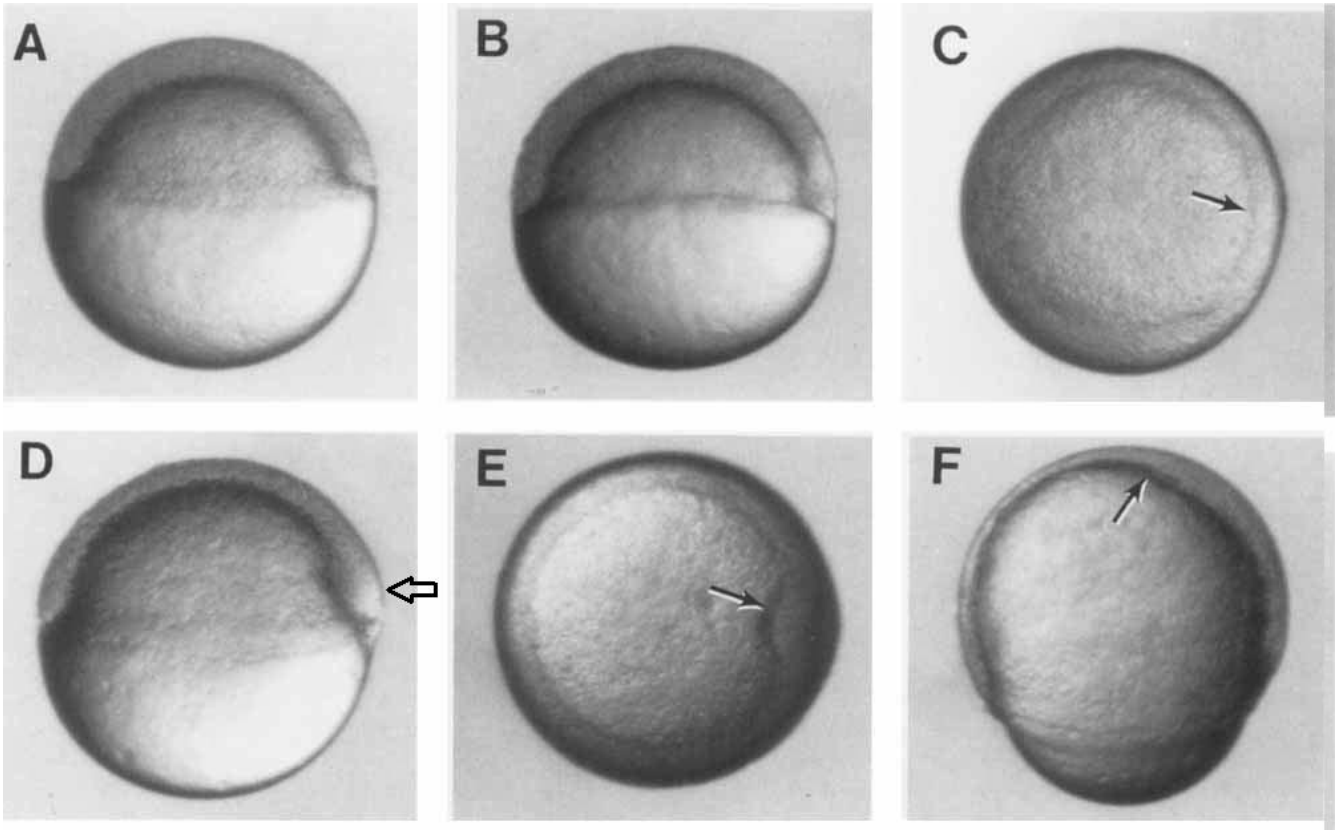

Figure 22: Development during the gastrula period. Left side views, except where noted, with anterior up and dorsal to the left. A: 50%-epibolystage (5.25 h). B: Germ ring stage (5.7 h). C: Animal pole view of the germ ring stage; the arrow indicates the germ ring; the embryonic shield will probably develop from the flattened region of the ring at the lower right. D: Shield stage (6 h). The embryonic shield, marking the dorsal side, is visible as a thickening of the germ ring to the right. E: Animal pole view of the shield stage; the arrow indicates the embryonic shield. ***F****: 70%-epiboly stage (7.7 h). The dorsal side of the blastoderm, to the left, is thicker than the ventral side, to the right. The anterior axial hypoblast, or prechordal plate (arrow), extends nearly to the animal pole.*

Gastrulation is defined by dorsal meso-endoderm internalization (not shown). This morphogenetic movement initiates the formation of the 3 layers and the embryonic axis during this period. During gastrulation, epiboly continues to progress (Figure 22 A to Figure 22 D), at around 50% there is a break in epiboly due to an accumulation of cell at a point of the germ ring that will form the embryonic shield (Figure 22 D arrow). This shield will mark the dorsal side of embryo, and the head of the embryo will develop at the animal pole (94 Wood and Timmermans, 1988). At this stage, one can therefore now, define the antero-posterior and dorso-ventral axis. After this period epiboly continue at a rate around 15% of recovering every hour. During this period the antero-posterior axis becomes longer. At 10 hpf the epiboly is complete.

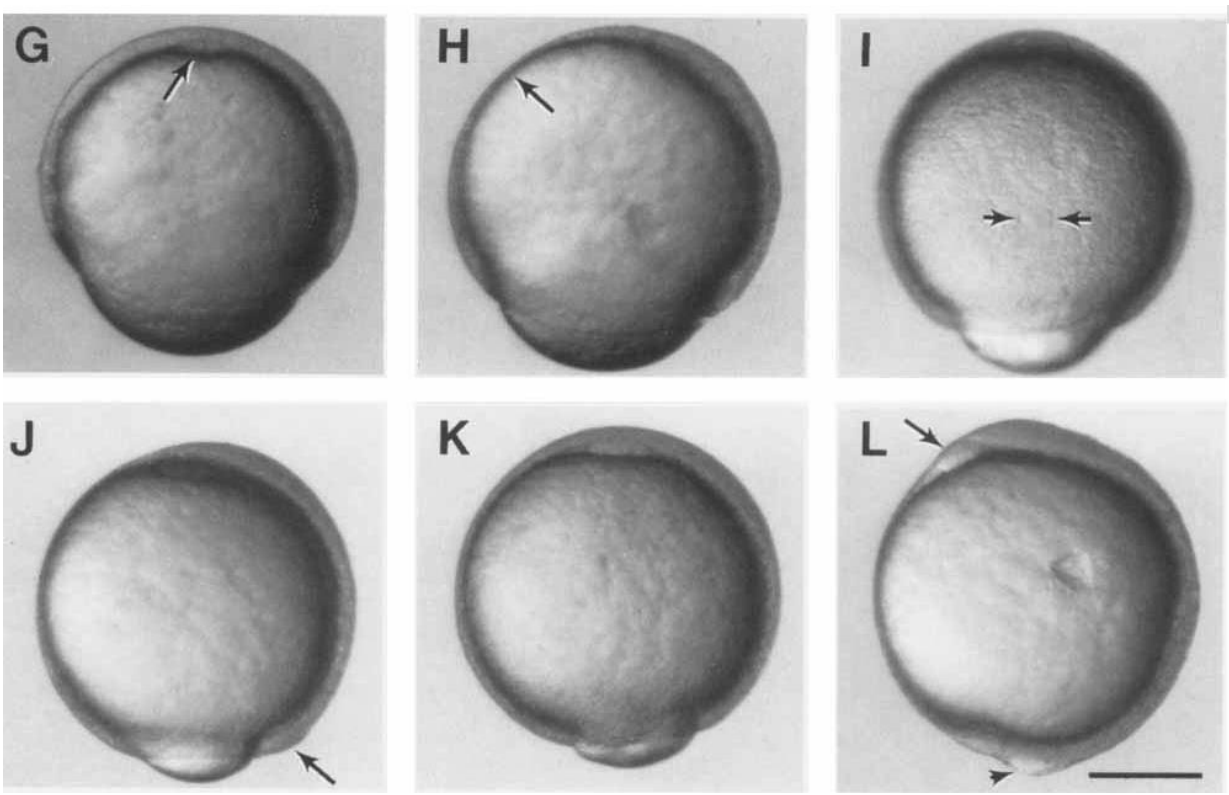

*Figure 23: **G**: 70%- epiboly stage, ventral view, but tipped slightly forward anteriorly to reveal the now well-delineated axial hypoblast (arrow) of the prechordal plate.**H**: 75%-epiboly stage (8 h). The arrow indicates the thin evacuation zone on the ventral side. **I**: 80%-epiboly stage (8.4 h), dorsal view. The arrows indicate the boundaries between axial mesoderm in the midline, and the paraxial mesoderm flanking to either side. **J**: 90%-epiboly stage (9 h). The tail bud (arrow) becomes visible in some embryos at this stage. **K**: 90%-epiboly stage, ventral view. The anterior prechordal plate (compare with G) enlarges as the polster. **L**: Bud stage (10 h). The arrow shows the polster, and the arrowhead shows the tail bud. A distinctive region just ventral to the tail bud (i.e., just to the left in this view) shows where the yolk disappears as epiboly ends. Scale bar = 250 pm (from Kimmel 1995).*

SEGMENTATION PERIOD (10-24 h)

The segmentation period starts with the somite development, with the rudiments of the primary organs formation becoming visible afterword, (Figure 25A). The somite appear at a mean rate of 2-3 somite per hour (95 Hanneman and Westerfield,1989). The main evolution in this part of development is the evolution of the tail. (96 Thisse et al 1993)(Figure 24). The mesoderm starts to be morphologically distinctive during this period, and mainly forms in the dorsal part of the embryo. At 5 somites, one can see the optic primordium (Figure 25D). At 20 somites the tail is detached, and one can see the first muscular movement of the embryo.

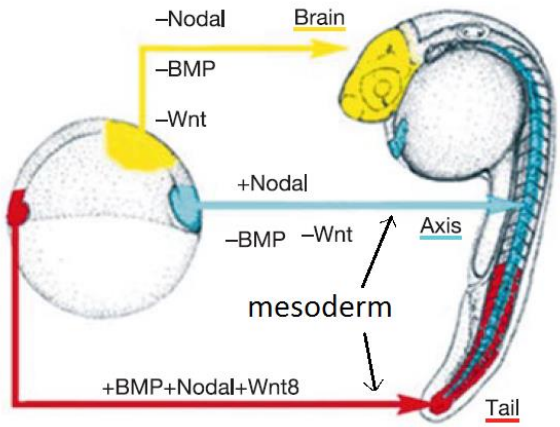

Figure 24 : (97 from Agathon et al 2003)The zebrafish embryo is patterned by the combined activity of BMP, Nodal and Wnt signalling pathways. The formation of the head results from the triple inhibition of BMP, Nodal and Wnt. Formation of the axis (prechordal plate, chorda-mesoderm and ventral neural tube) results from the inhibition of BMP and Wnt and stimulation by Nodal. The formation of the tail depends on the triple stimulation of BMP, Nodal and Wnt8 signalling pathways.

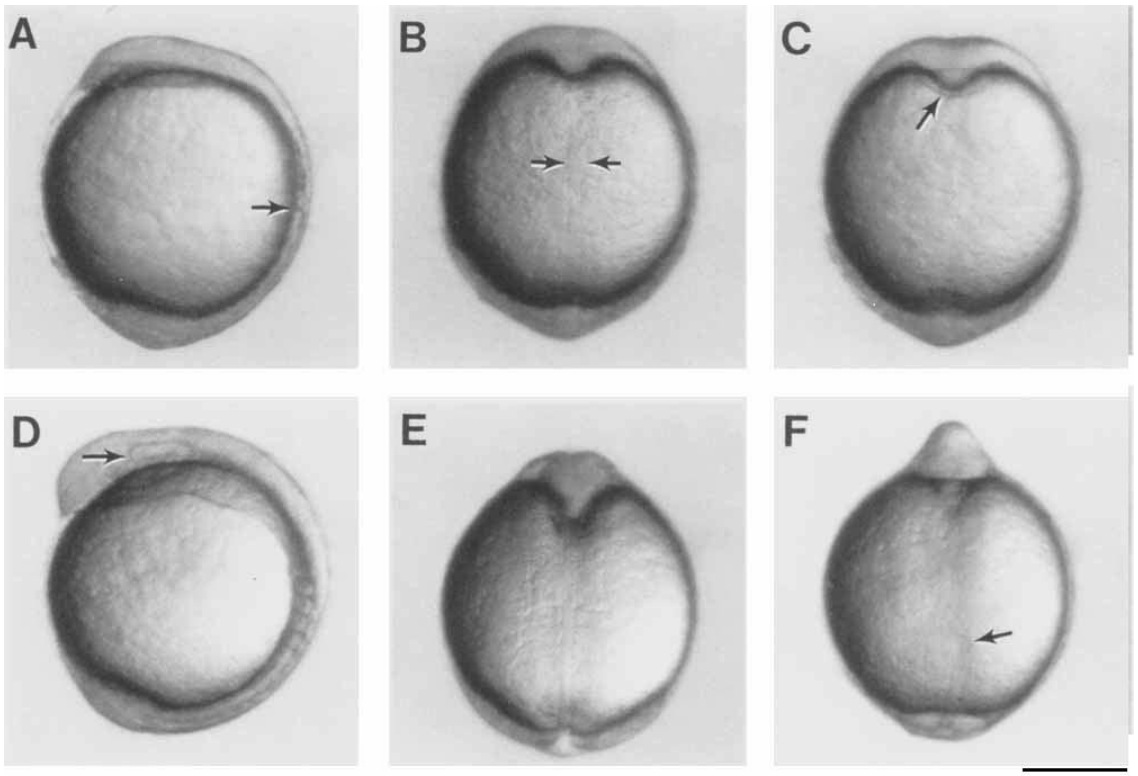

Figure 25 Development during the segmentation period. Left side views, except where noted, with anterior up and dorsal to the left. ***A:*** *Two-somite stage (10.7 h). Somite 2 is the only one entirely pinched off at this time, the arrow indicates its posterior boundary. Somite 1 is just developing a clear anterior boundary at this stage.* ***B:*** *Two-somite stage, dorsal view. The notochord rudiment shows between the arrows, just anterior to the level of somite 1.* ***C:*** *Two-somite stage, ventral view. The arrow indicates the polster.* ***D:*** *Four-somite stage (1 1.3 h). Somite 1 now has an anterior boundary. The optic primordium begins to show (arrow).* ***E:*** *Four-somite stage, dorsal view, focus is on the notochord at the level of the boundary between somite 2 and 3. Note at the top how the brain rudiment and underlying axial mesoderm prominently indent the yolk cell in the midline.* ***F:*** *Five-somite*

stage (1 1.7 h), ventral view, focus is on the newly forming Kupffer's vesicle (arrow).. Scale bars = 250 pm (from Kimmel 1995).

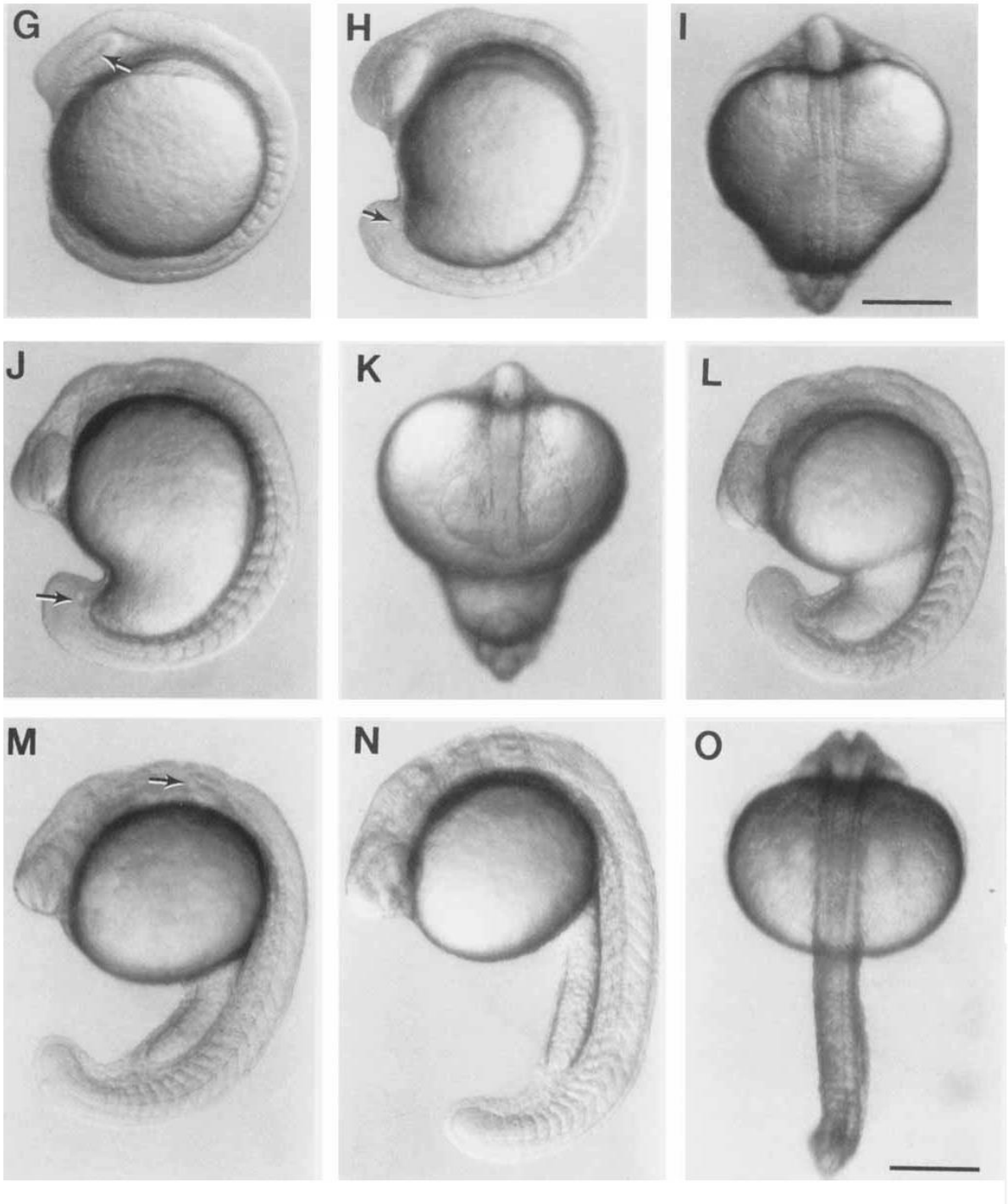

Figure 26: Fifteen-somite stage (16.5 h).The arrow shows Kupffer's vesicle. ***G:*** *Eight-somite stage (13 h). The optic primordium has a prominent horizontal crease (arrow). The midbrain rudiment lies just dorsal and posterior to optic primordium. The segmental plate, developing paraxial mesoderm posterior to the somite row, is clearly delineated. H: Thirteen-somite stage (15.5 h). Somite begin to take on a chevron shape. The yolk cell begins to look like a kidney-bean, heralding formation of the yolk extension. The tail bud becomes more prominent and Kupffer's vesicle shows from the side (arrow).* ***I:*** *Fourteen-somite stage (16 h), dorsal view, and posi-*

tioned so that the first somite pair is at the centre. Note at the top the shape of the brain primordium, at the level of the midbrain K: Fifteen-somite stage from a dorsal view to show the optic primordia. Kupffer's vesicle is also nearly in focus. L: Seventeen-somite stage (17.5 h). The otic placode begins to hollow.The yolk extension is now clearly delimited from the yolk ball as the tail straightens out. M: Twenty-somite stage (19 h). The arrow indicates the otic vesicle. N: Twenty-five-somite stage (21.5 h). The telencephalon is prominent dorsally, at the anterior end of the neuraxis. 0: Twenty-fivesomite stage, dorsal view. The hindbrain's fourth ventricle shows at the top (from Kimmel 1995).

PHARYNGULA PERIOD (24-48 h)

During the early pharyngula period, (98 Ballard 1981), the lengthening of the embryo continues during 7 hours. At this period, the embryo morphology is similar to the morphology of other vertebrates (99 Gould, 1977)(Figure 27A-C). At early pharyngula, the heart starts beating and the circulatory system forms (100 Reib, 1973). At 30 hpf one can see the first pigmentation and the stripes first dorsal then ventral are now observable. (101 Milos and Dingle, 1978)(Figure 27D-F). During the next hours of the development, the embryo will develop tactile sensitivity, and the uncoordinated movement will become more rare.

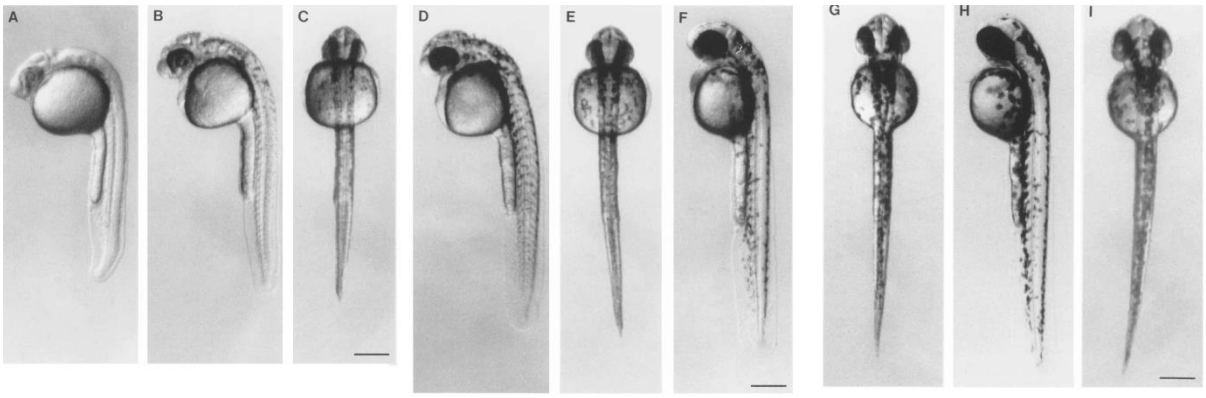

Figure 27: Development during the pharyngula period. Left-side and dorsal views (except for the prim-5 stage) of the same embryo at the given stage. A: Left-side view at the prim-5 stage (24 h). The brain is prominently sculptured (see Fig. 23 for a key to the brain subdivisions).Melanogenesis has begun, but is not yet evident at this low magnification.B,C: The prim-1 2 stage (28 h). Melanophores extend from the level of the hindbrain to about the middle of the yolk ball. D,E: The prim-20 stage (33h). A few pigment cells are now present along the axis dorsal to the yolk extension and on the dorsal part of the yolk ball. F,G: The prim-25 stage(36 h). Pigment extends almost to the end of the tail. The arrow in F indicates the ventral horn of melanophores. H,I: The high-pec stage (42h). Pigment now extends the whole length of the embryo. The dorsal and ventral pigment body stripes are filled in, but not so neatly as they will (from Kimmel 1995)

HATCHING PERIOD (48-72 h)

Individuals hatch sporadically during the 3rd day.

2- *notail* induction at the onset of epiboly

a- *notail* expression is β-cat dependent

During the early development of the zebrafish *Danio rerio*, nuclear translocation of β-cat occurs in two steps. The first step, starting at 128 cells and lasting until sphere stage (4 hours post-fertilization (hpf)), is under maternal genes control and defines the dorsal organizer by nuclear labelling restricted to a few cells ((Figure 28: 1,3,5, sphere stage, denoted by white arrows) (102 Schneider 1996). Please note that the details of all materials procedures and of the statistics of the findings are reported into the associated article in the end of this manuscript.

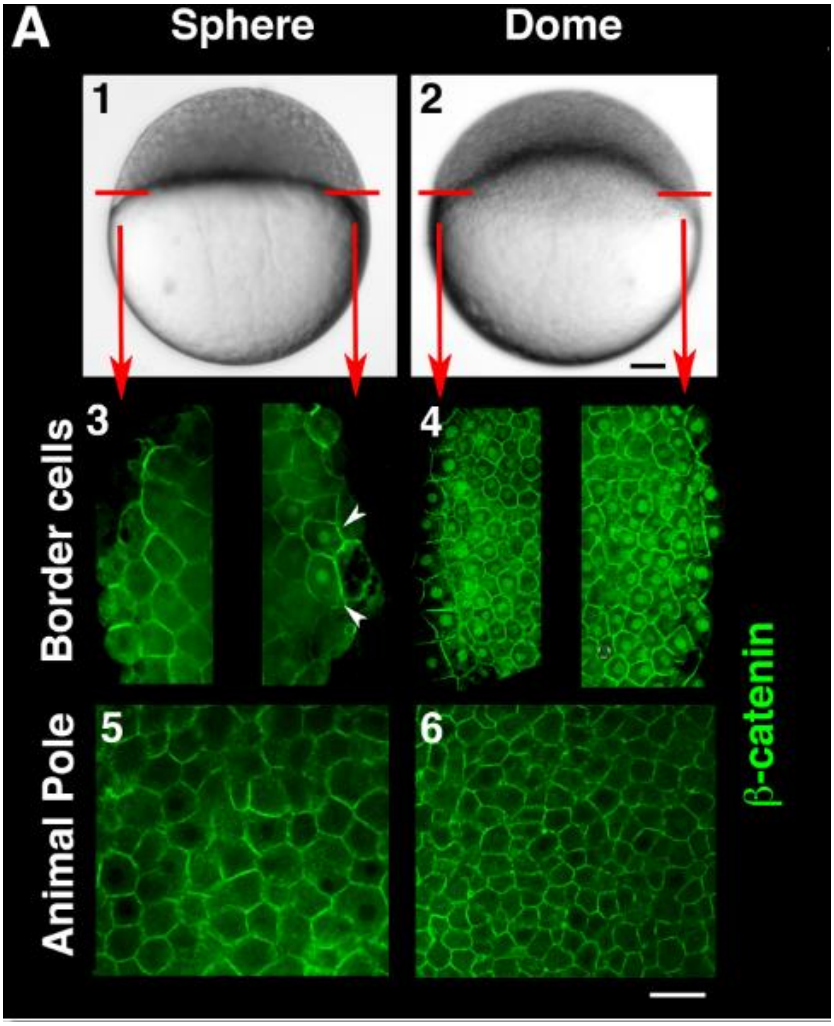

Figure 28: Start of epiboly in zebrafish embryo coincides with nuclear translocation of β-cat around the margin. (A1,2) The transition from sphere (A1, 4 hours post-fertilization (hpf)) to dome (A2, 4.3 hpf, epiboly initiation). The black bar is 100 microns. (A3,4) The margin is devoid of nuclear β-cat (A3 left) apart from the dorsal pole (A3 right, white arrows) at sphere, and is ubiquitous around the margin (A4, left and right) at dome. (A5,6) No nuclear β-cat is observed at Animal pole (upper pole) at either stages. The white bar is 20 microns.

In a second step, after epiboly has started, β-cat nuclear translocation expands to encompass the entire marginal zone (103 De Robertis 2008). By performing β-cat immunostaining on zebrafish embryos, we found that

marginal β-cat nuclear translocation initiates during the first 20 minutes of the epiboly morphogenetic movement (Figure 28 : 2,4,6, dome stage).

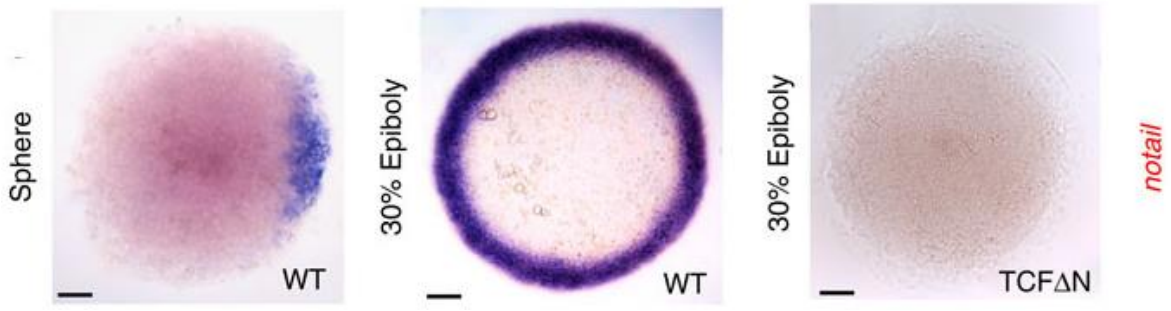

Figure 29:(1) Sphere: ntl expression initiation at dorsal pole. (2) 30% epiboly: ntl expression initiation spreads to the whole marginal zone. (3) Heat-shocked HS-TcfΔN-GFP embryos: ntl expression at the margin is undetectable at 30% epiboly.

The marginal zone out of the dorsal pole where nuclear β-cat extends gives rise to the mesoderm in zebrafish (104 Stern 2004)(Figure 20Figure 24). In Xenopus and mouse, β-cat has been shown to be necessary for early *brachyury* expression leading to mesoderm induction (105 Schohl 2003, 106 Valenta 2011). However, it has been so far unclear whether β-cat was necessary to establish the *brachyury* orthologous *notail* (*ntl*) expression in zebrafish. B-cat being the co-transcription factor of Tcf, we used a heat-shock-inducible Tcf-dominant negative-GFP (HS-TcfβΔN) transgenic strain to evaluate this possibility (107 Lewis 2004). In GFP-positive heat-shocked transgenic embryos, *ntl* expression is totally undetectable by *in situ* hybridization at 30% (4.7 hpf,) (Figure 29) and 50% (5.3 hpf,) epiboly (Figure 30).

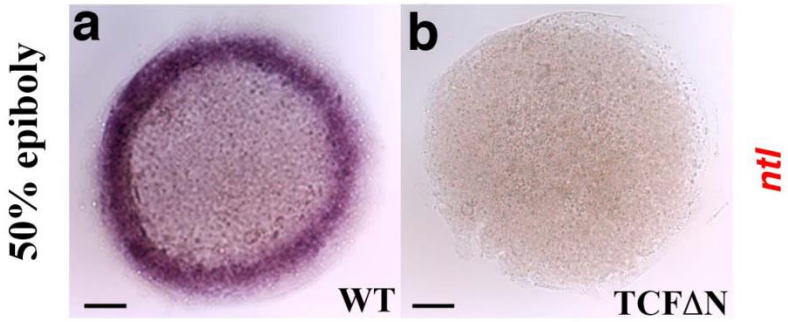

Figure 30: ntl expression at the marginal zone of 50% epiboly zebrafish embryo requires β-cat transcriptional activity (a) ntl is detectable by in situ hybridization on heat-shocked wild-type siblings at 50% epiboly (79/79). (b) ntl is undetectable by in situ hybridization on heat-shocked HSTcfΔN- GFP transgenic embryos (26/26). Experiments were replicated 2 times.

Consist*ntl*y, in wild-type (WT) fish *ntl* expression was observed in cells characterized by nuclear β-cat only, indicating that *ntl* transcription is a cell autonomous response to β-cat nuclear translocation β-cat transcriptional activity is thus necessary for initiation of *ntl* expression in zebrafish, suggesting that *ntl* expression is under the control of Wnt ligands that are known to activate β-cat transcription dependent events (Figure 33).

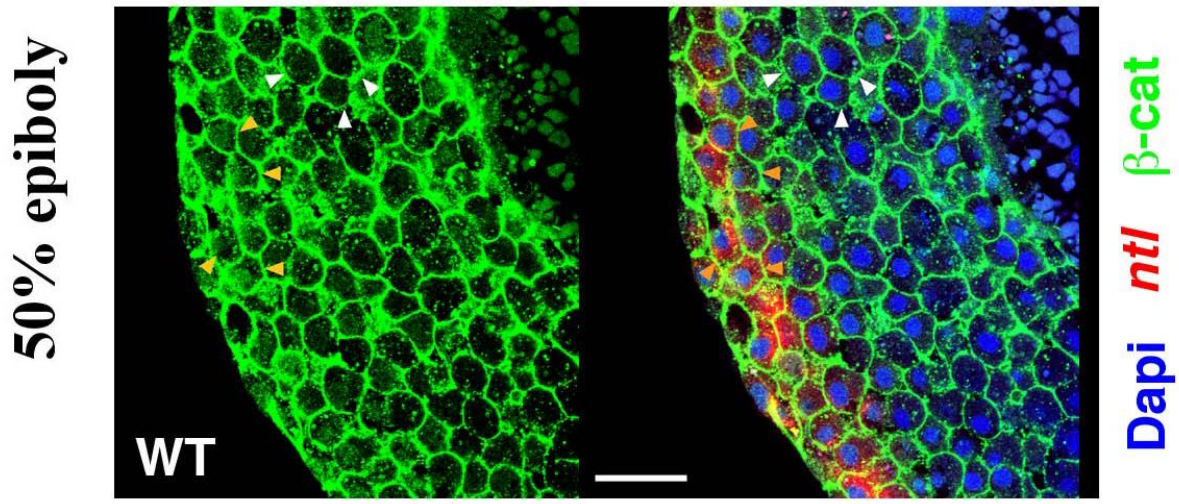

Figure 31: Confocal image of the marginal cells of a wild-type embryo (dome stage) labelled for β -catenin (green), notail in situ hybridization signal (red) and nuclei (DAPI, blue) (5/5). Note that the notail signal is only detected in cells displaying nuclear β -catenin (orange arrowheads), while cells without detectable nuclear β -catenin (white arrowheads) are devoid of notail signal. This suggests that β -catenin is necessary for notail expression in a cell-autonomous way. Some β -catenin-positive cells seem notail-negative, which might reflect the inability of the in situ hybridization procedure to detect low notail expression levels, or indicate that nuclear β -catenin alone is not sufficient to turn on notail expression and requires additional cofactors. Note that the ntl in situ labelling procedure is not optimal for β -catenin labelling and that β -catenin labelling is consequently less bright than in single labelling conditions. The black bars are 100 microns and the white bar is 20 microns.

b- β-cat -dependent *notail* expression is Wnt-independent

β-cat transcriptional activity is thus necessary for the initiation of *ntl* expression in zebrafish, which would suggest that *ntl* expression is under the control of Wnt ligands that are classically known to activate β-cat transcription dependent events. Strikingly, injection of the inhibitor of the Wnt receptors *dkk* did not result into the inhibition of *ntl* expression at 30% epiboly, while it does at the later 50% epiboly stages (108 Ueno 2007)(Figure 32).

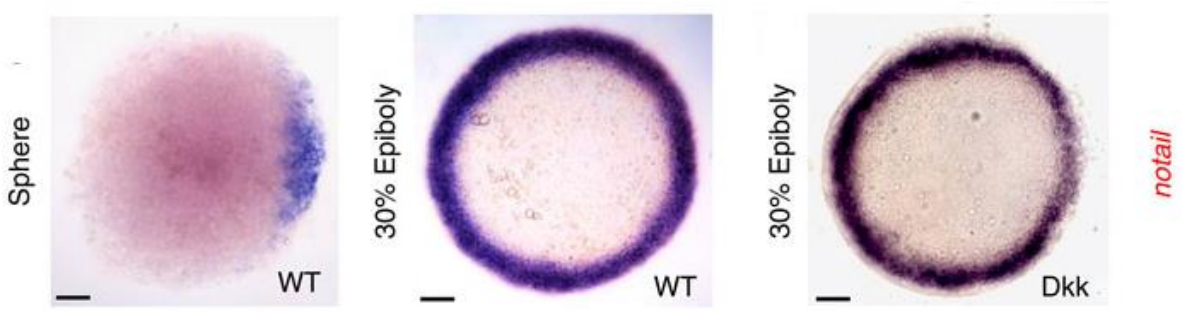

Figure 32: (1) Sphere: ntl expression initiation at dorsal pole. (2) 30% epiboly: ntl expression initiation spreads to the whole marginal zone. (3) Marginal ntl expression is readily detectable in dkk-injected embryos at 30% epiboly (8/8 controls, 8/8 dkk). The black bar is 100 microns.

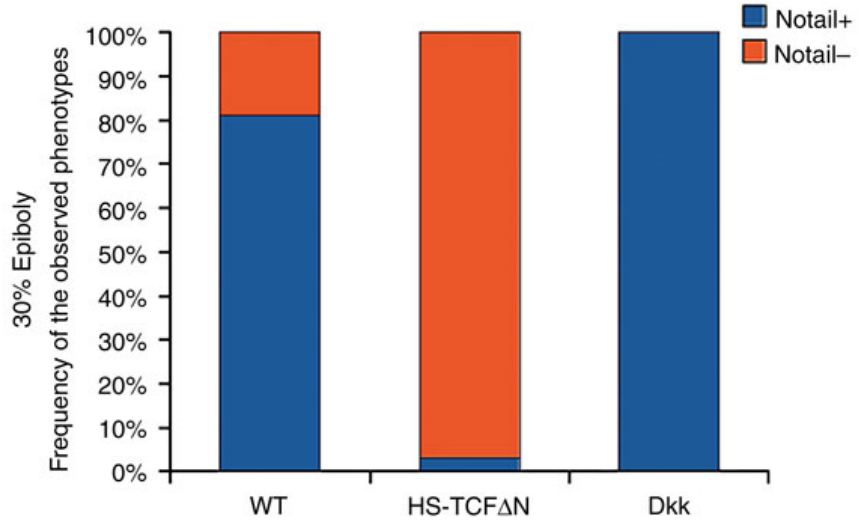

Figure 33: Quantification of ntl-expressing embryos in HS-TcfDN (n=35) and Dkk (n=15) compared with WT (n=37) at 50% epiboly in zebrafish. P<2.2E-16 by the w2-test. All experiments were replicated two times.

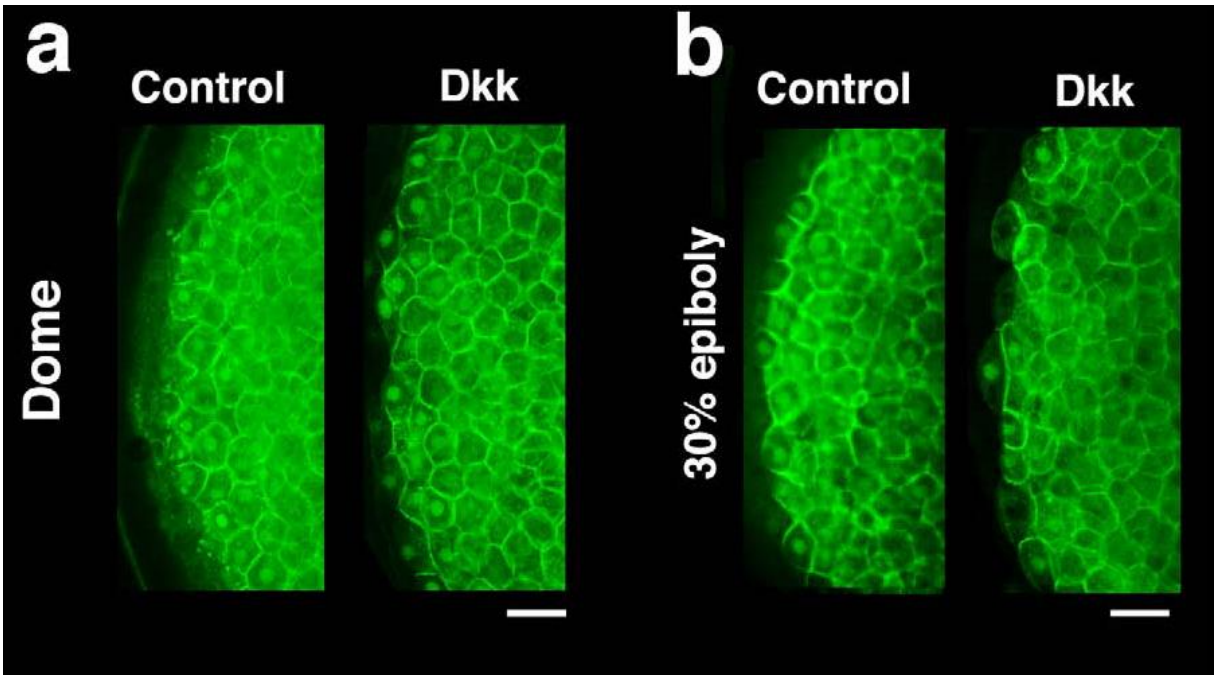

Figure 34: (a) Wnt ligands are not required to establish, but only to maintain, marginal nuclear translocation of β-cat during zebrafish epiboly. (A) Marginal nuclear translocation of β-cat is clearly visible in control dome stage zebrafish embryos. Marginal nuclear translocation of β-cat is not affected at dome stage by inhibition of Wnt co-receptors by dkk injection of dkk-GFP heat shock induced expression. (B) Marginal nuclear translocation of β-cat persists at 30% epiboly in control embryos. Marginal nuclear translocation of β-cat is severely reduced at 30% epiboly in dkk-injected embryos. The white bar is 100 microns.

Injections of the inhibitor of the Wnt receptors *dkk* did neither prevent the initiation of β-cat nuclear translocation in margin cells at dome stage, though it does at the later 30% epiboly and later stages. The initiation of marginal nuclear β-cat and *ntl* expression is thus Wnt independent (Figure 34).

3- Mechanical induction of β-cat nuclear translocation in mesoderm cells

Nuclear translocation of β-cat has been shown to be inducible by mechanical forces in *Drosophila Melanogaster* embryos (Farge 2003, Desprat 2008) as well as in mammalian cells (109 Kahn 2009 ,110 Sen 2008,Samuel et all 2011, Whitehead 2008). Because the onset of marginal β-cat nuclear translocation coincides with the first epiboly movements in zebrafish, we tested the hypothesis that nuclear translocation of β-cat at the margin of the zebrafish embryo is induced by the mechanical signals associated with epiboly movements.

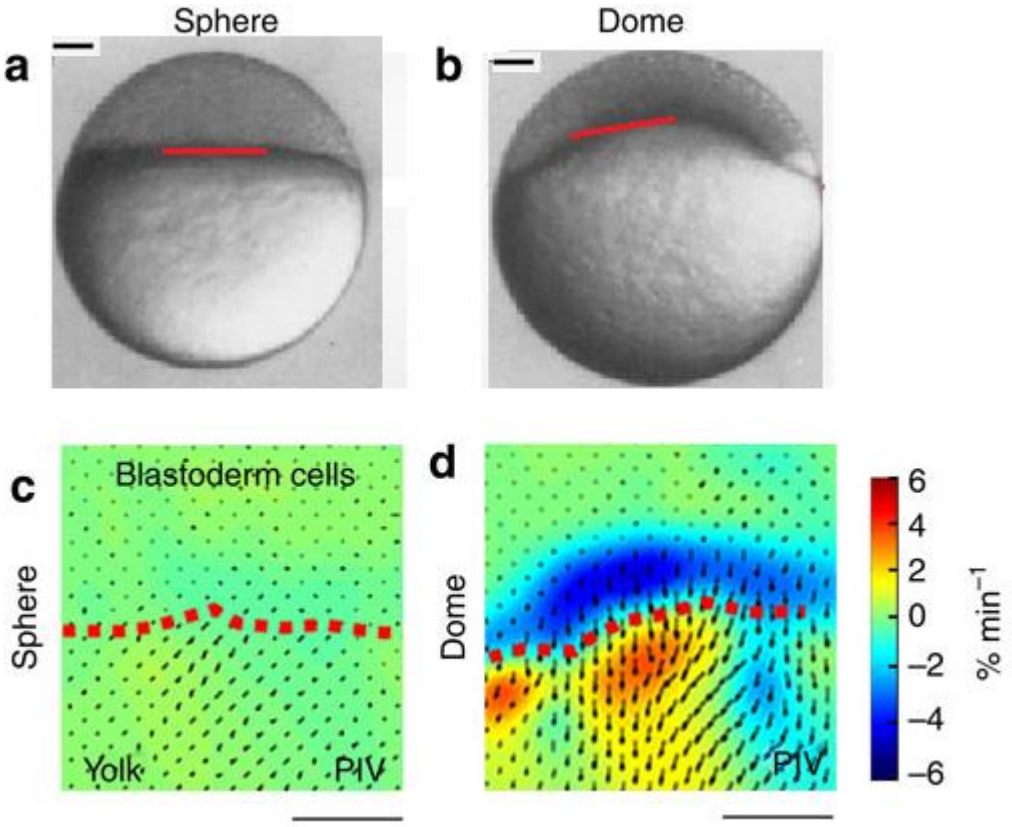

Figure 35: (a) sphere and(b) dome stage of wild type embryo. (c) PIV analysis with no significant cell deformation at sphere. (d) PIV analysis with marginal cell dilation at dome, coinciding with epiboly initiation. The black bar is 100 microns. The red bar represent separation between yolk and cells.

We first performed Particle-Image Velocimetry (PIV) analysis of FM-464-stained zebrafish embryos to test whether marginal tissue undergo specific deformations during epiboly and indeed found the marginal zone to undergo local dilation of the order of - 4%.min-1 of the tissue at the onset of epiboly (Figure 35).

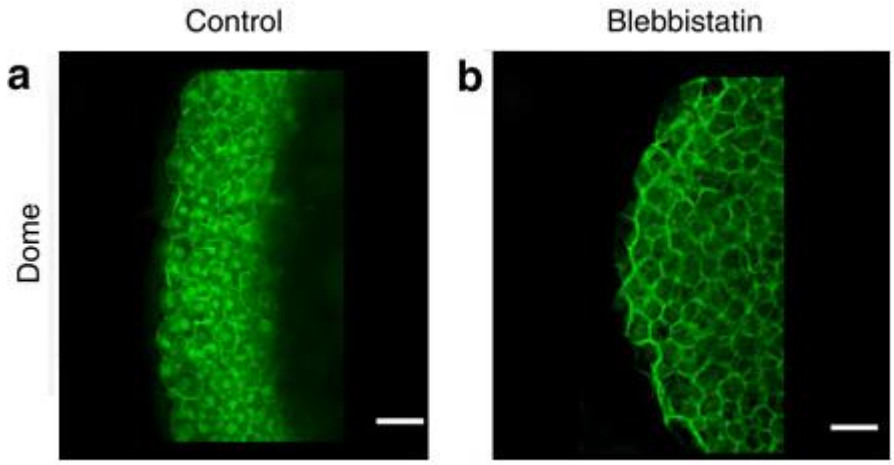

Figure 36: (a) β-cat labelling around the margin in dome non-treated embryo. (b) β-cat labelling around the margin in Blebbistatin treated embryos.

We thus tested whether such deformation was necessary for β-cat nuclear translocation around the margin. The objective was to block those deformations in the zebrafish as we can do with the *Sna* mutant in the *Drosophila (*Figure 8 *B first chapter of the manuscript)*. An equivalent mutant, Poky, exists. However it showed important local fluctuating movements at the margin (111 Fukazawa 2010), preventing the use of mutants to block any movement of epiboly. Therefore we had to use drugs to inhibit the deformation. We found that Blebbistatin, a specific non-muscle myosin II inhibitor (112 Limouze 2004), can block movement during zebrafish epiboly if treatment is started at the sphere stage (Figure 36).

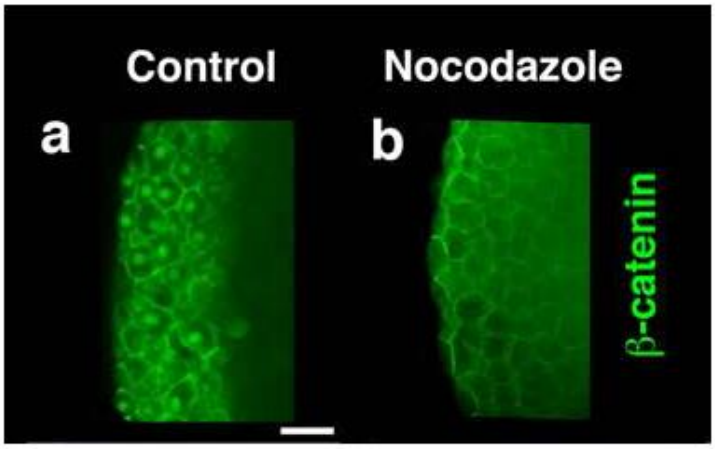

Figure 37: (a) β-cat labelling around the margin in dome non-treated embryo. (b) β-cat labelling around the margin in Nocodazole treated embryos.

To avoid producing results with one specific drug only we worked also using a microtubule-depolymerizing drug Nocodazole (113 Solnica-Krezel 1994). Nocodazole gave the same effect than Blebbistatin) (Figure 37).

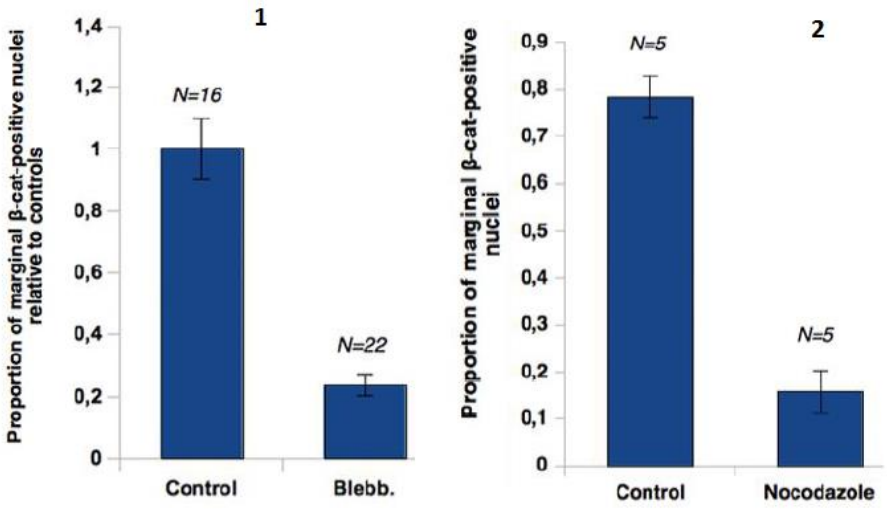

Figure 38: Blebbistatin (1) and Nocodazole (2) treatments severely decrease the proportion of marginal β-cat-positive nuclei.

Despite acting on different targets, both compounds were found to almost completely (80%) disrupt marginal β-cat nuclear translocation (Figure 38).

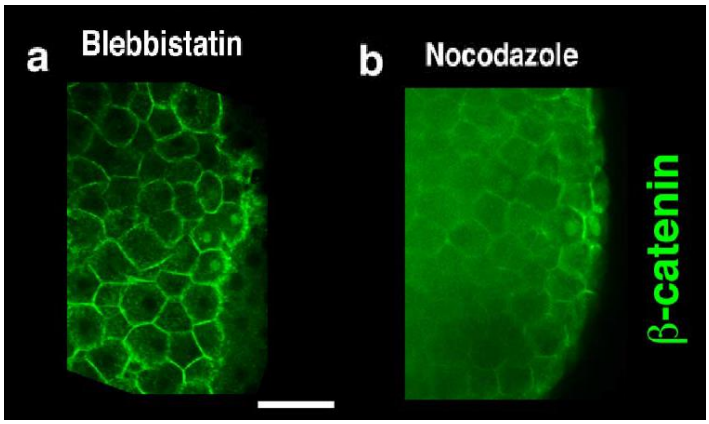

Figure 39: (a) Dorsal nuclear translocation of β-cat is not affected by Blebbistatin treatment (5/5) (b) Dorsal nuclear translocation of β-cat is not affected by Nocodazole treatment (8/8).

Consist*ent*ly, the dorsal centre of β-cat nuclear translocation established before treatment was unaffected by both treatment (Figure 39).

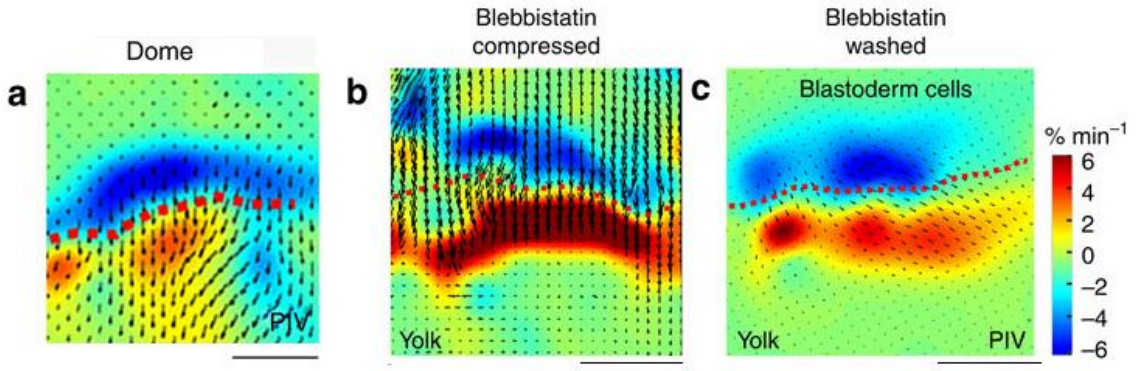

Figure 40: (a) PIV analysis with marginal cell dilation at dome, coinciding with epiboly initiation) (b) Blebbistatin-treated embryo compression and the resumption of epiboly movements and marginal cell dilation. (c) Blebbistatin washing and resumption of epiboly movements and marginal cell dilation. Deformations are assessed by PIV analysis. Note that velocity fields differ between c and d, but the dilations of the marginal cells in blue are the same. Scale bar, 100 mm.

To test whether β-cat nuclear translocation can be mechanically rescued by the mechanical strains developed by the endogenous epiboly morphogenetic movement, we first tested whether exogenous deformation of epiboly in inhibited embryos could rescue β-cat nuclear translocation by applying a soft uniaxial global compression of 35 mm during 20 min (Farge 2003). In addition, we took advantage of the fact that epiboly could be rescued in 5 minutes in the specific case of Blebbistatin by washing treated embryos. PIV analysis confirmed that the wild-type -4%.min-1 value of endogenous dilation characteristic of the dome shape change transition initiating epiboly was quantitatively restored in both cases (Figure 40,

Figure *41*, Figure 42).

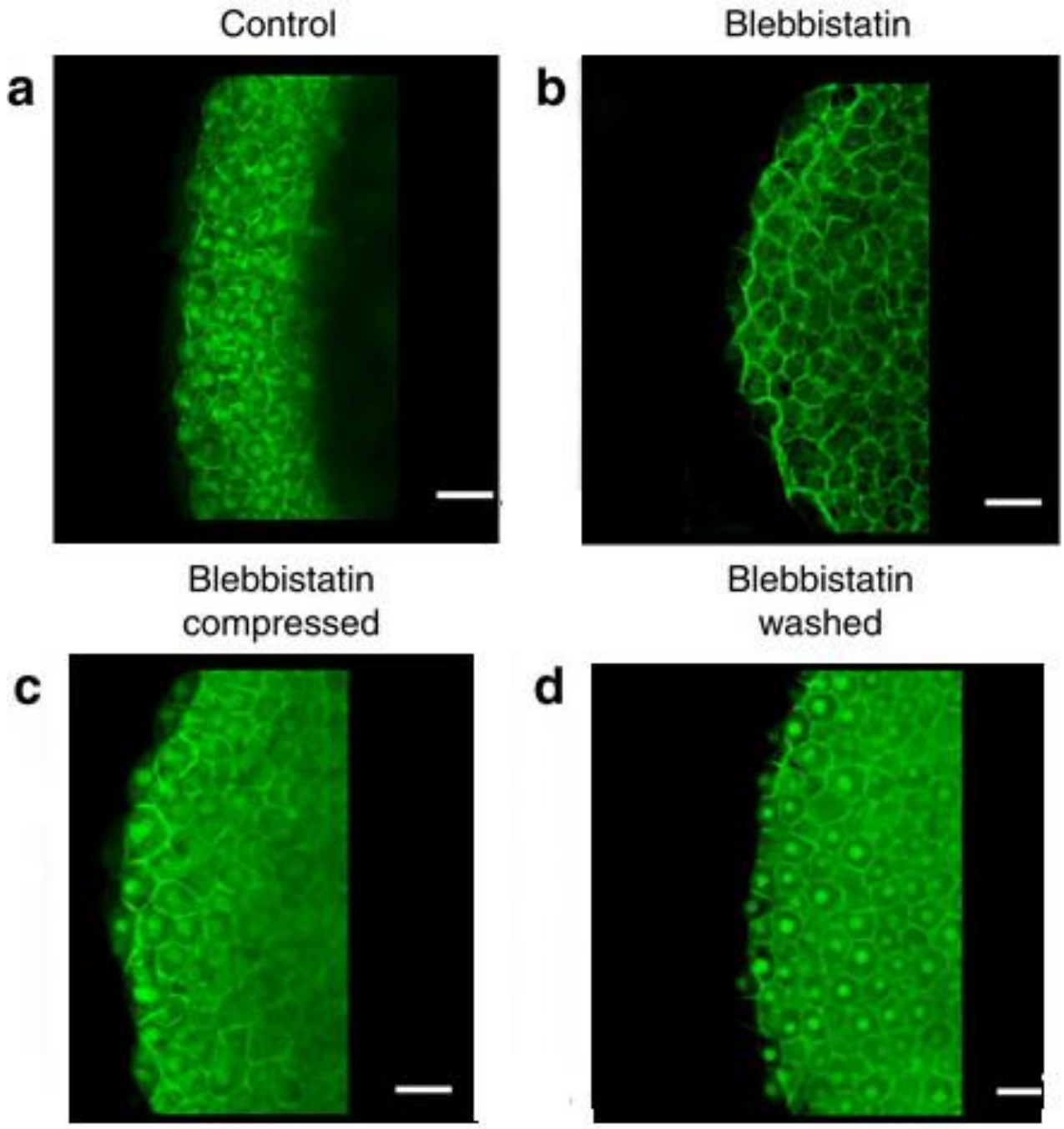

Figure 41: (a) β-cat labelling around the margin in dome to 5.7 hpf non-treated 50% epiboly embryos. (b) β-cat labelling around the margin in Blebbistatin treated embryos (c) β-cat labelling around the margin after global deformation of Blebbistatin-treated embryos. (d) β-cat labelling after Blebbistatin washing upon resumption of endogenous movements. Scale bar, 20 mm (white bar).

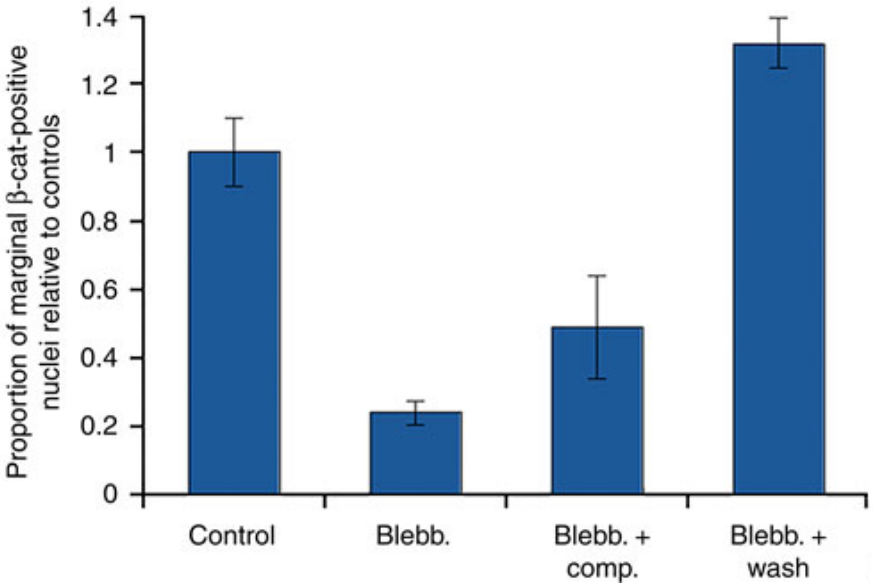

Figure 42: Quantification of marginal β-cat-positive nuclei in controls (n=16), Blebbistatin-treated (n=22), Blebbistatin-treated and globally compressed (n=16), Blebbistatin-treated and washed (n=10). Differences between control and Blebbistatin-treated embryos, and between treated embryos and rescued embryos, are statistically significant according to Mann–Whitney's exact test (P<0.001). Error bars are s.d. Note that ectopic positive nuclei (see figure 17) in Blebbistatin-treated and compressed individuals are not taken into account in this quantification.

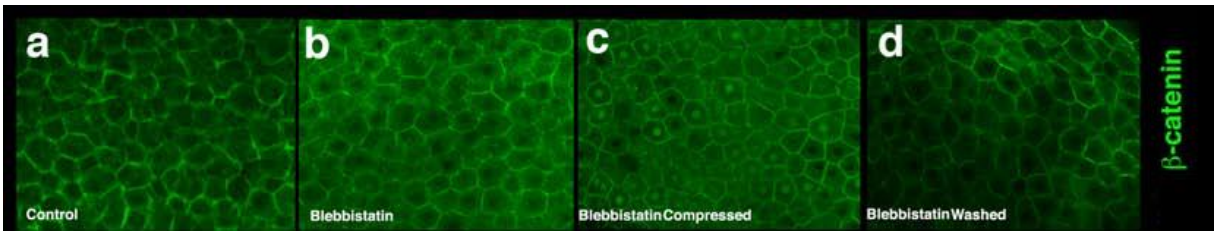

Figure 43: (a) In control and (b) Blebbistatin-treated, (d) and in Blebbistatin-treated and washed embryos, no ectopic β-cat-positive nuclei can be detected at the animal pole. (c) in Blebbistatin-treated compressed individuals in which some nuclear β-cat translocation can be detected at the animal pole.

This resulted in both cases in a partial but significant 50% rescue of the positive nuclei proportion, if only the margin is considered (Figure 42, Figure 43).

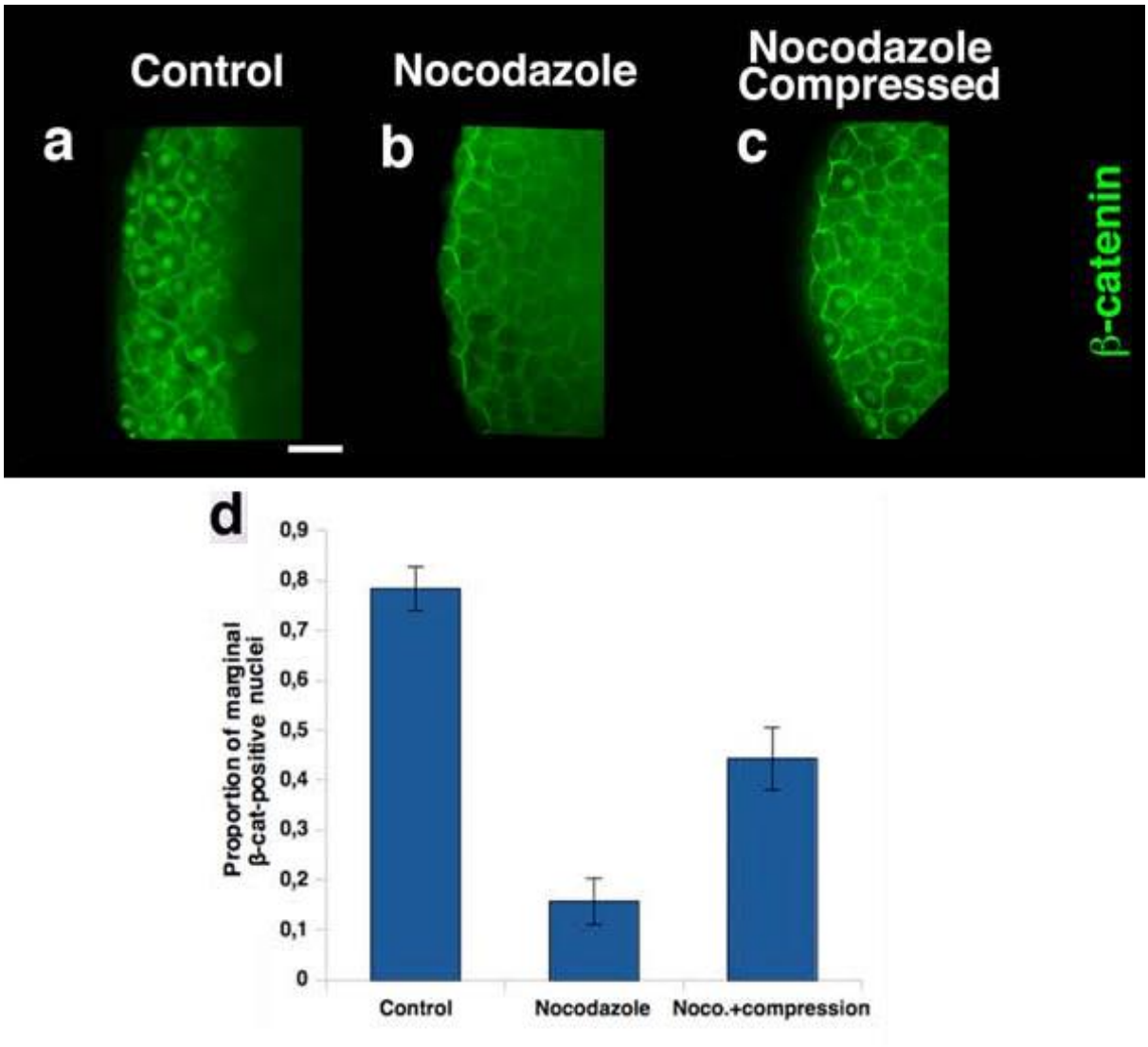

*Figure 44: (a) Marginal nuclear translocation of β-cat in 30% epiboly control embryos. (**b**) Marginal nuclear translocation of β-cat is abolished in Nocodazole-treated embryos when control siblings reach 30% epiboly. (**c**) Global compression rescues nuclear translocation of β-cat in Nocodazoletreated embryos. (**d**) Quantification of the number of β-cat positive nuclei in the control (n=5), Nocodazole treated (n=5) and Nocodazole treated compressed embryos (n=6). Differences between control and Blebbistatin or Nocodazole-treated embryos, and between treated and rescued embryos, are statistically significant according to Mann-Whitney's exact test (p<0.001). Error bars are standard error. All experiments were replicated 2 times. Note that ectopic positive nuclei in Nocodazole-treated and compressed individuals are not taken into account in this quantification.*

We obtained similar results with the Nocodazole (Figure 44). Note that washing effects of Nocodazole was less efficient preventing us to use Nocodazole for this experiment.

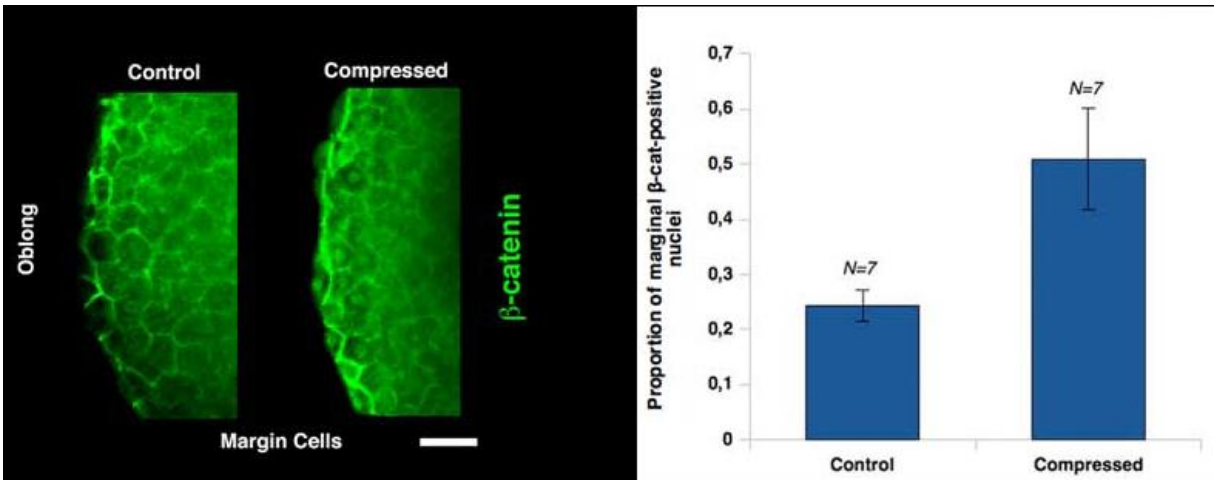

Figure 45: (a) No nuclear translocation of β-cat is observed at the margin out of the dorsal pole before the initiation of epiboly of dome stage (shown here at oblong stage) (n=20). (b) Rescue of margin nuclear translocation of β-cat in oblong stage compressed embryos (c) Quantification of nuclear translocation of β-cat induced by compression in pre-epiboly embryos (N=7) compared to control (n=7). Results are statistically significant according to Mann-Whitney's exact test (p<0.004). Error bars are standard deviation. All experiments were replicated 2 times. The white bar is 20 microns.

To exclude any permissive role of drug treatment in β-cat mechanically induced nuclear translocation, we performed compression of oblong-stage non-treated embryos having not yet initiated epiboly. In non-compressed oblong-stage embryos, no nuclear translocation of β-cat is observed around the margin out of the dorsal pole. β-cat nuclear translocation in the margin cells was also triggered at this pre-epiboly stage by compression in those non-treated embryos, thereby excluding any permissive role of drug treatment in mechanically induced β-cat nuclear translocation (Figure 45).

4- Mechanical induction of *notail* expression

We then explored the target of β-cat *ntl* expression in the margin cells of epiboly-inhibited embryos and compared this with mechanically and epiboly-rescued embryos. In epiboly-inhibited embryos, *ntl* expression displayed the following pattern. At the sphere stage, immediately after treatment, unipolar expression at the dorsal pole can be detected (Figure 46)

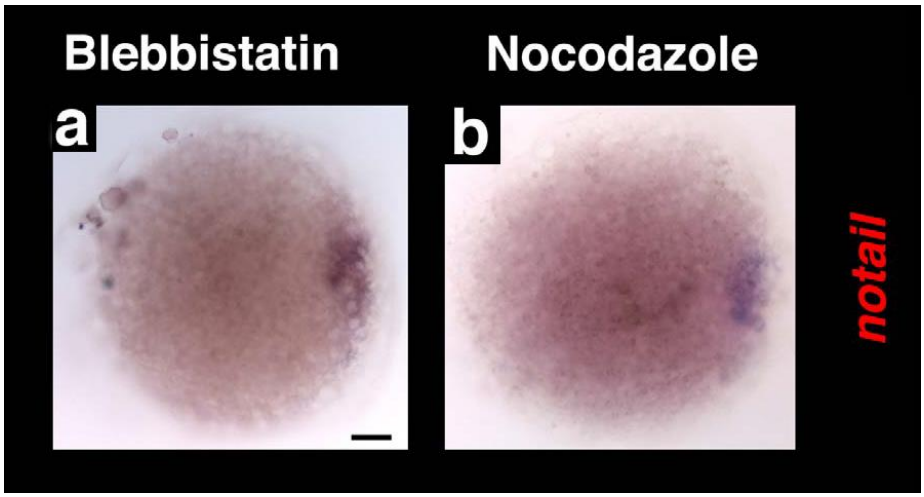

Figure 46: (a) When control siblings reach dome stage, Blebbistatin-treated embryos display persistent unipolar, presumably dorsal, expression of ntl (8/10). (b) An identical phenotype is observed in Nocodazole treated embryos at the same stage (9/12).

This corresponds to the maternally defined, *goosecoid* (gsc)-expressing part of the dorsal organizing centre (the future prechordal plate) specified by the maternally determined first wave of β-cat nuclear translocation that transiently expresses *ntl*. In WT embryos, *ntl* expression later spreads to the entire marginal zone and gets excluded from this *gsc* part of the organizer (Figure 47) (114 Schulte-Merker 1994, 115 Stachel 1995, 116 De Robertis 1995).

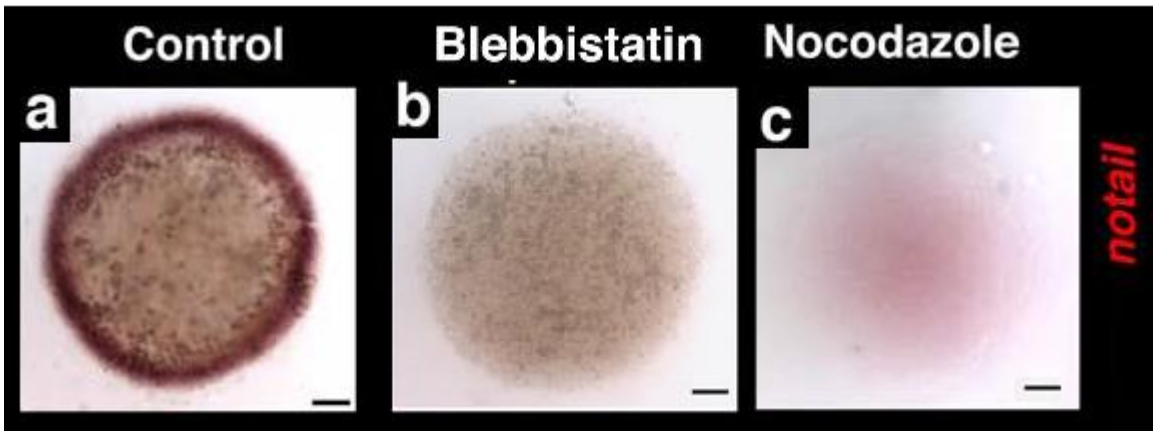

Figure 47: (a) ntl Expression in control embryos at the germ ring stage of 30% to 50% epiboly (5.7 hpf). (b) ntl labelling in Blebbistatin-treated embryos at the same stage, (c) ntl labelling in Nocodazole -treated embryos at the same stage.

In treated embryos, when control siblings reach 30% epiboly, *ntl* expression similarly vanishes from the *gsc* organizer cells but does not spread over the margin and thus becomes undetectable by in situ hybridization (Figure 47).

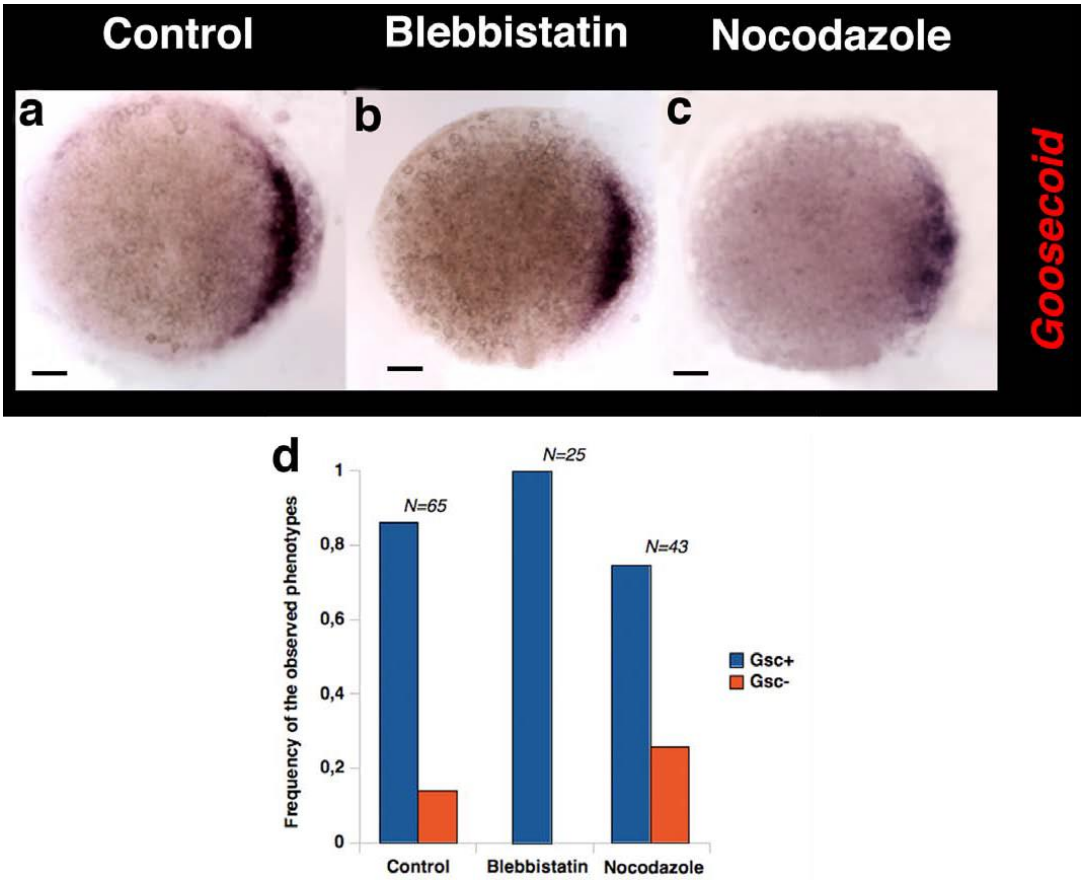

Figure 48: (a) gsc expression at 50% epiboly in control embryos. (b) gsc expression appears unaffected in both pattern and intensity in Blebbistatin-treated embryos. (c) gsc expression appears unaffected in pattern, but with detectably lower intensity, in Nocodazole-treated embryos. (d) Frequencies and statistical significance of the observed phenotypes. p=0.19 (resp. 0.11) for the control/Nocodazole (resp. control/Blebbistatin) comparison, indicating no statistically significant difference between the samples.

On the other hand, *gsc* expression remains readily detectable in the organizer of treated embryos (Figure 48).

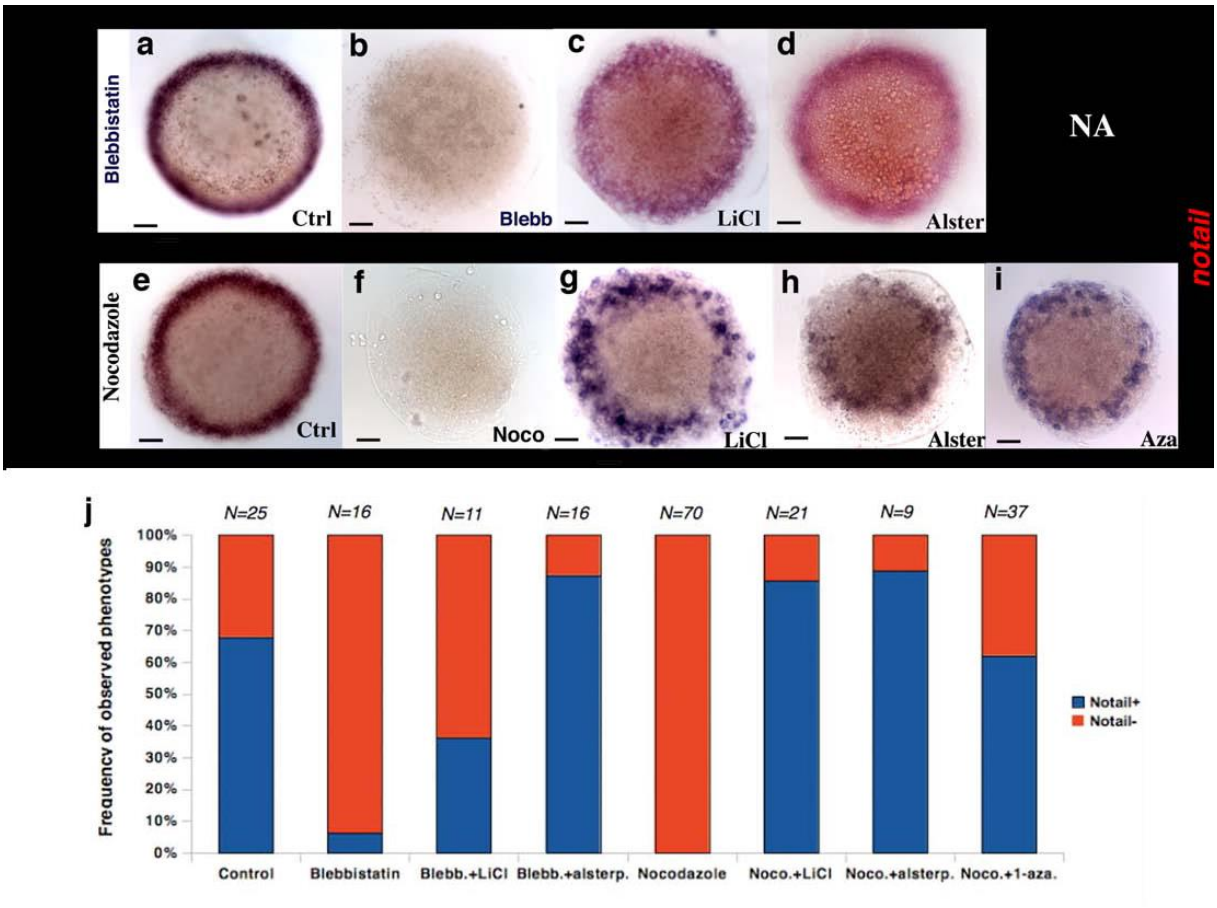

Figure 49: (a) Marginal expression of ntl (b) is abolished upon epiboly inhibition by Blebbistatin treatment, and can be rescued by chemical stimulation of β-cat nuclear translocation by GSK3β inhibitors: (c) LiCl and (d) alsterpaullone. (e) Marginal expression of ntl (f) is abolished upon epiboly inhibition by Nocodazole treatment, and can be rescued by chemical stimulation of β-cat nuclear translocation by GSK3β inhibitors: (g) LiCl, (h) alsterpaullone (i) and 1-azakenpaullone. The combination of 1- azakenpaullone and Blebbistatin turned out to be toxic at the concentrations used. (j) Frequencies and statistical significance of the phenotypes observed. χ_2 tests gave p<0.0001 for comparisons between control embryos and epiboly-inhibited embryos, as well as between epiboly-inhibited embryos and epiboly-inhibited embryos treated with GSK3β inhibitors. All experiments were replicated 2 times. The black bars are 100 microns.

Such selective clearance of *ntl* expression from the dorsal pole shows that treated embryos are not affected by a general developmental delay. We first checked that the *ntl* expression default is secondary to a failure in β-cat transcriptional activity using inhibitors of GSK3β. We treated embryos submitted to Blebbistatin and Nocodazole with either nonspecific (LiCl) or highly specific (alsterpaullone, 1-azakenpaullone) inhibitors of GSK3β known to activate the β-cat pathway, by impairing the GSK3β -dependent cytoplasmic β-cat degradation and thus allowing its nuclear translocation. We found that all of them efficie*ntl*y rescued *ntl* expression at the margin of epiboly-inhibited embryos (Figure 49).

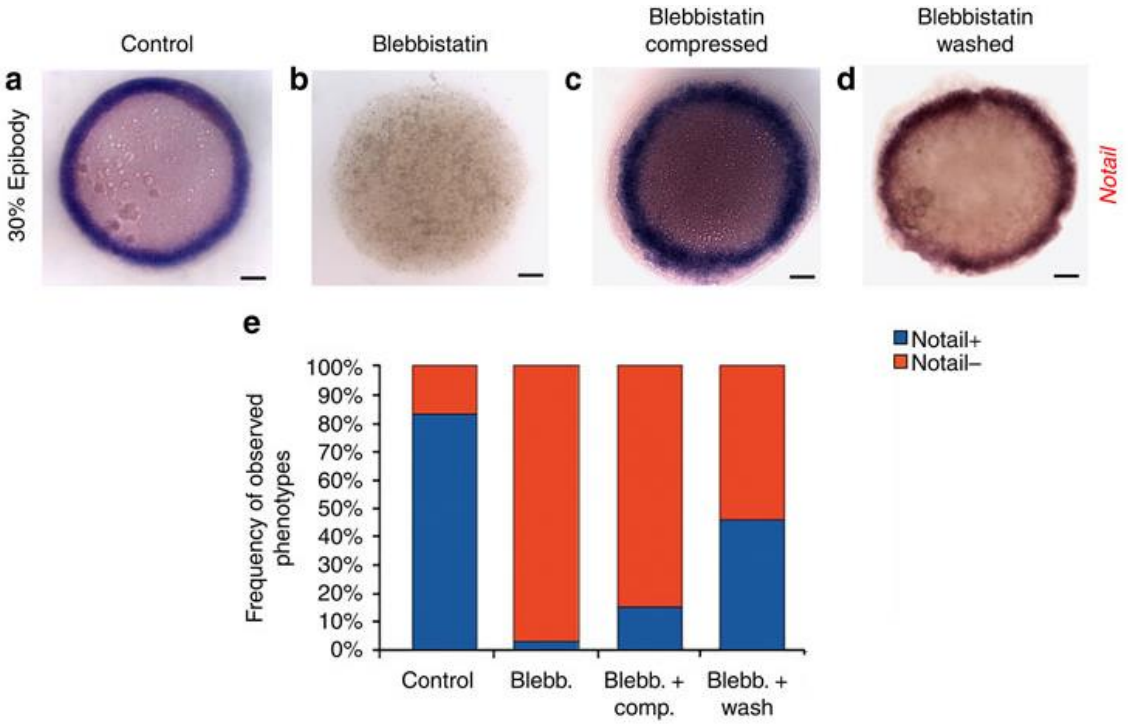

Figure 50: (a) ntl Expression in control embryos at the germ ring stage of 30% to 50% epiboly (5.7 hpf). (b) ntl labelling in Blebbistatin-treated embryos at the same stage, (c) in Blebbistatin-treated embryos globally compressed at the same stage (d) and after Blebbistatin washing at 4.8 and 5.7 hpf, when washed embryos morphologically reach 30–50% epiboly. Scale bar, 100 mm (black bar). (e) Quantification of the number of embryos showing in situ ntl expression in controls (n=97), Blebbistatin-treated (n=95), Blebbistatintreated compressed (n=73), Blebbistatin-treated and washed (n=24), Differences between control and Blebbistatin-treated embryos, and between treated and rescued embryos, are statistically significant according to the w_2-test ($P<0.001$). All experiments were replicated two times.

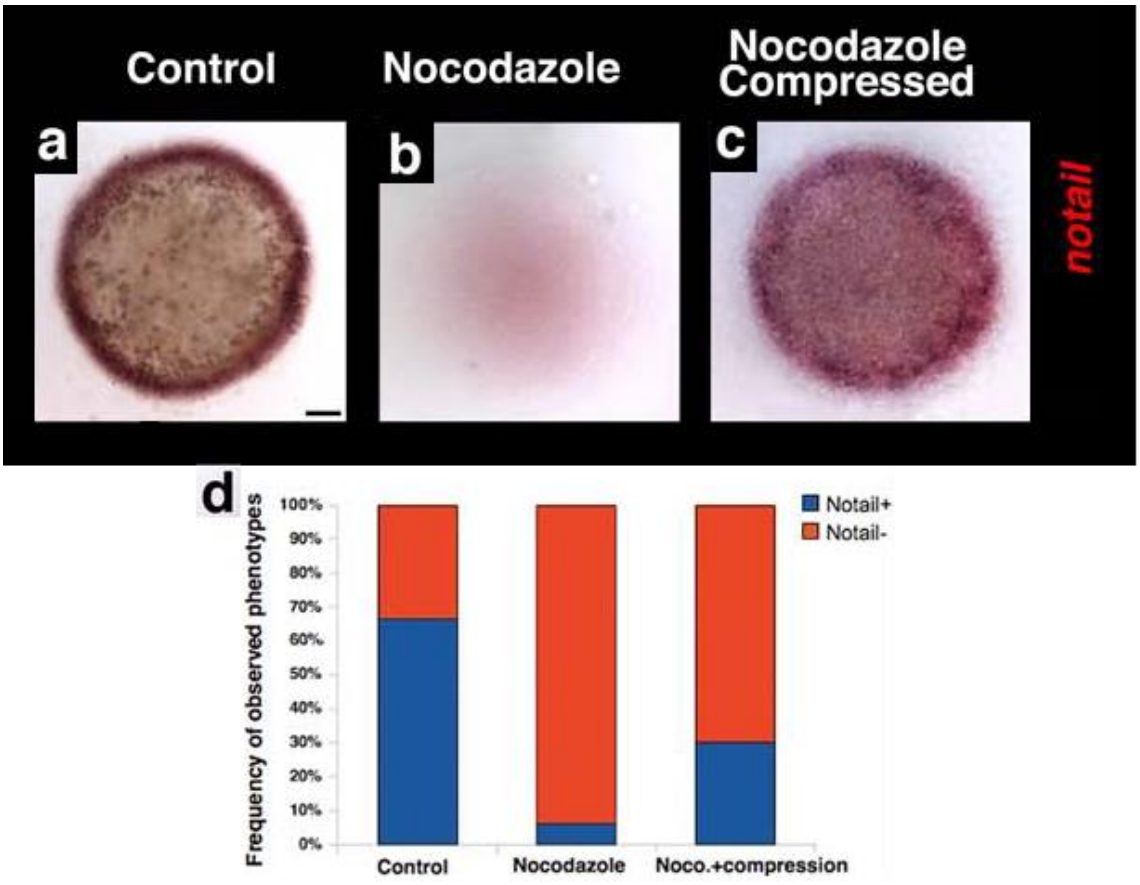

Figure 51: (a) Marginal ntl expression in 50% epiboly control embryos. (b) ntl expression is similarly abolished by Nocodazole when control siblings reach 50% epiboly. (c) Global compression rescues ntl marginal expression in Nocodazole-treated embryos.(d) Quantification of the number of embryos expressing ntl in the control (n=90), Nocodazole treated (n=96) and Nocodazole treated compressed embryos (n=30). $p<0.05$ by the w_2- test. All experiments were replicated 2 times.

Interestingly, ntl expression is rescued only at the margin and not ubiquitously, (

Figure 50) which is consistent with a previous report of ubiquitous Wnt8 overexpression that did not result in ntl ectopic expression. This indicates the existence of a β-cat-independent pre-pattern that restricts the competence for β-cat-induced ntl expression to marginal cells. We then tested whether exogenously applied mechanical strains could rescue ntl expression in epiboly-inhibited embryos. Uniaxial compression resulted in a partial but significant rescue of patterned ntl marginal expression, the re-establishment of the endogenous mechanical strains by drug washing of treated embryos, fully rescued ntl marginal expression, as shown by in situ hybridization (

Figure 50, Figure 51).

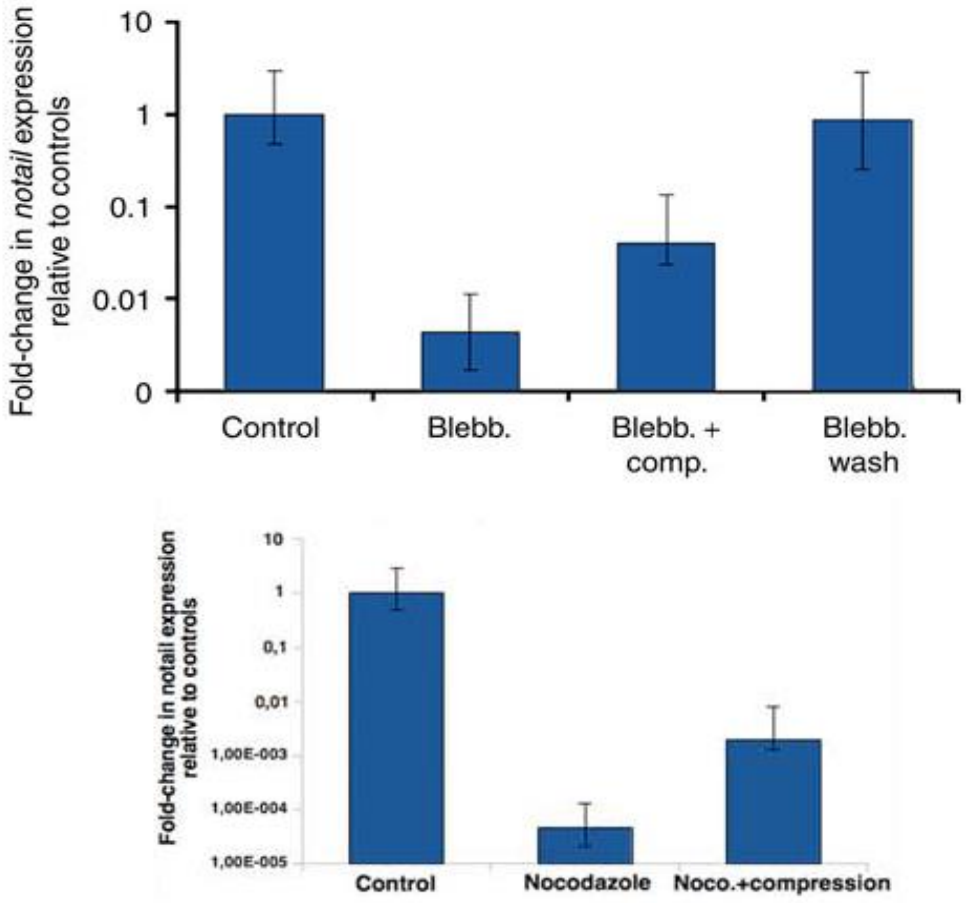

Figure 52: (Up) Quantitative reverse-transcription PCR quantification of ntl expression in controls, Blebbistatin-treated, Blebbistatin-treated compressed, Blebbistatin-treated and washed embryos (each reaction realized in technical triplicates). Differences between control and Blebbistatin-treated embryos, and between treated and rescued embryos, are statistically significant according to the Student's t-test (Po0.001). Error bars are s.d. All experiments were replicated two times. (Down) RT-qPCR quantification of ntl expression in controls, Nocodazole treated, Nocodazole treated compressed embryos (every reaction realized in technical triplicates). All experiments were replicated 2 times. The white bar is 20 microns and the black bar is 100 microns.

In order to have quantitative analysis to complete these results we measured the expression of *ntl* by realizing quantitative reverse-transcription PCR (Figure 52). We found that level of expression were at least 10 times bigger in the case of drugged compressed compare to the drugged one. This expression is still below the expression of the control. To improve our results we tried to replace the global compression by a magnetic deformation with Utra Magnetic Liposomes to get closer to physiological movements.

5- Mechanical induction of β-cat dependent *ntl* expression by magnetic forces quantitatively mimicking the onset of epiboly dynamics

In order to improve the previous results, we took advantage of the lab skill in using magnetization of living embryos, to quantitatively mimic endogenous morphogenic movements (Desprat et al 2008). Here I developed a new method of deformation specifically mimicking epiboly. This method consists in injecting Blebbistatin-treated zebrafish embryos with ultramagnetic liposomes (UMLs) and exposing them to a permanent magnet ring positioned 400 µm below the margin cells (Figure 53, Figure 54).

This magnetization method is based on two innovative microscopic elements. The first one consists in a external magnet ring 15µm thick of 800µm diameter and the second one consists in 200nm ultramagnetic liposomes.

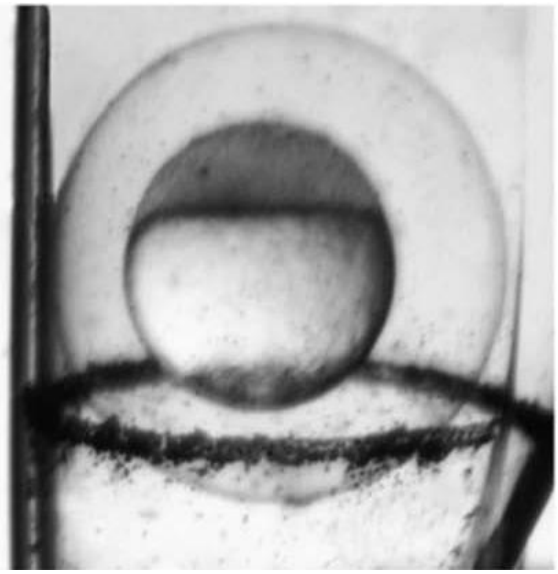

Figure 53: zebrafish embryo submitted to the magnetic field

Ultramagnetic ring: This ring has been created by our collaborating team at institute Néel in Grenoble. Especially by Frédéric Dumas-Bouchiat, Damien Le-Roy in Dominique Givord and Nora Dempsey team. The ring is radially magnetized of average cross section 800 µm, and was prepared using the micro-Magnetic Imprinting technique (117 Dempsey 2007). NdFeB particles of average size 15 µm and are trapped along the pre-magnetized stripe and then covered by pdms. This pdms is then circled with a plastic ring in small enough to prevent the chorioned embryo to cross the magnetized section (Figure 53). This ring was not able to rescue movement and initiate beta-catenin translocation in non UML injected embryo (N=6)(not shown).

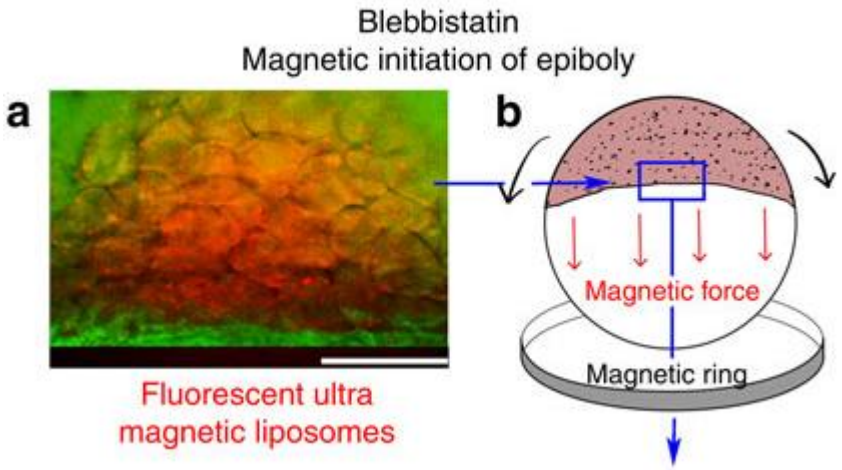

Figure 54: a) Embryos injected with UML (in red, green counter colour in transmission, surface lateral view). (b) Magnetic force applied to magnetically loaded margin cells by the ring micro-magnet.

Tissue magnetization : To be able to magnetize all the tissue of the embryo we had to inject the micro magnets at the one cell developmental stage and led the magnet spread inside the cell (Figure 54). The first particles we tested were magnet beads of 1µm diameter and 5 nm ferro-nano particles. The first one didn't diffuse enough in the embryo and the second one was toxic at concentrations required for force development. We thus decided, to work with Ultra Magnetic Liposomes (118)(Collaboration with Christine Ménager at UPMC) which were not toxic at concentration required for force development. 10 nano-litre of this UML was injected in the one stage cell embryos. These developed normally until we blocked the movement with Bebbistatin. Note that the injection in itself was not enough to induce β-cat translocation (Figure 55, Figure 56).

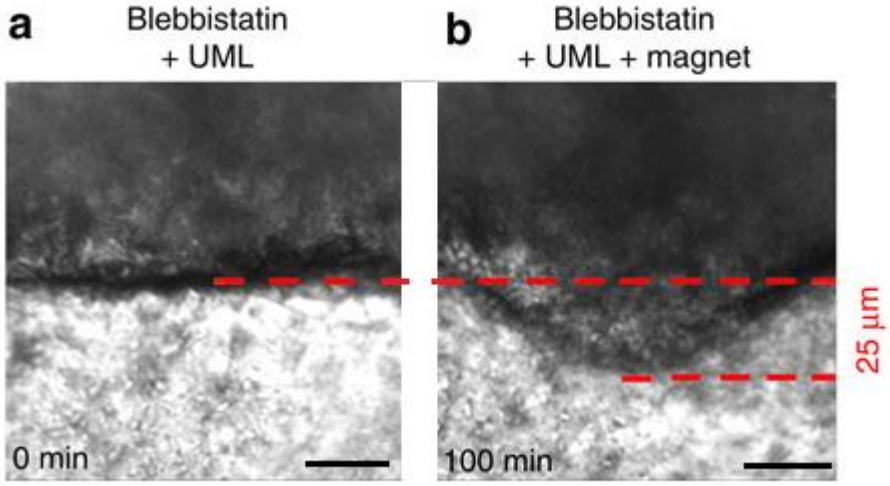

Figure 55: (a) Margin tissue in Blebbistatin-treated UML-injected embryos at time zero of magnetic field application, (b) and after 100 min of application. In the two later cases, the loss of resolution due to the ring micro-magnet setup impaired PIV analysis. Note also that all experiment were realized with an UV filter in a dark room, preventing Blebbistatin degradation.

Using this method, we rescued front epiboly movements in local margin cell domains, with a mean value of 0.25±0.06 mm/min (n=4). This is comparable with the value of 0.22±0.04 mm/min (n=5), which is characteristic of the onset of the first hour of the endogenous margin cell front movement at dome stage (Figure 55).

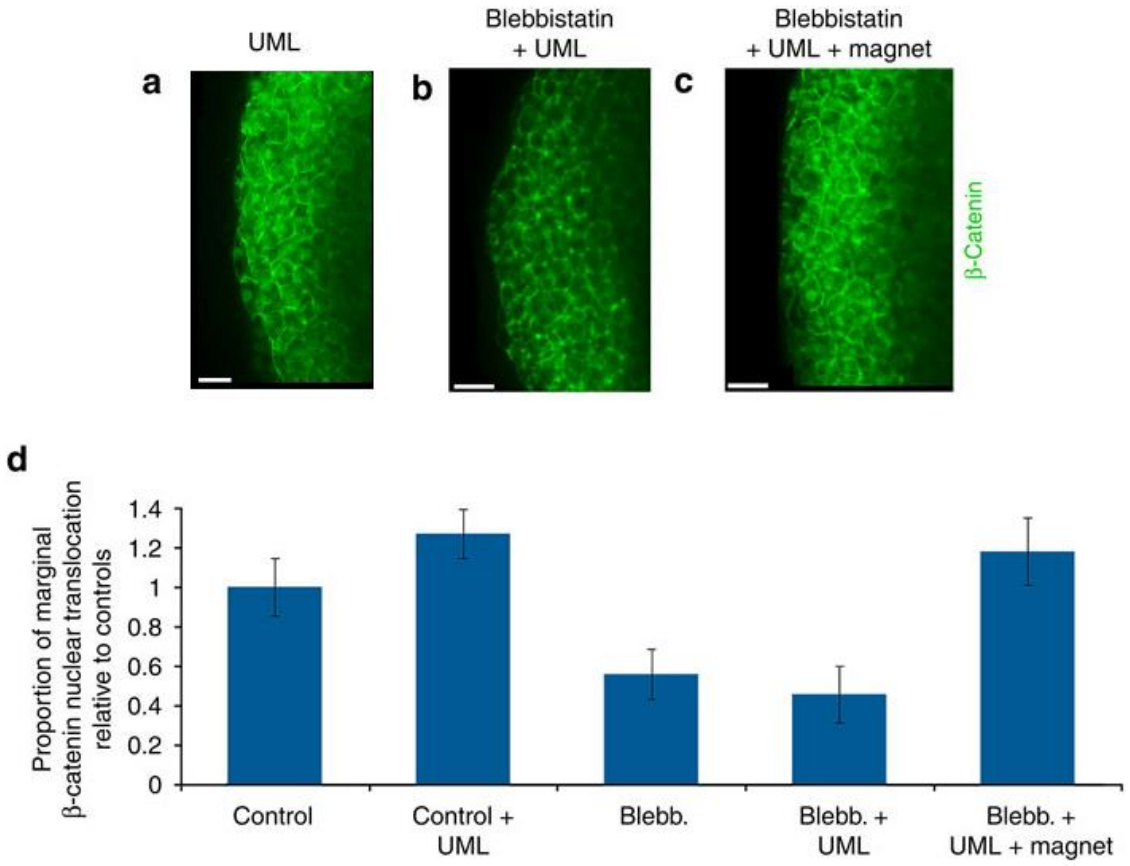

Figure 56: (a) Labelling of β-cat UML-injected embryos in the absence of ring micromagnet. (b) Labelling of β-cat in Blebbistatin-treated UML-injected embryos in the absence of ring micromagnet. (c) Labelling of β-cat in Blebbistatin-treated UML-injected embryos after exposure to the ring micromagnet. Quantification of nuclear translocation of β-cat in controls (n=5), UML-injected controls (n=5), Blebbistatin-treated embryos (n=35), Blebbistatin UML-injected embryos (n=4) and Blebbistatin UML-injected embryos submitted to the ring micromagnet (n=17). All data are characterized by P<0.001 using Mann–Whitney's exact test. Error bars are s.d. All experiments were replicated at least two times. Scale bars, 20 μm.

We observed that UML injection in itself was not perturbing the expression of β-catenin. We completely rescue the nuclear translocation around the deformed marginal zone after the rescue of margin epibolic movements in margin cells (Figure 56 C-D).

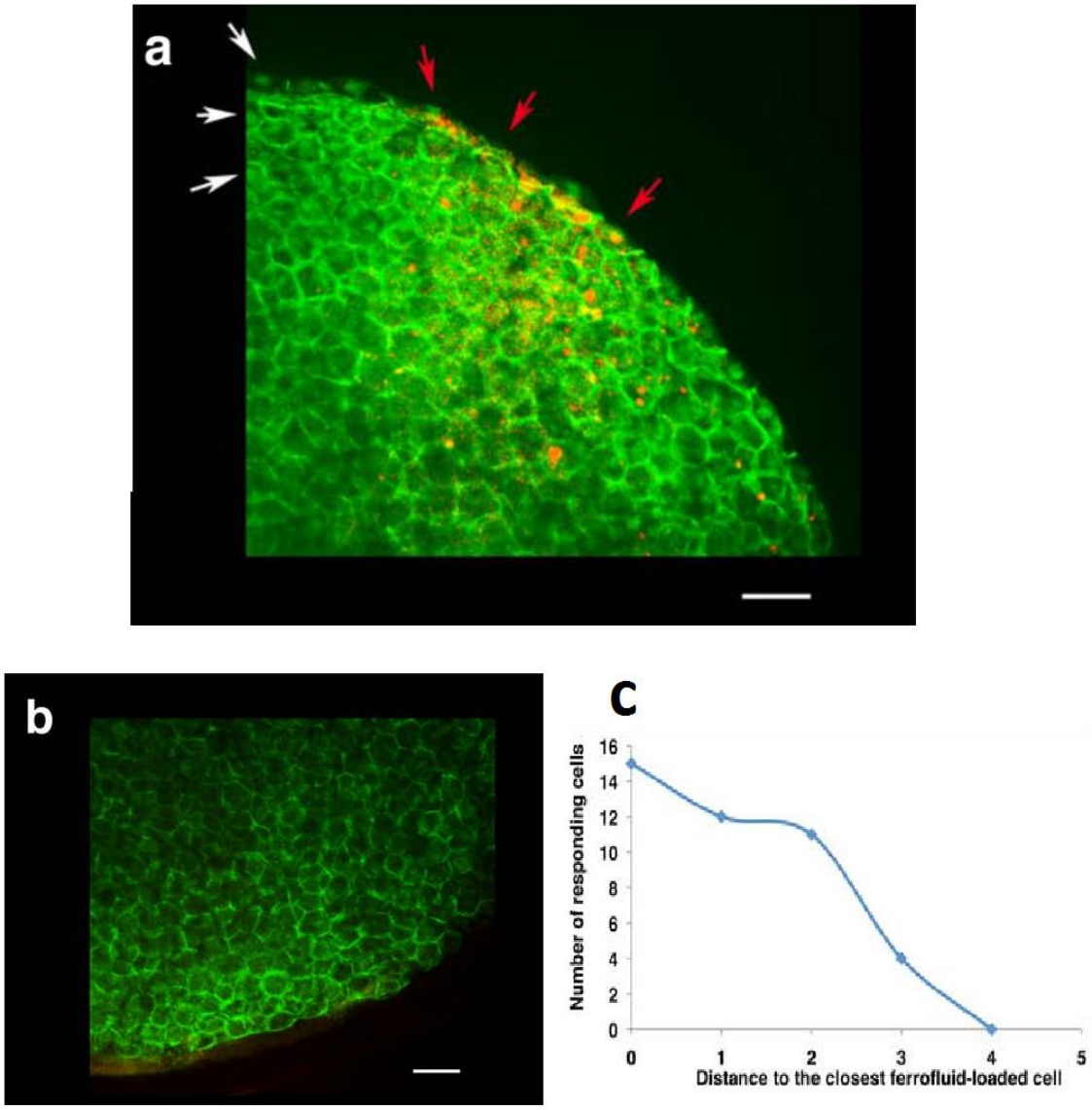

Figure 57: (a) Few-cell-deep vegetal view in the magnetically loaded domain. Note β-catenin nuclear translocation in magnetically loaded cells (red arrows), but also nonmagnetically loaded cells (white arrows) as far away as 3 cells distant from the loaded cells. (b) No β- catenin nuclear translocation is observed more far away from the magnetically loaded domain. (c) Quantification of the action range of non-cell-autonomous mechanical cues. The white bars are 20 microns. Representative of n=6 embryos on the N=6 embryos injected.

Interestingly we found that the magnetic loading of a quarter of the embryo by injection at a four-cell stage led to the nuclear translocation of β-cat in magnetically loaded cells, and at a short distance from magnetically loaded cells. Some individual margin cells that were not loaded with magnetic liposomes effectively also showed β-cat nuclear translocation (Figure 57). These cells can be as distant as three cells away from magnetically loaded cells, indicating that mechanical cues lead to non-cell-autonomous nuclear translocation of β-cat (Figure 57).

Together, these results demonstrate that nuclear translocation of β-cat is highly sensitive to non-cell-autonomous mechanical activation in margin cells, which are specifically deformed by the morphogenetic movement of epiboly initiation.

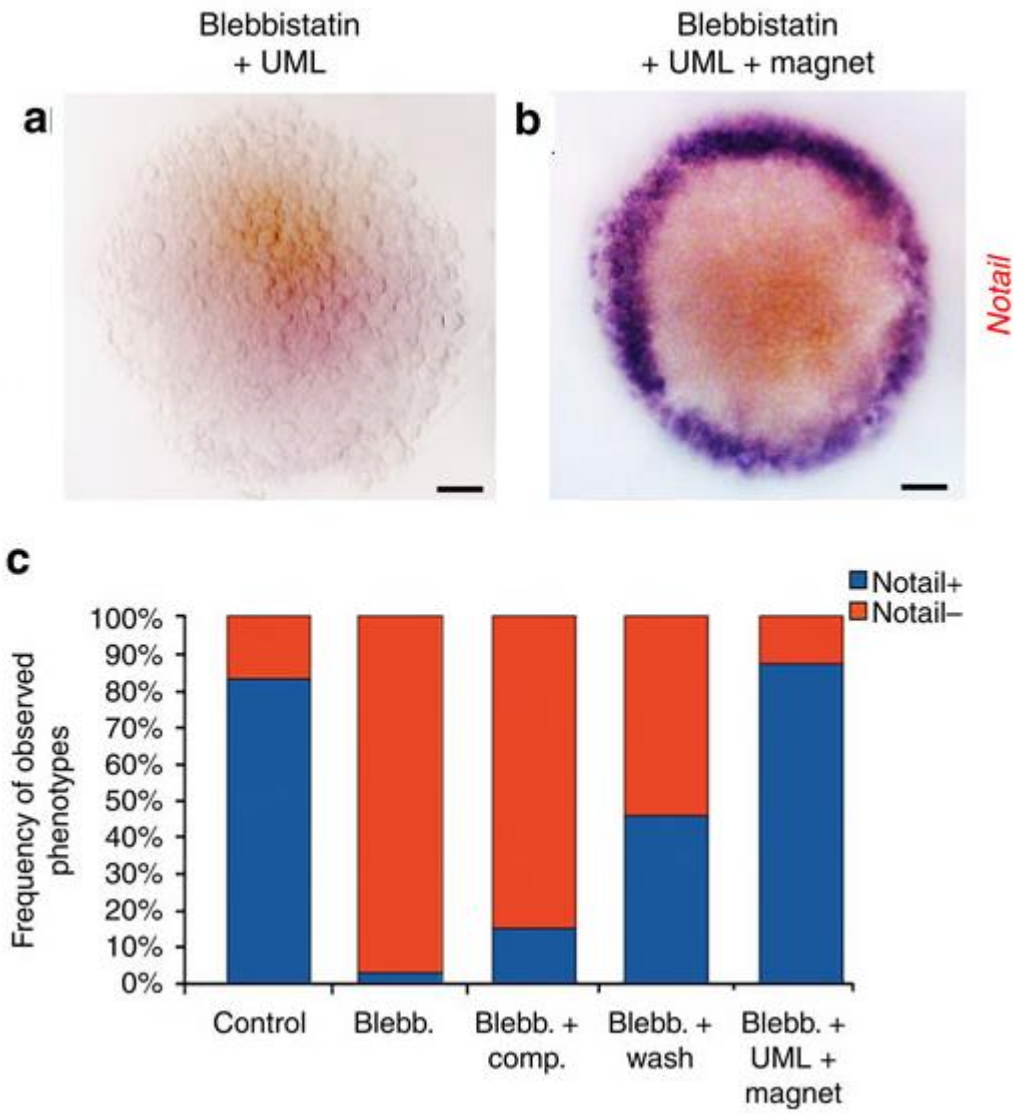

Figure 58: (a) ntl *Labelling in Blebbistatin-treated UML-injected embryos in the absence of ring micromagnet (representative of n =12 embryos on n =15 injected embryos). (b)* ntl *Labelling after the ring micromagnet applied forces to UML-injected embryos. (c) Quantification of the number of embryos showing in situ* ntl *expression in controls (n =97), Blebbistatin-treated (n =95), Blebbistatin-treated compressed (n =73), Blebbistatin-treated and washed (n =24), and Blebbistatin-treated embryos with epiboly rescue by magnetic forces (n =8). Differences between control and Blebbistatin-treated embryos, and between treated and rescued embryos, are statistically significant according to the w_2-test ($P<0.001$).*

As for β-cat, the re-establishment of the endogenous mechanical strains by magnetic rescue of epiboly of treated embryos, fully rescued *ntl* marginal expression. Interestingly we observe that using such physiological deformation the results on both β-catand *ntl* were very close to the untreated normal embryos (Figure

56,Figure 58). Thus, the onset of epiboly movements induces a specific dilation of marginal cells and provides mechanical signals that trigger β-cat nuclear translocation to initiate *ntl* expression in the presumptive mesoderm of zebrafish embryos.

6- Mechanical induction of β-cat molecular translocation and of *ntl* expression by Y667 β-cat phosphorylation

In the *Drosophila* embryo anterior mid-gut, as well as in mice colon cancer lines, the mechanically induced nuclear translocation of β-cat permissively requires Src family kinases that phosphorylates the tyrosine present in one of the sites of interaction between β-cat and E-cadherin, and represses their interaction (Desprat 2008, Whitehead 2008). In mice, the phosphorylation of the β-cat Y654 site by Src family kinases impairs the interaction of β-cat with E-cadherin, leading to the release of β-cat into the cytoplasm and into the nucleus in the case of defective Adenomatous polyposis coli (APC) degradation (Whitehead 2008). We thus decided to search of for any change of the phosphorylation status of the y667-β-cat in response to mechanical deformation.

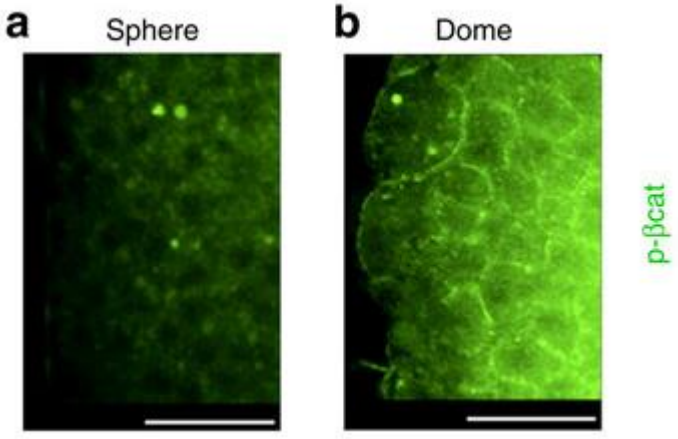

Figure 59: (a) Phospho-β-cat labelling in zebrafish marginal cells before epiboly (sphere stage). (b) Phospho-β-cat labelling at the start of epiboly (dome stage).

A statistically significant 20% increase in the conserved phospho-Y654 β-cat concentration can be detected by immunofluorescence at the marginal zone during the first 5 min of epiboly, predomina*ntl*y near junctions (Figure 59).

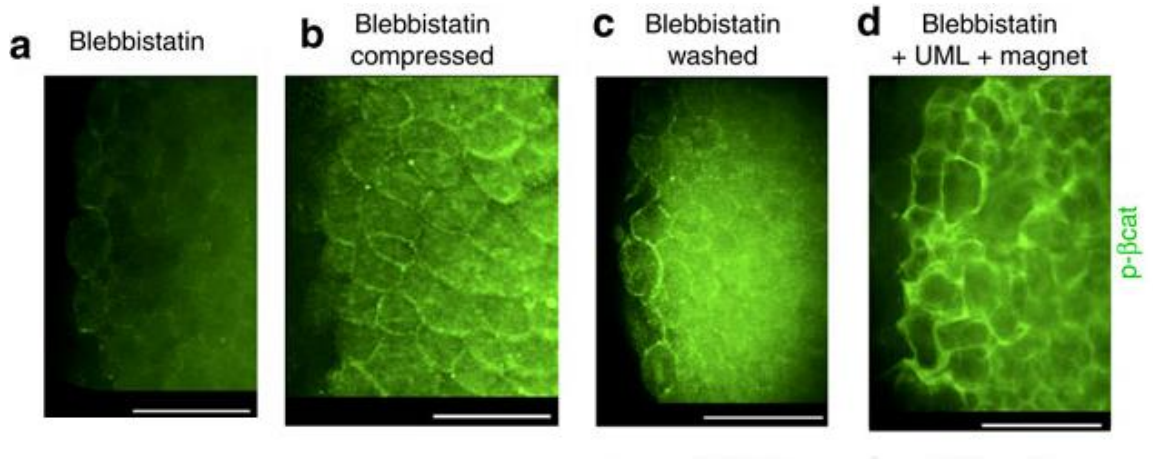

Figure 60: (a) Phospho-β-cat labelling after Blebbistatin treatment that suppressed movements. (b) Phospho-β-cat labelling after Blebbistatin treatment with epiboly movements rescued by global compression. (c) Phospho-β-cat labelling after Blebbistatin treatment with epiboly movements rescued by drug washing. (d) Phospho-bcat labelling after Blebbistatin treatment rescued by magnetic manipulation of UML-injected embryos leading to epiboly movement resumption.

Such phosphorylation is suppressed by blocking epiboly and subsequently rescued by compression, washing and magnetic manipulation (Figure 60).

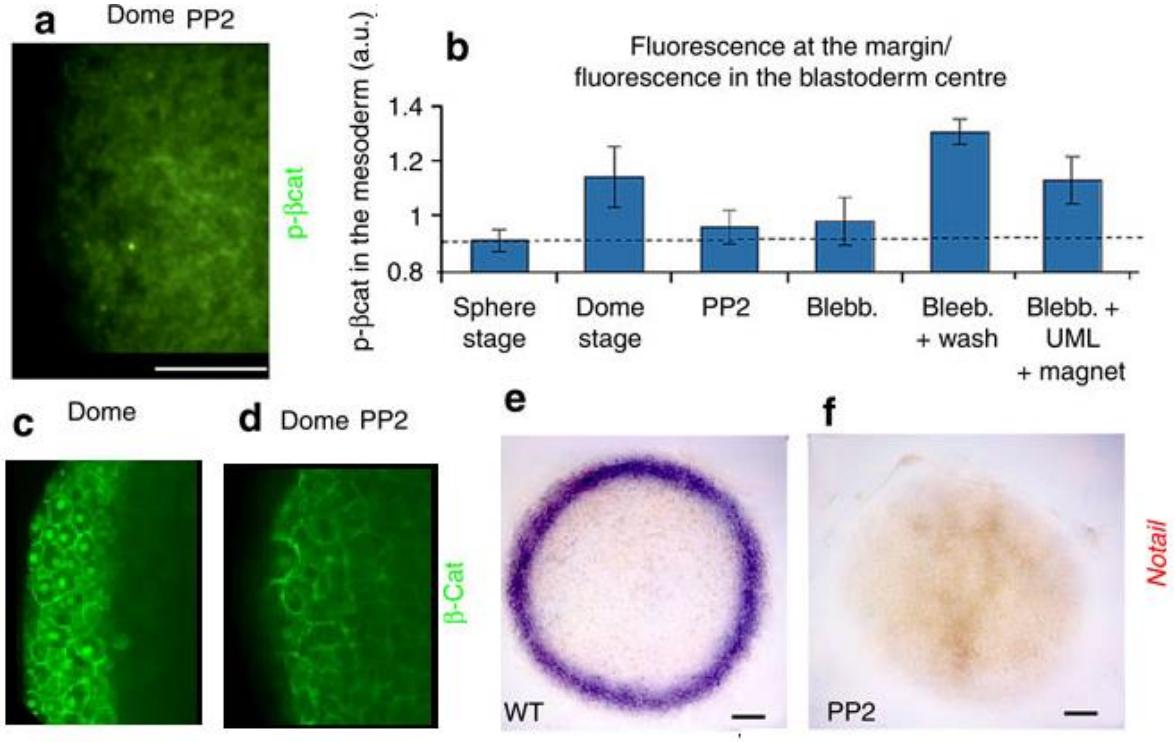

Figure 61: (a) Phospho-β-cat labelling in the presence of PP2 Src-family inhibitor treatment at(b) Levels of pY667 β-cat in the margin relative to the blastoderm centre and in the margin relative to the background in sphere stage (n =6), dome stage (n =9), PP2 treated (n =7), Blebbistatin-treated (n =22), Blebbistatin-treated and washed (n =7), and Blebbistatin-treated UML-injected magnetically rescued embryos (n =9). Differences between control dome, Blebbistatin-washed or Blebbistatin-compressed embryos and all other conditions are sta-

tistically significant (P<0.05 according to Mann–Whitney's exact test. Error bars are s.d. All experiments were replicated two times. (c) Marginal nuclear translocation of β-cat in dome stage zebrafish (d) Marginal nuclear translocation of β-cat is abolished in dome stage zebrafish embryos treated with the Srcfamily kinase inhibitor PP2. (e) ntl expression at 30% epiboly. (f) ntl expression at 30% epiboly upon PP2 treatment in Blebbistatin-treated embryos.

Note that the phospho-Y654 β-cat is more concentrated in the cortex, suggesting a process of rapid dephosphorylation after release from the membrane (Figure 61). In addition, β-cat phosphorylation, nuclear translocation and *ntl* expression at 30% epiboly are abolished by PP2 Src family kinase inhibitor treatment at the onset of epiboly (Figure 61).

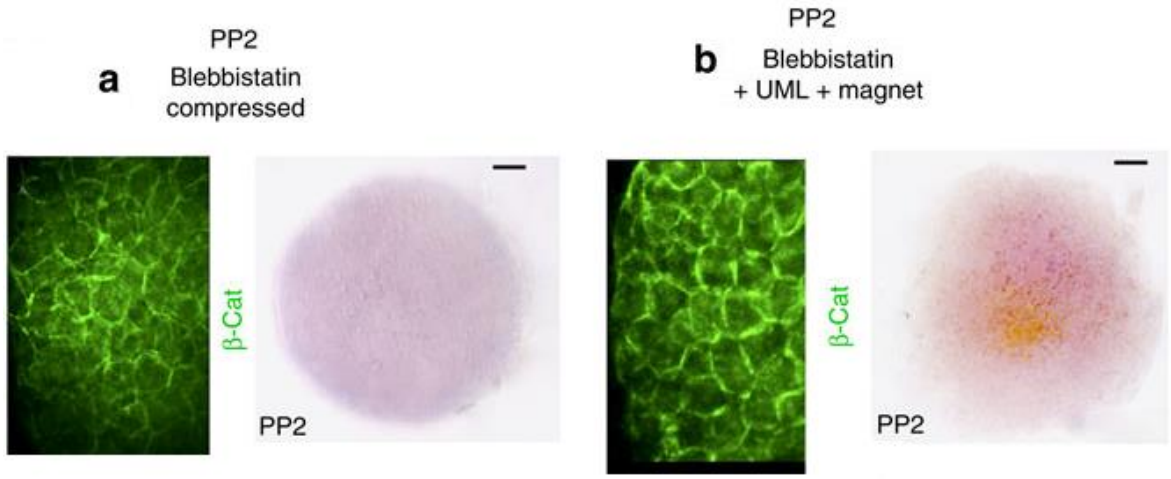

Figure 62: (a) β-cat labelling in Blebbistatin globally compressed embryos treated with PP2. ntl expression at 30% epiboly upon PP2 treatment in Blebbistatin-treated embryos with margin cell epiboly deformation rescued by global compression. (b) β-cat labelling in Blebbistatin magnetically deformed UML-injected embryos treated with PP2. Associated quantitative results in Supplementary Fig. S15b. ntl expression at 30% epiboly upon PP2 treatment in Blebbistatin-treated embryos with margin cell epiboly deformation rescued by magnetic forces.

Neither could be re-established in Blebbistatin-treated embryos rescued with global compression or magnetic forces in the presence of PP2, (Figure 62) showing the requirement of Y654 β-cat phosphorylation for β-cat-dependent *ntl* mechanical induction.

Therefore, Y667- β-cat phosphorylation, leading to nuclear trabslocation of β-cat and activation of ntl target endo-mesodermal gene transcription, are mechanically induced by the mechanical strains developed at magin cells by the onset of epiboly.

7- Pathways synergising with Y667-β-cat mechanically induced phosphorylation

a- Bmp and Nodal

Here we proved that *ntl* expression was not dependent of Wnt before 50% of epiboly but was induced by Y667 β-cat phosphorylation. However, such mechanical induction of *ntl* in early mesoderm specification might naturally require additional biochemical signalling, such as Nodal, which is known to be expressed all around the embryo in margin cells at the onset of epiboly (119 Rebagliati 1998, 120 Feldman 1998) and to be involved in mesodermal *ntl* expression at the 90% epiboly stage (9hpf) (121 Hagos 2007).

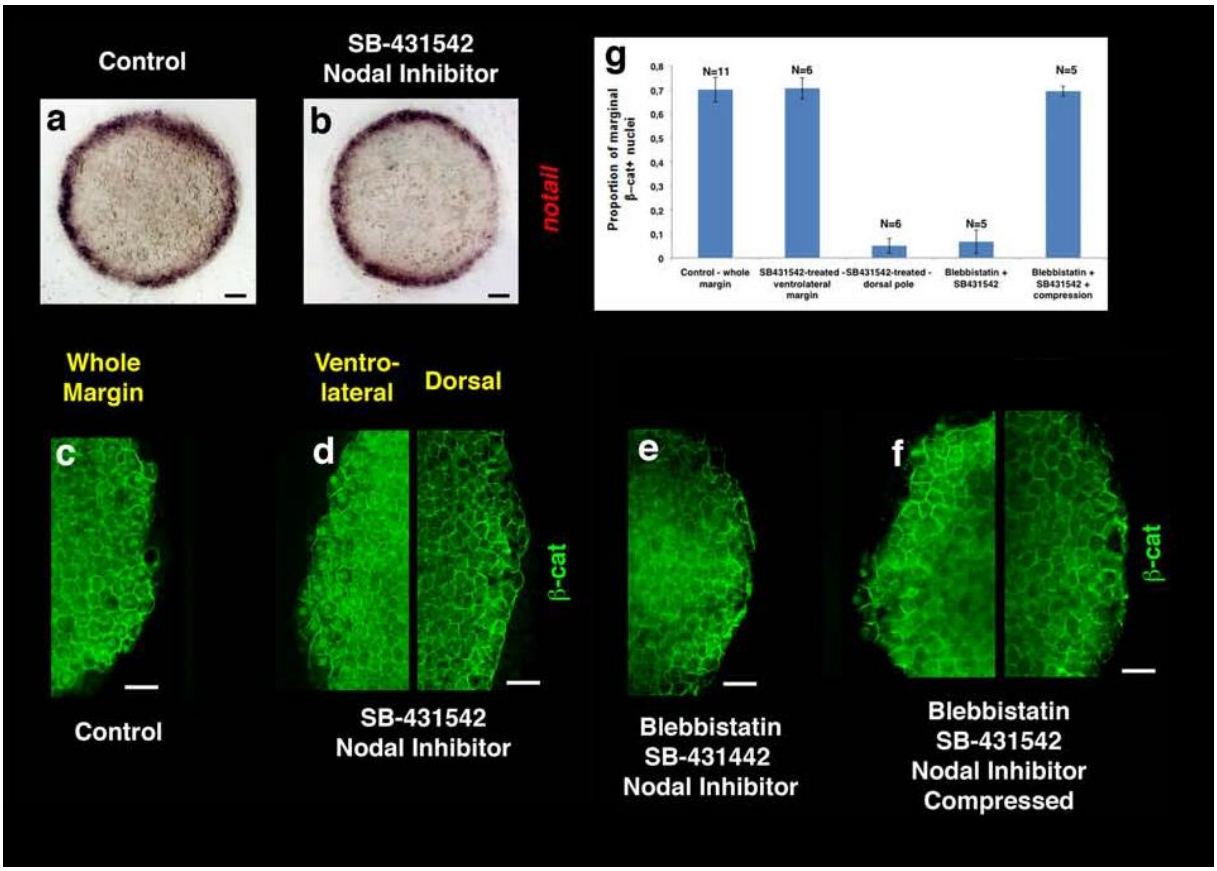

Figure 63: Nodal activity is required for nuclear β-cat translocation and notail expression at the dorsal pole, but dispensable in the rest of the marginal zone (a) notail in situ hybridization signal at dome stage in a control embryo (b) and a sibling treated with the Nodal inhibitor SB-451342. (c) β-cat immunostaining signal at dome stage, control. (d) SB45-treated sibling, showing loss of nuclear β-cat translocation at the dorsal pole, and maintenance of nuclear β-cat around the ventrolateral margin. (e) SB45- blebbistatin double-treated embryo, showing loss of nuclear β-cat all around the margin. Note the relatively noisy effect of double treatment with SB-45 and blebbistatin on labelling. (f) Compressed SB45- blebbistatin double-treated sibling, showing rescue of

nuclear β-cat around the ventrolateral margin, but not at the dorsal pole. Note that embryos did not resist in situ labelling in addition to blebbistatin, SB-45 and compression treatment, preventing the observation of ntl expression within these conditions. (g) Quantification of the results. Note that the β-cat positive nuclei in compressed SB45-blebbistatin double embryos have been quantified around the ventrolateral margin, excluding the dorsal pole. $p<10^{-6}$ by Student's t-test for the comparison between the dorsal pole of treated individuals and their ventrolateral margin; for the comparison between the dorsal pole of treated individuals and the margin of control siblings; for the comparison between the ventrolateral margin of compressed doubletreated embryos and the margin of uncompressed double-treated siblings. Error bars are standard deviation. Black bars are 100 microns and white bars are 20 microns.

However, except for the dorsal-most margin, we found no inhibition of *ntl* expression after inhibition of Nodal signalling in the complete mesoderm by treatment with the Nodal receptor inhibitor SB-431542 (Figure 63 a,b,g) and, consistently, no inhibition of β-cat nuclear translocation at the onset of epiboly in most of the margin cells (Figure 63 c,d,g). In addition, except at the dorsal pole, the rescue of the β-cat nuclear translocation was still observed in embryos treated with blebbistatin and deformed by uniaxial global compression, in the presence of the Nodal receptor inhibitor SB-431542 (Figure 63 e–g). This indicates the requirement of the biochemical factor Nodal for the mechanical induction of β-cat nuclear translocation and *ntl* at the dorsal pole only, but no requirement of Nodal for mechanotransductive β-cat -dependent early-mesoderm *ntl* expression in the majority of margin cells in the ventro-lateral domain.

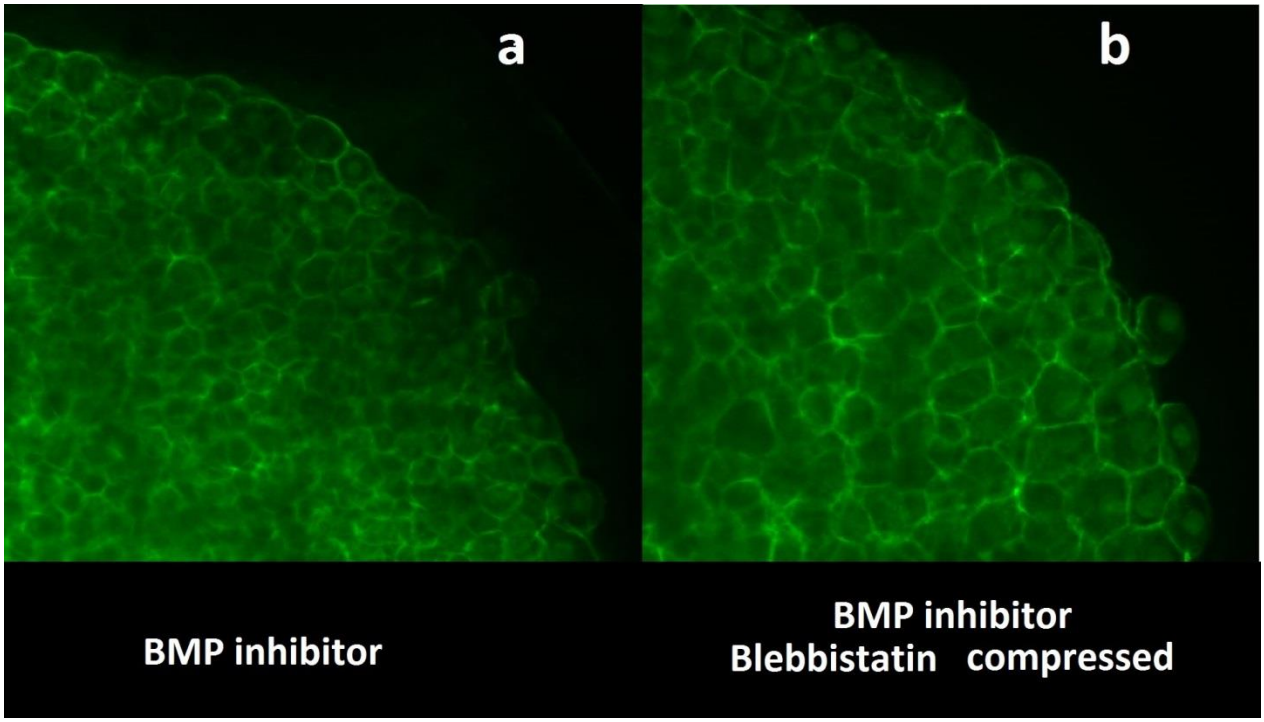

Figure 64: (a) BMP inhibitor treated embryo showing loss of nuclear β-cat all around the margin exept for the most external line of cells. This expression is the same in (b) Double treated Blebbistatin and BMP inhibitor compressed embryo.

The BMP signalling protein is also known to be required for mesoderm differentiation in the ventral part of the zebrafish embryo (Agathon et al 2003). Here we find that the biochemical factor BMP is indeed also required for the mechanical induction of β-cat nuclear translocation in the ventral part of the embryo (122 Thisse 1999). Inhibition of BMP inhibits the nuclear expression of β-cat in the mesoderm, but not in the most YSL external cell (Figure 64 a).

The same result is obtained in embryos treated with Blebbistatin and the BMP inhibitor, compressed by exogenous uni-axial compression (Figure 64B). In contrast these non-compressed embryos show no nuclear translocation of β-cat in margin cell, like in Blebbistatin embryos (not shown).

Therefore, both Nodal and BMP are required in different mesoderm domains, with the mechanical induction of the phosphorylation of Y667 β-cat by the morphogenetic movements of the onset of epiboly, for the nuclear translocation of β-cat leading the *ntl* expression inducing earliest mesoderm differentiation in 30% epiboly zebrafish embryos. We thus propose that Nodal and BMP pre-pattern a mechanical induced nuclear translocation of β-cat leading to mesoderm induction in margin cell only.

b- Mapk and phospho-GSK3β

The phosphorylation of the Y654 β-cat site is known to be sufficient to trigger nuclear translocation (123 Van Veelen, W. et al. 2011). Moreover, we demonstrated that mechanically induced MAPK activation, leading to specific inhibition of GSK3 by dephosphorylation of the Y279-GSK3a/Y216-GSK3b (Figure 65,Figure 66) site in margin cells, combines with the 20% increase in Y654 phosphorylation in zebrafish to allow nuclear translocation of the junctionally released β -cat. Notail expression is repressed by the inhibition of Mapk activity (Figure 67).

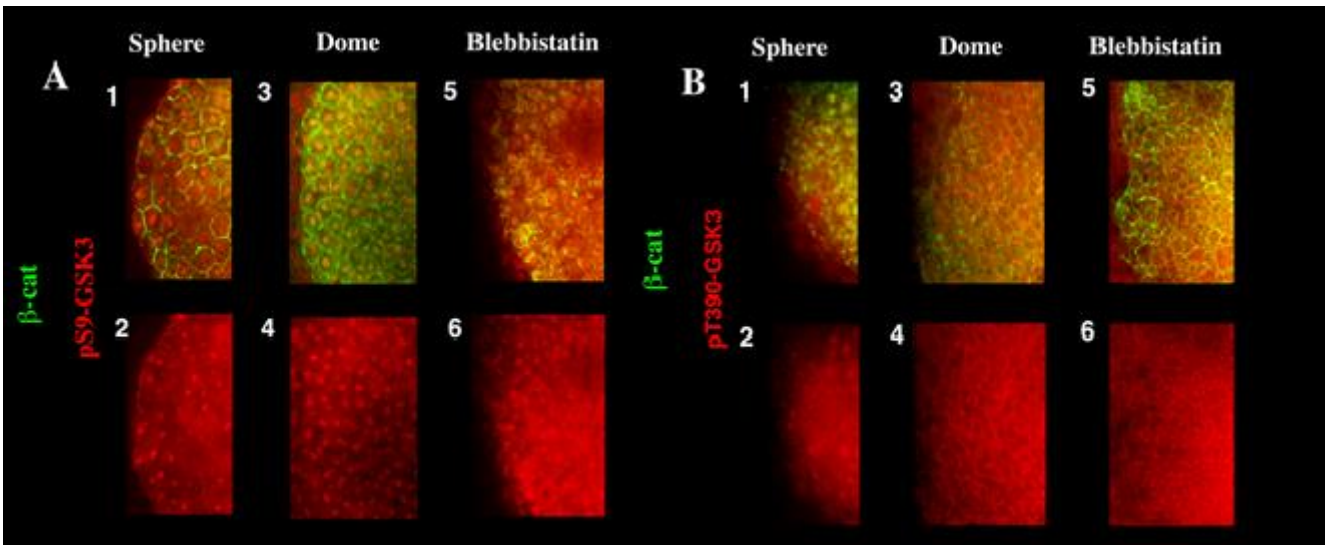

Figure 65: Mesoderm induction is not correlated to GSK3 inactivation by serine phosphorylation or threonine phosphorylation in zebrafish : (A) No specific increase of GSK3β inhibition by Serine 9 phosphorylation is detectable during mesoderm specification in zebrafish. (1,2) The sphere stage zebrafish blastula is characterized by an ubuquitous level of pS9-GSK3β located predominantly in the nuclei (all detectable nuclei positive with DAPI as a counterstain, N=20). (3,4) The distribution of pS9-GSK3β detected at dome stage is identical to sphere stage without any detectable increase in the mesoderm (all detectable nuclei positive, N=25). (5,6) Persistence of pS9-GSK3β after blebbistatin treatment indicates serine 9 phosphorylation is movement-independent (all detectable nuclei positive, N=7). (B) No specific increase of GSK3β inhibition by Threonine 390 phosphorylation is detectable during mesoderm specification in zebrafish. (1,2) The sphere stage zebrafish blastula is characterized by an ubiquitous level of pT390-GSK3β (I=1.52±0.05 normalized by extracellular background, N=5). (3,4) The distribution of pT390-GSK3β detected at dome stage is identical to sphere stage without any detectable increase in the

mesoderm (I=1.62±0.10 normalized by extracellular background, N=8). (5,6) Persistence of pT390-GSK3β after blebbistatin treatment indicates Threonine 390 phosphorylation is movement-independent (I=1.76±0.14 normalized by extracellular background, N=5).

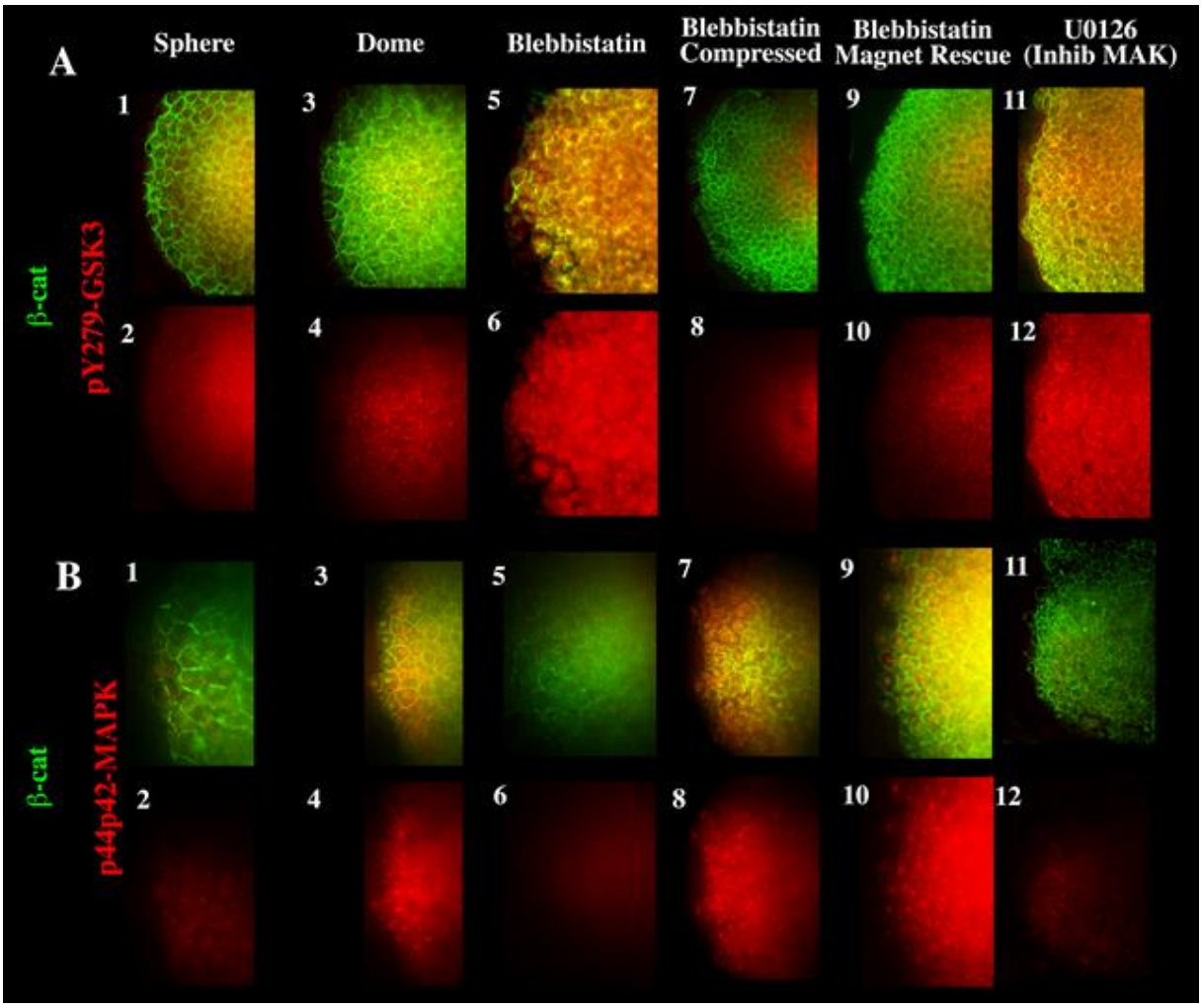

Figure 66: Mechanically induced Erk1/2 MAP kinases inactive GSK3 by promoting its tyrosine 279 dephosphorylation in the margin cells at gastrulation: (A) Mechanical signals induce GSK3 inactivation by tyrosine 279 dephosphorylation in the margin cells. (1,2) Tyrosine 279 dephosphorylation of GSK3 in margin cells is apparent already at sphere stage and (3,4) maintained at dome stage. (5,6) Tyrosine 279 dephosphorylation of GSK3 in margin cells at dome stage is inhibited when epiboly is blocked by blebbistatin treatment (7,8) and rescued by compression and (9,10) magnetic deformation. (11,12) It requires Erk1/2-MAPK activity as indicated by the sharp increase of GSK3 tyrosine 279 phosphorylation in the margin cells, up to the same intensity as in the centre of the blastoderm, after U0126 treatment. (B) (1,2) Erk1/2-MAPK (p44p42-MAPK) activity is stimulated by mechanical signals at the margin at dome stage. No MAPK activity is detectable at sphere stage. (3,4) A strong increase restricted to the margin signal appears at dome stage, (5,6) is strongly reduced after epiboly blocking by blebbistatin treatment (7,8) and rescued by exogenous compression and magnetic deformation (9,10). (11,12) U0126 treatment leads to an important down-regulation of Erk1/2-MAPK marginal activity

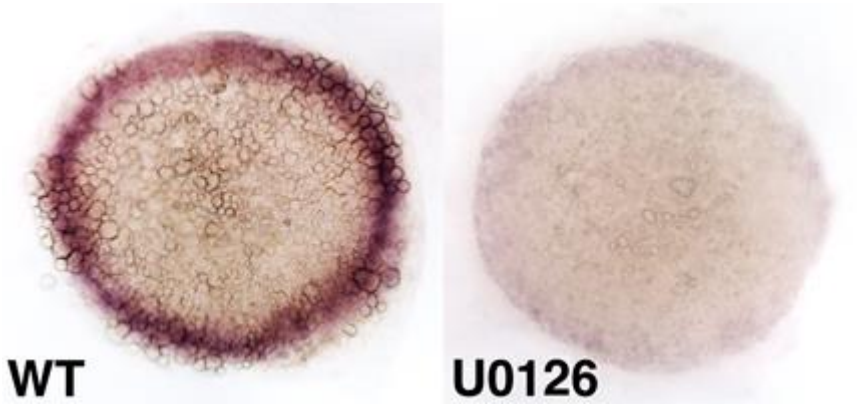

Figure 67: ntl expression at 30% epiboly (WT: representative of 94% of n=15, U0126: representative of 85% of n=20).

We propose that a second mechanotransductive process, that MAPK dependent mechanical induction of the phosphorylation of the Y279-GSK3β leading to Gsk3-β inactivation, synergize with the mechanical induction of phosphorylation of the Y667- βcat mechanotransductively released from the junctions, thereby allowing its translocation into the nuclei.

8- Comparison with *Drosophila* and evolutionary consequences

a- Mechanical induction of Twist expression by Armadillo/ β-cat nuclear translocation

Mechano-induced β-cat/Armadillo (Arm) nuclear translocation is also known to act in the *Drosophila* anterior mid-gut to induce the expression of the mesendodermal gene *twi*st (*twi*) in response to compression by germ band extension at Gastrulation (Desprat 2008 , Farge 2003). In the prospect of making a close comparison with zebrafish, we proceeded to test β-cat/Arm-dependent *twi* mechanosensitivity in the mesoderm of *Drosophila*. The *twi* expression is initiated by the maternal transcription factor Dorsal, but in *sna*il (*sna*)-null mutants, which lack mesoderm invagination, *twi* expression vanishes prematurely at stage 8, 45 min to 1 h after WT invagination (124 Leptin 1991) (Figure 68). This had led to speculation that the mechanical cues associated with mesoderm invagination could act to maintain a high level of *twi* expression in the mesoderm (125 Brouzès 2004).

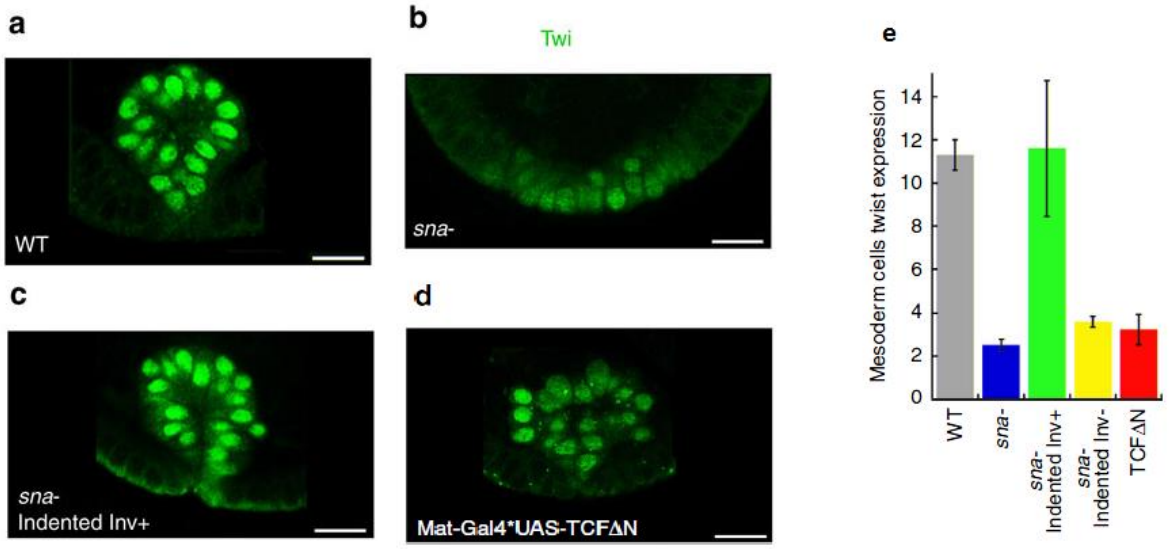

Figure 68: (a) Twi expression in the mesoderm of Drosophila embryos at stage 8 after WT invagination (n=6). (b) Twist expression in non-invaginating sna⁻/⁻ mutants (n=7). (c) Twist expression after invagination rescue through indentation of sna⁻/⁻ mutants (n=6). Twi expression in the mesoderm of TcfDN embryos at stage 8 (n=6). (e) Quantification of Twi expression in the mesoderm of WTembryos (n=6), sna⁻ embryos (n=7), sna⁻ indented embryos with rescue of mesoderm invagination (n=6), sna⁻ indented embryos without rescue of mesoderm invagination (n=6), TcfΔN embryos (n=6), Src42A-RNAi embryos (n=12) and Arm667m embryos (n=10). Data are characterized by a Mann–Whitney's exact test $P<0.001$. Error bars are s.d.

To test the involvement of a mechanotransduction β-cat/Arm pathway leading to *twi* expression during mesoderm invagination, we rescued the mesoderm invagination in a *sna* mutant, taking advantage of the Myo-II mechanotransduction response of *sna* embryos to soft indentation (chapter I Figure 8 B-C). This is known to rescue, with 70% success, the apical accumulation of Myo-II, leading to mesoderm invagination lacking in *sna*, in a Fog dependent process. Indeed this led to the full rescue of *Twi* protein levels (Figure 68). Here the indent experiments were realized by Benjamin Driquez and Démothene Mitrosillis.

To test that β-cat/Arm is involved in the mesodermal Twi mechanical induction process; we quantified *Twi* expression in Tcf-ΔN overexpressing individuals. We found that Twist expression dramatically dropped in the mesoderm of transgenic individuals at stage 8, thereby demonstrating the transcriptional activity of Arm in mesodermal *Twist* expression at gastrulation (Figure 68 d,e).

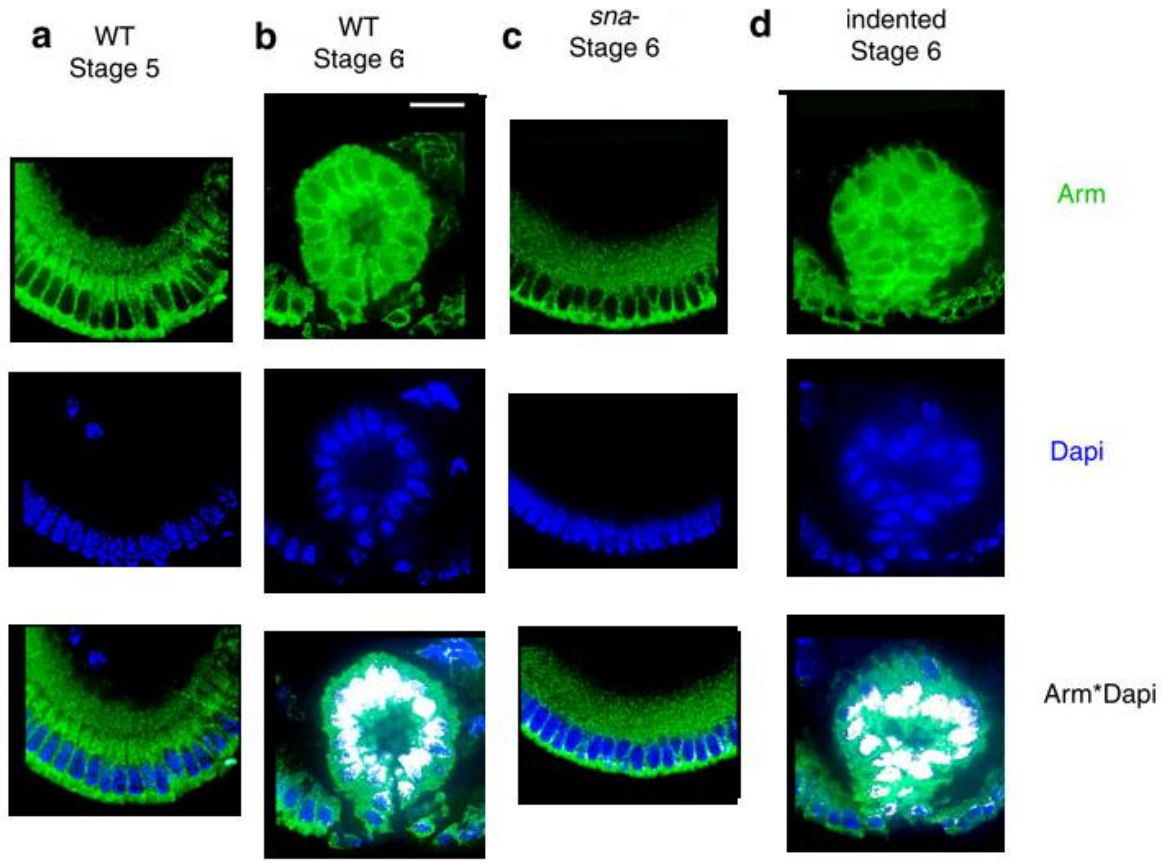

Figure 69: (a) Arm labelling at stage 5 before mesoderm invagination. (b) Arm labelling during mesoderm invagination at stage 6. (c) Arm labelling in stage-6 sna⁻/⁻ mutants. (d) Arm labelling in mesoderm-invaginated sna mutants after indentation.

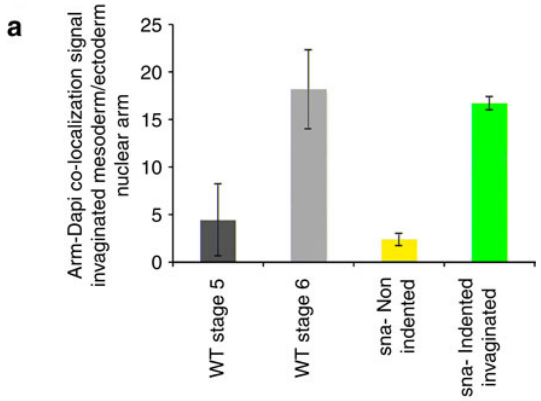

Figure 70: Quantification of Arm nuclear translocation (ratio of average mesodermal co-localization signal (density of white pixels) over ectodermal co-localization signal) in the mesoderm of WTat stage 5 (n=7), at stage 6

(n=6), in the sna⁻ at stage 6 (n=6), in the sna⁻ indented with rescue of invagination at stage 6 (n=6), Arbitrary units (a.u.). Data are characterized by a Mann–Whitney's exact test P<0.01 for all relevant comparison. Error bars are s.d. sna⁻/⁻ mutants were selected by phenotype a priori (no mesoderm constriction and invagination before the onset of germ band extension and a delay of 10 min in anterior gut invagination14), as well as a posteriori (profound lateral dorsal folds characteristic of sna mutants as described in (126 Leptin 1990) and by Snail labelling,. All embryos are at stage 8. Note that indented WT showed no inhibition of mesoderm invagination of Snail expression and of twist expression, additionnaly ensuring that embryos expressing no Snail are sna⁻.

Immunofluorescence staining confirmed that Arm is released from apical cellular membranes to the cytoplasm, with translocation observed in the nuclei upon invagination at gastrulation (Figure 69). In contrast to strong nuclear labelling in zebrafish, signalling Arm in early *Drosophila* embryos is known to be more diffusively found in the cytoplasm with some degree of localization in the nuclei (127 Peifer 1994), consistent with our observations. Arm nuclear translocation was further evidenced by Dapi/Arm colocalization analysis quantification. Arm membrane release from apical junctions to the cytoplasm and nuclei is lost in sna⁻/⁻ mutants and rescued in invaginating indented individuals, demonstrating mechanical induction of Arm release from the junctions to the cytoplasm and nuclei in response to mesoderm invagination strains (Figure 69, Figure 70).

b- Mechanical induction of Y667 β-cat phosphorylation

We then found that immunostainings for Y667 phospho-β-cat at stage 6 showed a strong localized signal in the mesoderm during invagination (Figure 71 a-b). To ensure the specificity of this antibody we worked with a mutant which unable the phosphorylation of Y667 β-cat and we observe the loss of the signal (Figure 71 c).

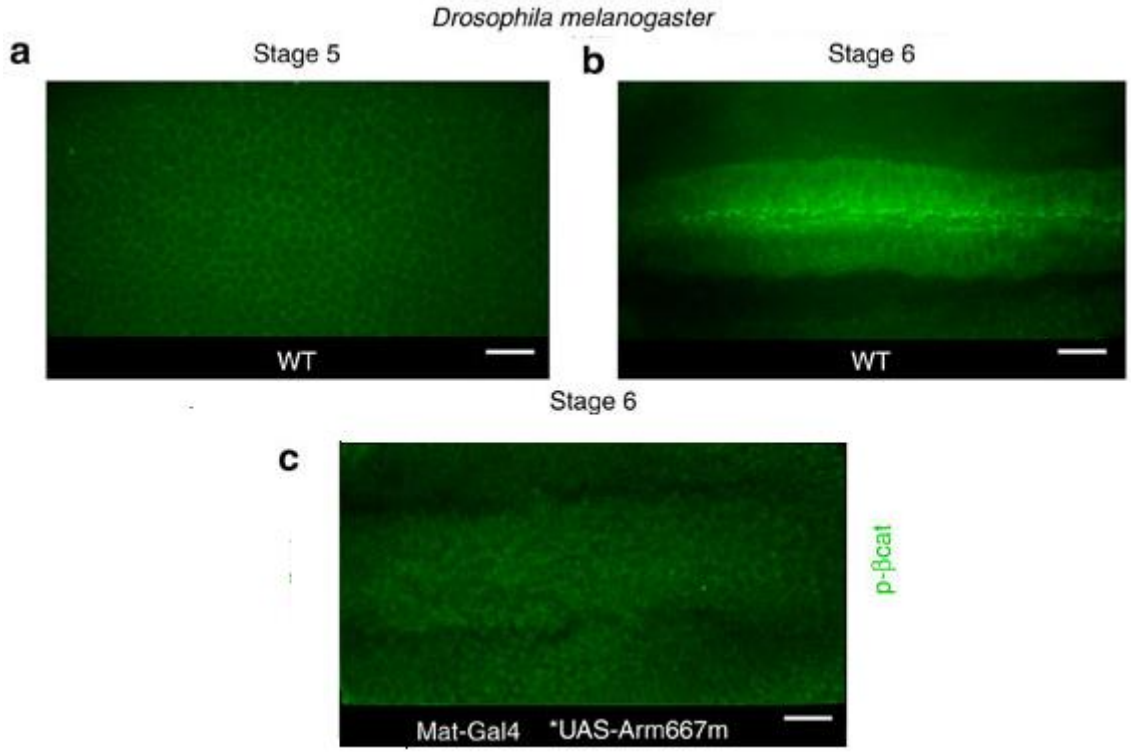

Figure 71: (a) Phospho-Y667-bcat labelling in stage-5 Drosophila embryos. (b) Phospho-ß-cat labelling in stage-6 invaginating embryos. (c) Phospho-ß-cat labelling in Src42A-RNAi invaginating embryos. (d) Phospho-ß-cat labelling in Arm667m stage-6 invaginating embryos. Scale bar, 10 mm (white bars).

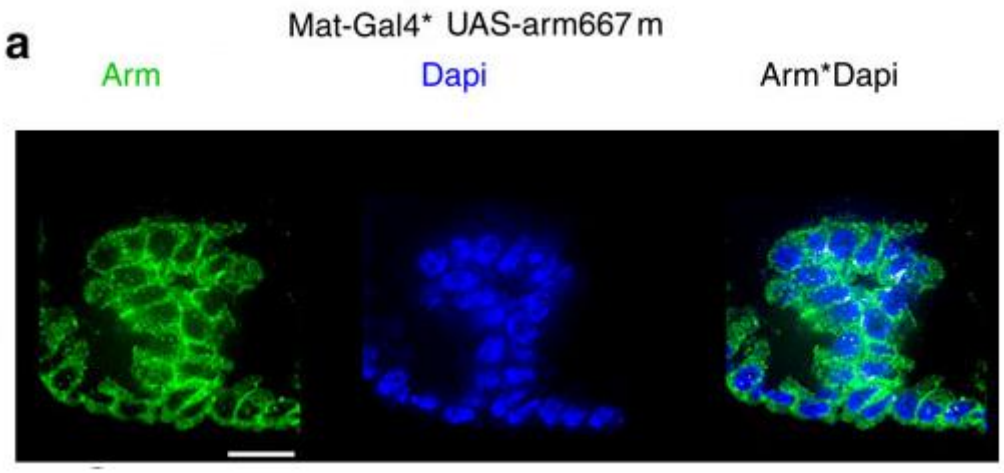

*Figure 72: Arm labelling in Mat-Gal4*Arm667m Y667 unphosphorylable Arm mutants.*

Consistent with this, apical release of Arm from membranes to the nuclei (Figure 72) and late Twist expression (Figure 73) are lost in a Y667-dependent specific way.

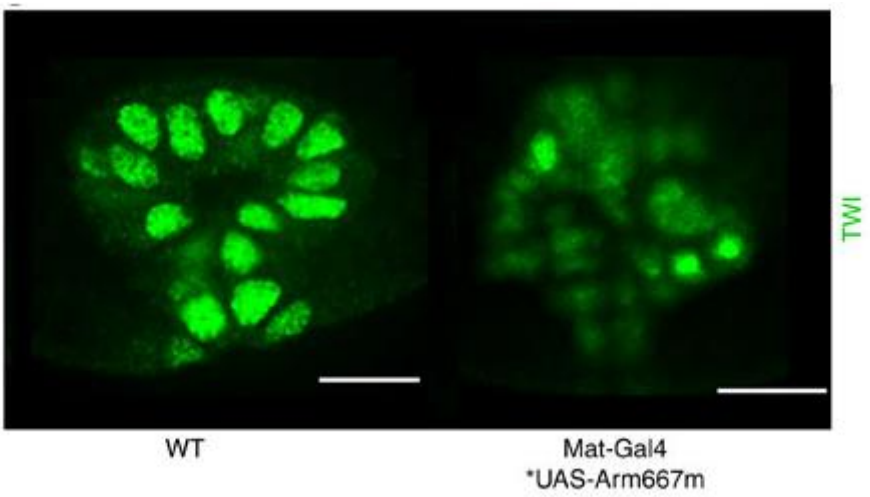

Figure 73: (a) Twist expression in the WT at stage 8. (b) Twist expression in Arm667m embryos at stage 8.. Scale bar, 10 mm (white bars).

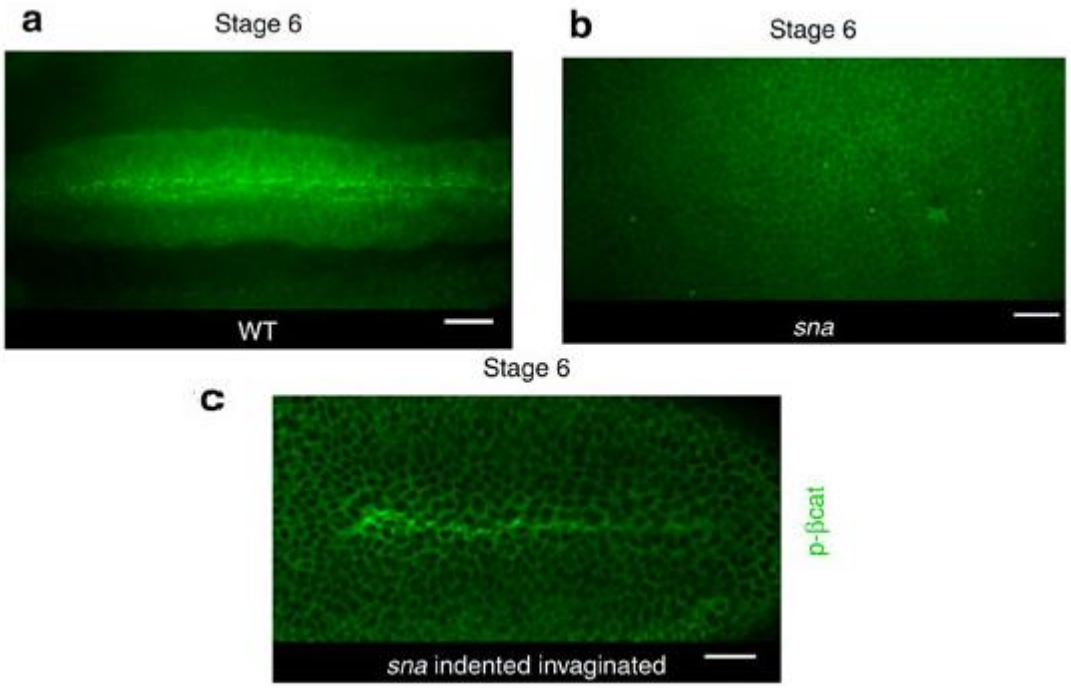

Figure 74: (a) Phospho-β-cat labelling in Src42A-RNAi invaginating embryos.(e) Phospho-β-cat labelling in the non-invaginating mesoderm of stage 6 sna^{-}/$^{-}$ Drosophila embryos. (f) Phospho-β-cat labelling in the indented invaginating sna^{-}/$^{-}$ mutants rescued in mesoderm invagination Scale bar, 20 mm (white bars).

Furthermore, Arm Y667 phosphorylation was absent in sna^{-}/$^{-}$ mutants and restored after invagination rescue due to soft indentation (Figure 74).

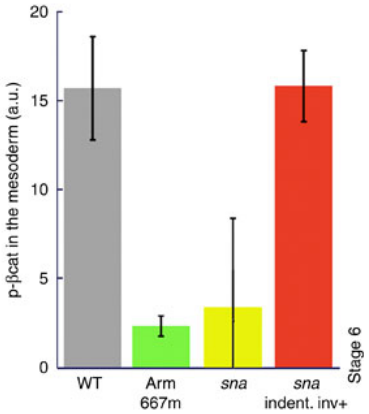

Figure 75: Quantification of Arm Y667 phosphorylation in the ventral furrow of Drosophila WTembryos (n=18), , in Arm667m (n=8), in sna^{-}/$^{-}$ embryos (n=7) and in indented invaginated sna^{-}/$^{-}$ embryos (n=6). P<0.001 according to Mann–Whitney's exact test. Error bars are s.d. All experiments were replicated two times.

In addition, dominant negative embryos of Sarc42A, known to be involved in the phosphorylation of Armadillo prevention its interaction with E-cadherins (128 Takahashi et al 2005) prevented Y667 β-cat phosphorylation, Arm nuclear translocation and Twist expression in the mesoderm, confirming the requirement of a Src family kinase as permissive in the β-cat mechanotransductive process, in a line with zebrafish results.

All together these results demonstrate that in both in *Drosophila* and zebrafish, β-cat Y667 phosphorylation is mechanically induced in a Src-dependent process. This allows β-cat to be released from junctions to the nucleus and leads to the stimulation of mesoderm transcription-factor expression during gastrulation. Here we thus find that the triggering of the zebrafish *ntl* expression and the maintenance of the *Drosophila* Twist expression in presumptive mesoderm cells are mechanically induced in a β-cat dependent mechanotransductive process by the first morphogenetic movements of gastrulation in both species. We demonstrate that the phosphorylation of the Y667 site of β-cat that prevents the interaction with E-cadherin is the key mechanotransduction molecular event, leading to the release of β-cat from the junctions to the cytosol leading to nuclear translocation and expression of mesodermal genes in both species. We conclude that an identical mechanosensitive pathway acts in early mesoderm development in two dista*ntl*y related bilaterians, *Drosophila* and Danio. This detailed similarity indicates common inheritance of this pathway from the Urbilateria, the last common Protostomia–Deuterostomia bilaterian ancestor.

9- Conclusion: a mechanotransductive origin of mesoderm emergence in the common ancestor of bilaterians ?

The search for a common biochemical pathway leading to mesoderm formation across Bilateria has so far proved to be difficult (129 Arendt 2004, 130 Martindale et al 2004, 131 Schol 2003, 132Harvey 2010) especially owing to the case of the protostome superphylum Ecdysozoa, for which there has been no reports of a role for β-cat in early mesoderm specification. As we demonstrate Y667/654-β-cat phosphorylation-dependent mechanical induction of early mesoderm specification to be a common pathway in two such dista*ntl*y related species as *Drosophila* and zebrafish, thereby introducing a role for β-cat signalling in early mesoderm specification in a member of Ecydosozoa—that is, *Drosophila*—we suggest that mesoderm specification by mechanical signals could be of ancient bilaterian origin. If the mechanotransduction pathway we describe dates back to the Urbilateria, the last common ancestor of Protostomes (*Drosophila*) and Deuterostomes (zebrafish), there should be potential for its conservation in other Bilateria. Indeed, our results have interesting parallels in other organisms. In Xenopus, it was shown that the marginal nuclear translocation of β-cat at stage 9 was surprisingly independent of Wnt ligands and necessary for mesoderm induction (Schol 2003). Strikingly, this coincides temporally with the first detectable morphogenetic movements in the Xenopus ectoderm (133 Keller 1980). In artificially bent Xenopus animal explants, mesodermal identity is mechanically induced in the convex (dilated) side (134 Kornicova 2010). In sea urchins, *bra* is downstream of the Wnt canonical β-cat pathway and is strictly expressed at the highly curved deformed margin of the blastopore with extinction of transcription on internalization, an observation that could be elega*ntl*y explained by control through mechanical signals (135 Gross 2001). In amniotes, such as mice and chicken, the movements of epiboly (that happen at the rim of the blastoderm) are uncoupled from the process of mesoderm induction which, instead, takes place at the primitive streak (136 stern 2004). Interestingly, the primitive streak is established by strong morphogenetic movements (known as polonaise in chick embryos), which might provide the required strains for mechanical mesoderm induction in amniotes. More investigations are required to test this point. So far, data obtained in mouse indeed confirm that the transcription activity of β-cat is required for the initiation of *bra* expression (137 Velenta 2011). These observations suggest broad conservation for the mechanotransduction pathway we describe at least among deuterostomes.

From a morphogenetic point of view, gastrulation movements are strikingly diverse across Metazoans, including invagination, epiboly-driven involution, ingression and delamination. Is this diversity compatible with the idea of a conserved requirement for mechanical cues in the establishment or maintenance of gene expression patterns? In this respect, we note that the two bilaterians we compare, *Drosophila* and zebrafish, display strikingly divergent modes of gastrulation, as *Drosophila* gastrulate only by invagination while the zebrafish embryo is strictly epibolic at our stage of interest. Indeed, *Drosophila* and zebrafish are practically as different, as far as modes of gastrulation are concerned, as two bilaterians can possibly be. Nevertheless, these radically different morphogenetic movements are compatible with conservation of the same mechanosensitive pathway during mesoderm specification. This indicates that the conservation of mechanotransduction pathways, even though it consta*ntl*y requires cell deformation, is not tightly constrained by the exact type of morphogenetic movement involved. In the case we report here, it is sufficient that mesoderm cells undergo a specific and localized

deformation before or during mesoderm specification. The comparison between the two species we studied demonstrates that this is compatible with important divergences in morphogenetic mechanisms.

From a mechanistic point of view, the phosphorylation of the Y654 β-cat site was found in different contexts to reduce β-cat affinity with E-cadherins and in several cases to be sufficient to trigger nuclear translocation (Van Veelen 2011, 138 Sharma 2012, 139Polakis 2012 140 Tamade 2012). Within the present mechanotransductive context, how cytoplasmic β-cat, having been released from the junctions after Y654 phosphorylation, escapes Axin/ APC-mediated degradation to translocate in the nucleus in the mesoderm is an interesting question that will be addressed in future investigations. It might either be due to a parallel mechanical inhibition of the APC/Axin complex, a process known in other biochemical contexts(141 Samuel 2011), or to an overflow of cytoplasmic β-cat due to a burst of mechanical signals that could saturate and bypass the degradation machinery and lead to partial nuclear translocation. Consiste*ntl*y with the latter hypothesis, it is worth noting that in the case of *Drosophila*, weakly observable β-cat nuclear translocation (Peifer 1994) is known to be sufficient for transcriptional activation, with β-cat transcriptional activity having been demonstrated by defects in target gene expression in TCF dominant-negative mutants,(142 schweizer 2003). From an evolutionary perspective, our results are consistent with the reconstituted ancestral fate map of bilaterians, where the mesoderm is proposed to originate at the blastoporal margin, which, indeed, is by definition a strongly deformed zone (143 Arendt 1997). Adding to the cell–cell adhesion ancient metazoan role of β-cat allowing the constitution of epithelia (144 Dickinson 2011), we thus propose that in the last common ancestor of protostomes and deuterostomes, mechanical deformation associated with gastrulation at the blastoporal margin could have induced Y667/654 phosphorylation of β-cat and nuclear translocation, and, in turn, activated the expression of mesodermal transcription factors. In conjunction with the mechanical induction of β-cat transcriptional activity, additional signalling pathways such as Nodal37 and Dorsal (145 Roth 2004) were differentially recruited to contribute to mesoderm induction in independent branches of the animal evolutionary tree, probably consolidating the output of the ancestral mechanotransduction pathway. Indeed, Nodal and Dorsal have no conserved role in mesoderm determination in *Drosophila* and zebrafish, respectively (146 Shen 2007, 147 Lynch 2011). In contrast, here we find that mechanical induction of Y667/654 phosphorylation of β-cat in early mesoderm determination is conserved in both species. This suggests that the mechanotransductive β-cat pathway is more ancient than the protostome-specific or deuterostome-specific pathways previously identified in mesoderm induction, and dates back to the last common ancestor of zebrafish and *Drosophila* more than 570 million years ago, the period during which the mesoderm is thought to have emerged (148 Douzery 2004, 149 Peterson 2004). A conserved mechanotransductive origin of the mesoderm specification in Bilateria embryos thus suggests that the mesoderm could have developed in diploblastic ancestors through the emergence of the mechanical control of the phosphorylation of the β-cat Y667/654 site in response to gastrulation morphogenetic movements.

10- Perspectives

In this work we demonstrated the conserved role of mechanical strains developed by the first morphogenetic movement of embryogenesis in the mesoderm differentiation in both a vertebrate (zebrafish) and invertebrate (*Drosophila*) embryos. This suggests the Y654 β-cat mechanically induced phosphorylation underlying mechanism at the origin of mesoderm emergence in the last common ancestor of bilaterian. A “definitive” conclusion is currently being tested by reproducing the experiments realized in the zebrafish and *Drosophila* embryos, on *Nematostella vectensis*, in collaboration with Thibaut Brunet and Detlev Arendt at EMBL. Indeed the *Nematostella vectensis* is a diploblast without mesoderm, but possesses an emerging precursor rudiment of mesoderm, which makes it a perfect representative of the ancestor of the last common ancestor of bilaterians characterized by a mesoderm. Finding the same conclusions in *stella* than in zebrafish and in *Drosophila* would thus encircle the common ancestor in the evolution tree, and allow a definitive conclusion.

III- Mechanically Induced Heritable Modulation of Developmental Biochemical Regulation

In this project in development, we mechanically perturbed *Drosophila* embryos germ cells and found anomalies in the development of the resultant progeny generations. We thus studied the molecular processes underlying the inheritance of such anomalies. Specifically, our results show that gentle mechanical compression on the posterior pole germ cells of stage 5 embryos (cellularisation stage), leads to early embryonic dorso-ventral polarity phenotypic anomalies, in the progeny produced after the crossing of the adults having developed from the indented embryos.

1- Introduction

a- Epigenetics in *Drosophila*

Historically, the term “epigenetics” was dedicated to specify developmental or homeostatic process that could be actively modulated by “external” factors, namely factors that are not consequences of the state of expression of the genome. Today, the sense of the “epigenetics” term has evolved to define any feature of a living system, which is heritable generation after generation in a genetic independent process.

Such feature can be with the requirement of genetic perturbations. For instance, the progeny of Drosophila fly mutants for Hsp90/83 show numerous morphological defects that can become independent of the Hsp90 mutation, and therefore heritated, once enriched by selection (150 Rutherford 1998). Such process can be be enhanced by environmental factors, temperature (Rutherford 1998).

Here we will not make an exhaustive introduction to the very large spectra of underlying mechanisms involved in the many epigenetics phenomena that can be found in living systems. However, one of the best characterized mechanisms of epigenetic transmission belongs to the methylation of DNA in response to environmental factors, which is able to silence the expression of specific genes, even in the presence transcription factors (151 Walsh, Christopher 2006). Such methylation can be achieved by the activation of methyltransferases in response to environmental factors, and can be transmitted mitosis after mitosis in somatic cells. Not only the methylation state of the DNA can be modulated, but also of the Histones, which state of methylation can regulate the histone activity in compacting DNA in a heterochromatin state un-abled to transcript genes (152 Grewal, 2004). However, there exists a process of methylation washing up in germ cells, making generational epigenetic transmission a priori independent of methylation processes (153 Carroll 2008).

An alternative mechanism of trans-generational epigenetic transmission has thus been proposed to involve pi-RNAs, which are very small 24-25pb RNAs involved in the silencing of transposons during the all life cycle of the organism in somatic cells, and in a specifically robust process in germ cells (154 Sato ,Siomi 2013). Importantly, a modulation of germinal pi-RNAs production at a given stage of the life cycle of the organism can perturb the expression of the same population of pi-RNAs all along the life of the organism, and be maternally transmitted generation after generation in an epigenetic process (155 Vanssay, Ronsseray Nature 2012).

b- The pi-RNA transposon repressing complex

In eukaryotes, a large proportion of genomes consists in the sequence of various transposable elements (TEs). For instance, 45% of the human genome and 15–22% of the *Drosophila* genome contain TE sequences (156 Biemont and Vieira, 2006; 157 Lander et al., 2001). A major class of TEs consist in retro-transposons, which abundance is due to a "copy -paste" mode of amplification (158 Finnegan 2012; 159 Gogvadze and Buzdin, 2009). When TEs are inserted into a genomic location, gene expression patterns may become altered, which can compromise cell viability (160 Callinan 2006, 161 Hancks 2012).

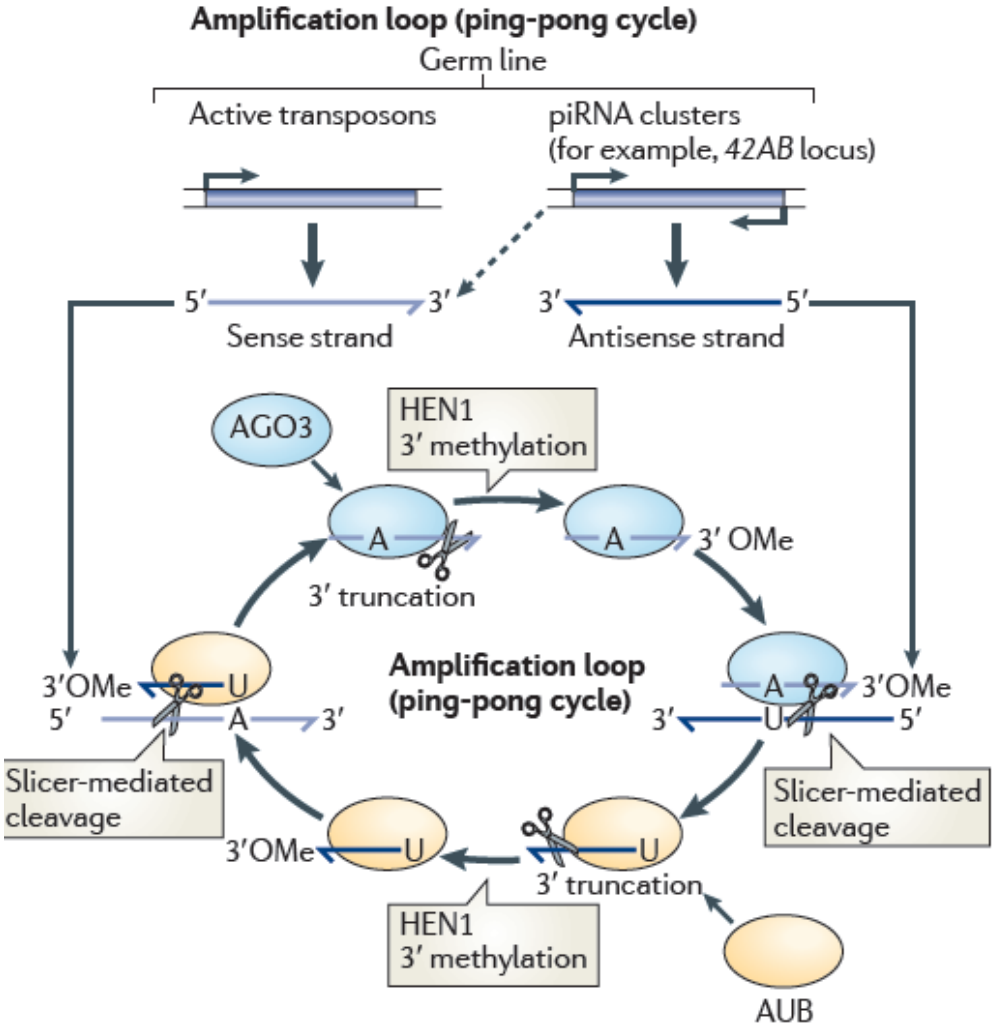

*Figure 76: Amplification loop (ping-pong cycle**)** (from162 siomi et al 2011). This amplification mechanism (also known as the ping-pong cycle) is most likely to involve Slicer activity of AUB and Argonaute 3 (AGO3), but not PIWI itself. AUB associated with antisense piRNA cleaves piRNA precursors in the sense strand. This reaction determines and forms the 5′ end of piRNAs that are loaded onto AGO3. AGO3 associated with sense piRNA cleaves antisense piRNA precursors, generating the 5′ end of antisense piRNAs that subsequently are loaded onto AUB. The 3′ end of piRNA is formed by an unknown nuclease (or nucleases), which is followed by 2′-O-methylation mediated by HEN1. piRNAs that induce the amplification loop may also be deposited from the mother .*

PIWI-interacting RNAs (piRNAs) are endogenous small noncoding RNAs that act as guardians of the genome, protecting it from these invasive TEs in the germ line. Their main role is to silence the TEs. Other proteins are also needed for the TE leading to a total of 3 major protein involved :

- Aubergine (AUB), participates at the amplification of the piRNA during a so-called ping-pong cycle process (Figure 76).

- AGO3, participates at the amplification of the piRNA during the ping-pong cycle (Figure 76).

Once amplified piRNA are bound to PIWi proteins that will target TE and silence TES through the cleavage activity of PIWI. PIWI can recognize and cleave transposon transcripts (Brennecke 2007; 163 Gunawardane) because they are associated to piRNAs that are anti-sense to TEs.

c- The checkpoints DNA integrity guardians

During mitosis or meiosis, the replication of the genetic information can be compromised. Safety pathways, called cell cycle checkpoints are in place to make sure that the genetic information can be replicated, without being altered. At each phase of the cell cycle, there is a check that a given phase has been done accurately before the starting of the next phase. So, the chromosome genetic information can be safely transmitted across cell lineages and generations. These checkpoint pathways are highly conserved among species. They mainly consist in 4 elements: initiating signals, sensors, transducers and effectors (164 Masrouha 2003). There exists mainly 3 checkpoints: the first one (G1 checkpoint) checks that the cell is large enough to enter S phase. The G2 checkpoint checks that the DNA is correctly replicated and that replication errors have been repaired (Figure 77). The last one checks that the chromosomes are correctly aligned on the spindle. Here we will focus on the second checkpoint.

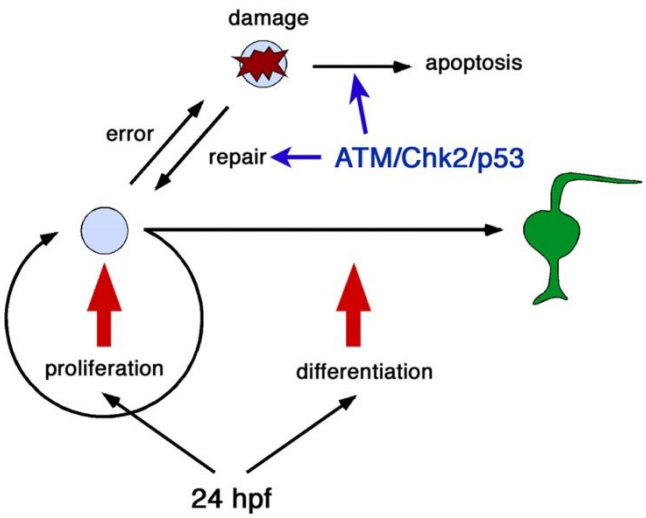

Figure 77: From (165 Masahiro Yamaguchi 2008) "Model of ATM-Chk2-p53 pathway in zebrafish retinal neurogenesis. In the zebrafish retina, mitotic progenitor cells start to generate neurons at 24 hpf. After 24 hpf, the cell cycle duration of retinal progenitor cells shortens and the cell proliferation rate increases. The increase in cell proliferation rate may increase the number of DNA replication errors during retinal neurogenesis. One possible model is that the ATM-Chk2-p53 pathway repairs the replication errors or induces apoptosis to remove retinal neurons with unrepaired DNA damage. This pathway might prevent the accumulation of abnormally differentiated neurons, which possibly compromise the subsequent formation of neural circuits, and might also remove cancer-predisposing cells."

Activation of a meiotic checkpoint due to the persistence of unrepaired Double Strand Breaks (DSBs) is a conserved features common to many species, from yeast and worms to flies and vertebrates (166 Tanakami 1998; 167 Gartner 200; 168 Edelman 1996; 169 Prittman1998).

However, a comprehensive understanding of the underlying mechanism of the checkpoint has not yet been completely achieved. Nevertheless, such mechanism has been well studied in *Drosophila*. Indeed we know that in *Drosophila*, the checkpoint protein-2 kinase (Chk2) and its downstream effector protein, Dmp53 (P53), are required for DNA damage-mediated cell cycle arrest, DNA repair or apoptosis. After recognition of DNA lesions and particularly double strand breaks (DSBs), Chk2 is activated upstream of the repair process. The p53 kinase is activated downstream, and will induce apoptosis following non-repaired DNA damage events (170 Brodsky et al 2000 , 171 Ollman et al 2000, 172 Titen 2014). Chk2 is also essential for the activation of a second meiotic checkpoint due to mutations in genes in the repeat associated small interfering RNA pathway (173 Klattenhoff 2007, 174 Chen 2007, 175 Pane 2007).

As a side effect, Check-2 activation leads to the disruption of microtubule organization during *Drosophila* oogenesis, which will perturb axis specification. In 2007 Klattednhoff showed that, in contrast to normal polarities establishment (176 Fichelson, P. et al, 2010), Mnk/Check-2 activation creates a perturbation in *gurken* expression, leading to a perturbation in dorso-ventral axis formation.

2- Mechanically induced herited early developmental phenotypic defects

In a first set of experiments, we induced a deformation on the germ cells of embryo just before the end of the cellularisation (around 3 hpf) (Figure 78), namely at stage 5, before the initiation of morphogenetic movement of gastrulation.

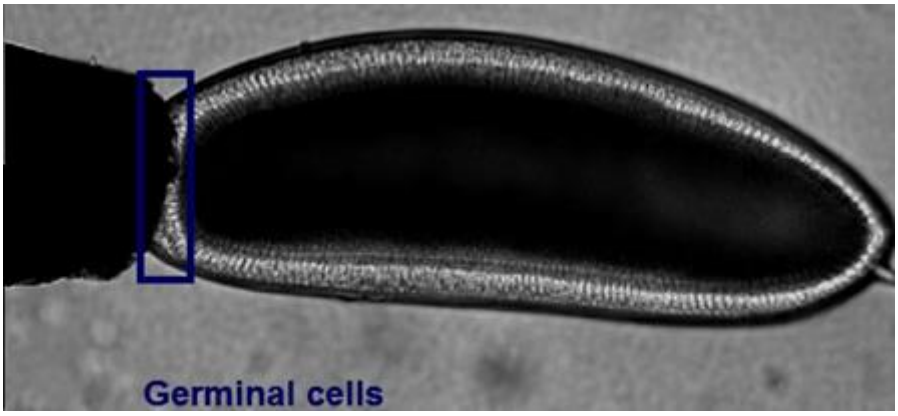

Figure 78: Indent of germinal cells a Drosophila embryo at stage 5. This is indentation procedue 1.

In a second set of experiments, we indented before the formation of the pole cells, around stage 2-3 at 1.5hpf (Figure 79).

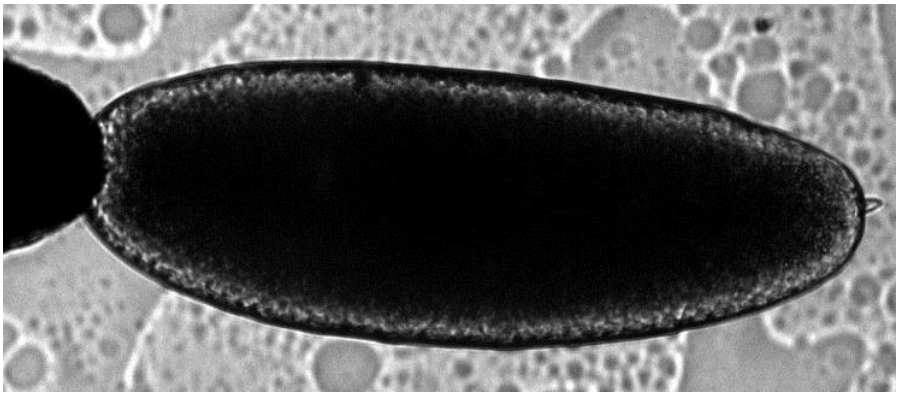

Figure 79: Indent of germinal cells a Drosophila embryo at stage 2. This is indentation procedure 2.

After the germ cells compression, we led the embryos develop until they become adult flies. In a first approach, we crossed those flies together and let them reproduce. In the perspective of refined experiments, we also followed the progeny of single indented couples by crossing one virgin female with on male together, both flies emerging from compressed embryos.

We worked with their progeny called {F1,F2,F3, Fi}, “i “ representing the number of the generation. The only mechanical input has been realized in generation G0 embryos. At no other time were realized new indents on embryos.

a- Mortality and morphological approach to study the progeny

To measure early anomalies, we let the embryo lay for 1 hour and observed the embryos at 8hpf. We then compared the phenotype of the indented progeny embryos to the WT ones. To analyze the early death rate, we grouped embryos by 5 and we counted them. Then between 24-28 hpf we counted the number of "remaining" embryos that didn't become larvae.

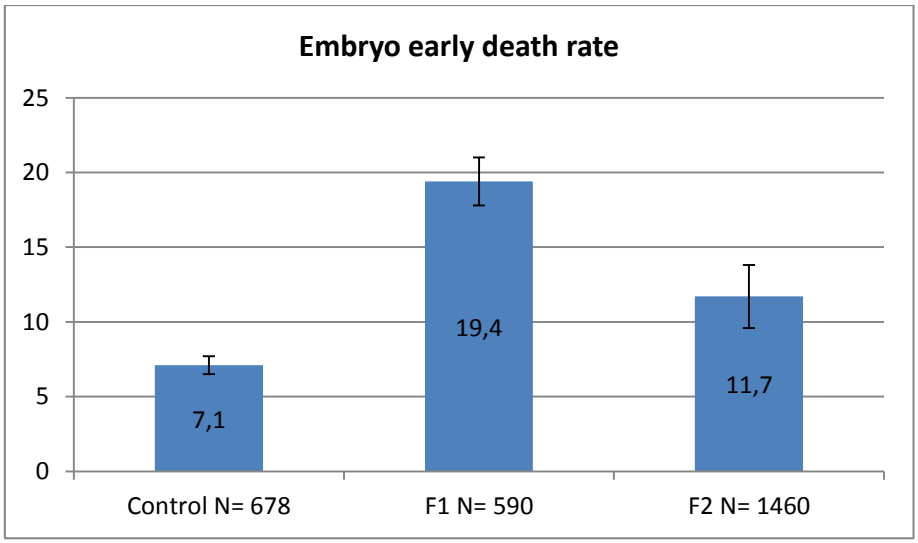

Figure 80: Observation of embryo death rate before larva hatching.

In controls, we observed a larva-hatching rate of 93% meaning an early death rate of 7%. This result is consistent with literature (177 Olsen 2001). In the first generation F1, we observed that the early death rate is around 20% (Figure 80). We thus observed a strong increase of early mortality. In addition, when we looked at the development before 8hpf we observed that around 49**%** of the embryos, compared to 13% in non indented showed phenotypic anomalies (Figure 81, Figure 82).

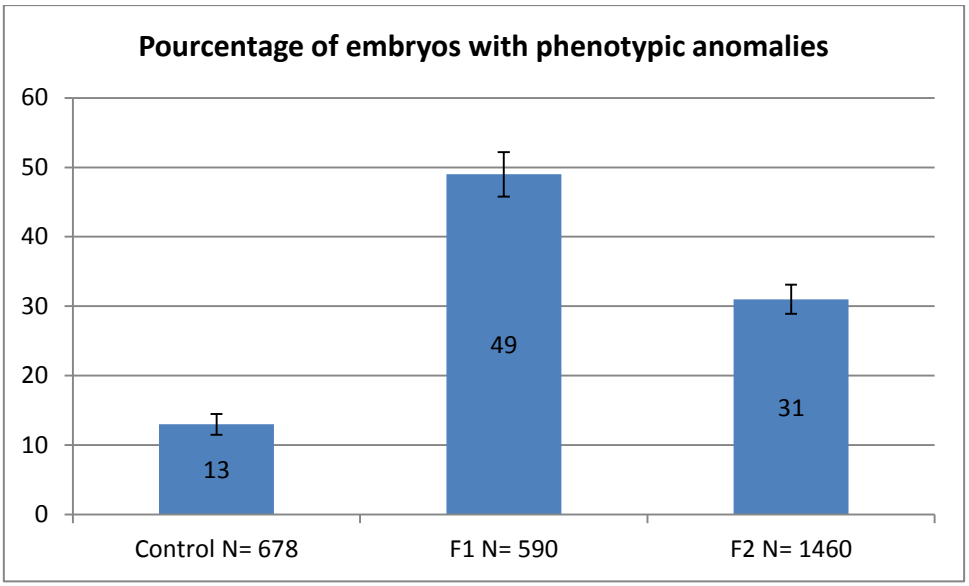

Figure 81: Percentage of embryo with phenotypic anomalies observed under binocular. This is a first approach that determined if the lineage has trouble that could explain lethality.

The phenotypes we considered as anomalous were the following:

- Dead embryos/non-fertilized embryos: the embryos visually looks like fixed in time. They didn't continue development. In case of synchronized laying they are not at the same stage than the other embryos. The particularity of F1 is the abundance of phenotypes we called "zebra patches" (Figure 82).

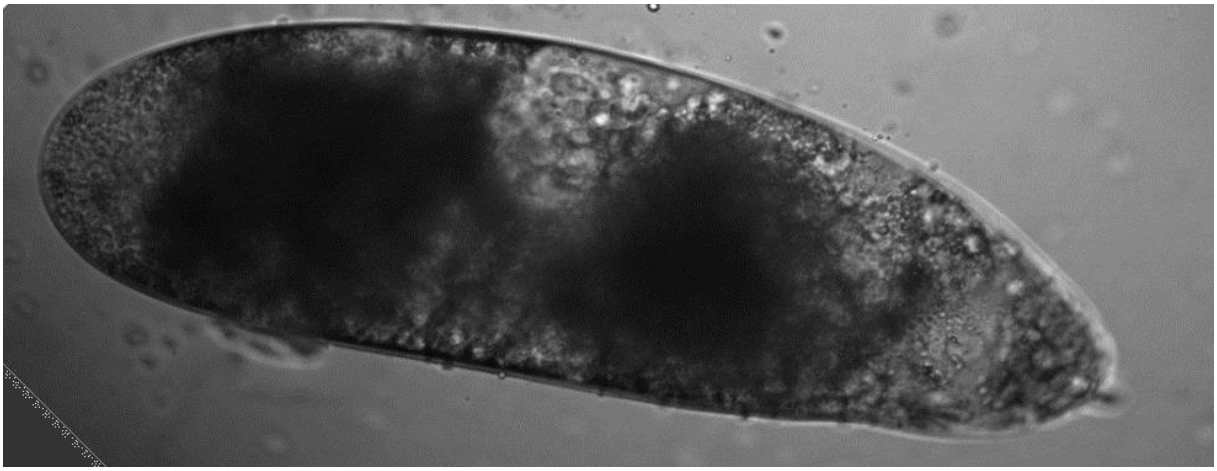

Figure 82: Dead embryo with representative phenotype of darker and clearer stripes called zebra patches.

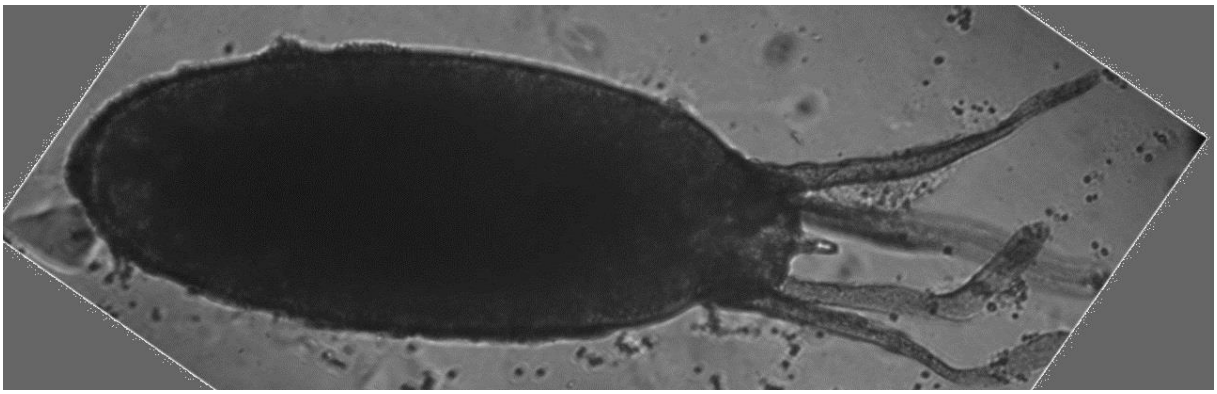

Figure 83: Embryo with 4 appendices.

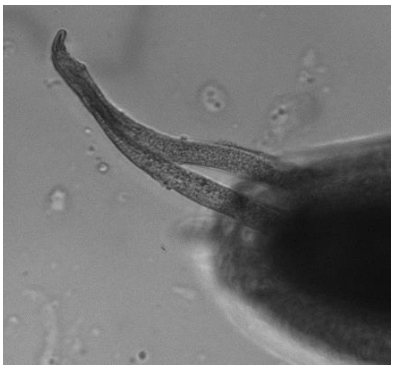

Figure 84: Embryo with a fusion of the dorsal appendice. This fusion can be representative for dorsal polarity anomalies (178 Wiechaus 1978).

- Anomalies in the appendices: we could observe some times four appendices (Figure 83), but the usual phenotype was only one appendix or more precisely the fusion of the 2 appendices in around 1% of cases, compared to 0.1% in controls $p<0.001$ (Figure 84).

- Anomalies in dorso-ventral polarities and anterior holes in gastrulating embryos.This categorie represent around 30% of the embryos,most of them associated to phenotypic anomalies in the dorso-ventral polarity. Analysis showed that around 30% of the embryos of this category do not reach the larva hatching in both category wild type and F1.

The difference between the anomalies and the hatching rate can be explained by the robustness of development. Even though embryos are characterized by some anomalies, a certain proportion appears to be rescued and to finally develop until larvae stage. For example, in WT 6% of embryos show appendix fusion. Embryos with this phenotype have a higher death rate (27% in the subpopulation N=110).

This first analysis revealed that the progeny of indented embryo is anomalous. The next question is thus: are those anomalies induced by malformations of reproductive organs due to the indent, or are they alternatively heritable from one generation to another.

b- Inheritance of anomalies in the progeny of indented embryos

To answer this question, I studied F2 embryos, progeny of F1 (itself progeny of the G0 indented embryos). Importantly, the F1 flies leading to the F2 embryos have not been indented. Therefore, if anomalies remain in F2, it will necessarily be transmitted from G0 to F2 generation through a heritable process.

I indented Wild type strains have thus been generated in a set of 5 distinct independant experiments. As a result, we observed in the second generation that one third of the embryos showed anomalies in their development (Figure 81) before 8 hpf with the same phenotype observed in F1. The early death rate was around 12% in F2 (N=590) (Figure 80).

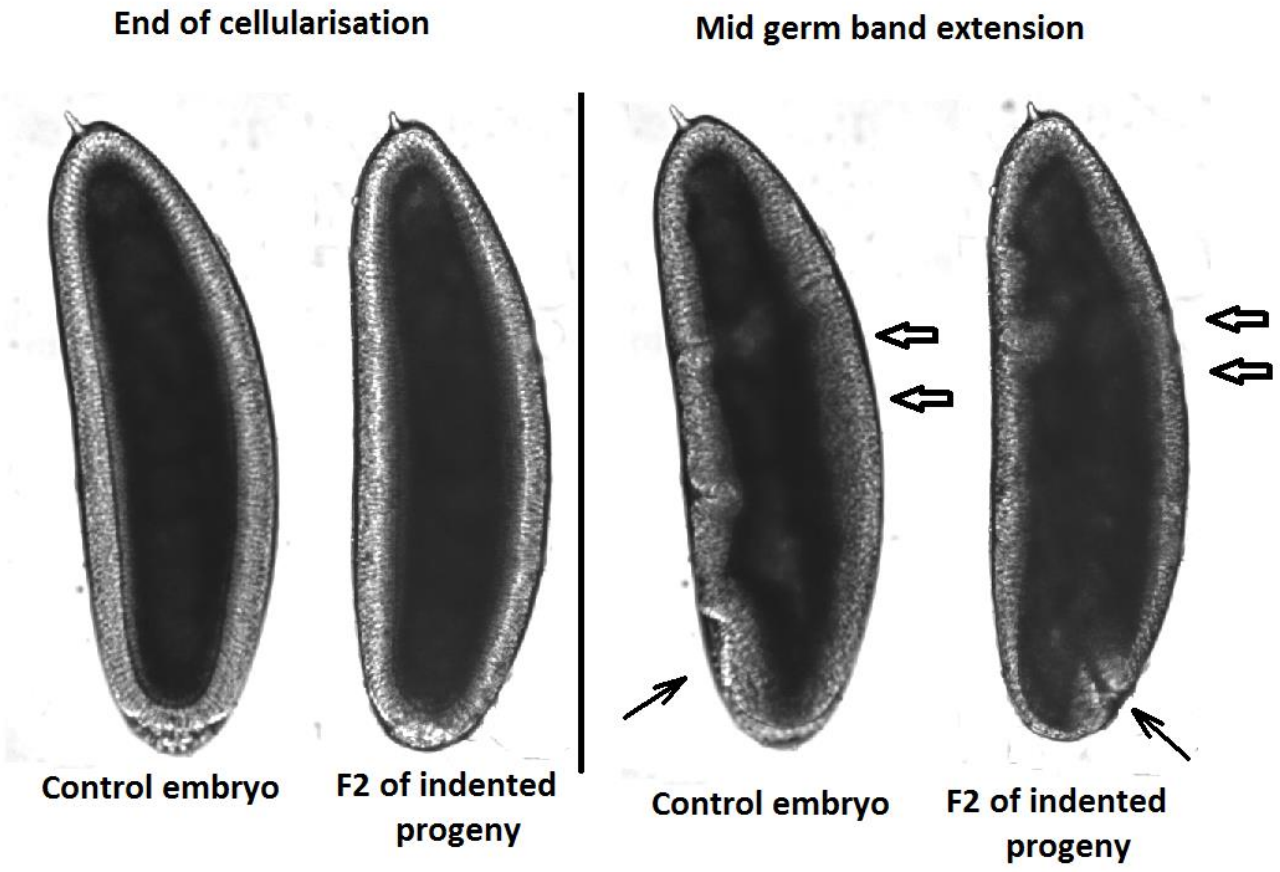

Figure 85: F2 embryo of indented progeny showing a defect in germ band extension localization single arrow) and in mesoderm invagination (double arrow).

In addition to appendix fusion(1% of cases) (179 Abdu 2002), the observation of gastrulating embryos showed that a high number of these anomalies are associated to dorso-ventral polarity anomalies, sepcifically exhibit-

ing dorsalised phenotypes, or changes in the dorso-ventral polarity orientation(30% of cases). Such dorsalised phenotypes were characterized by a germ band extension (GBE, the convergent extension movement of gastrulation) on the lateral or ventral side of the embryo, instead of on the dorsal, as well as defects of mesoderm invagination (Figure 85). Therefore we focused on the mesoderm invagination and germ band extension the first movement of gastrultion reflecting the embryo axis establishment.

We mainly focused on F2 the generation to have enough material to work on, as well as to make sure of a trans-generational effect inheritance from G0 indentation. We also assumed that effects may decrease with time so F2 is the best generation we can study to observe heritable defects with *a priori* most sensitive effects.

c- Microscope analysis

After careful analysis of the produced phenotype under classical light microscopy, we found that all anomalies consisted in:

- delay in cellularisation and in mesoderm invagination,

- defects in mesoderm invagination

- anomalies in the initiation of the germ band extension (Figure 86)

- perturbed dorso-ventral orientation of the embryo inside doso-ventral correctly orientated vitelline membranes (Figure 87)

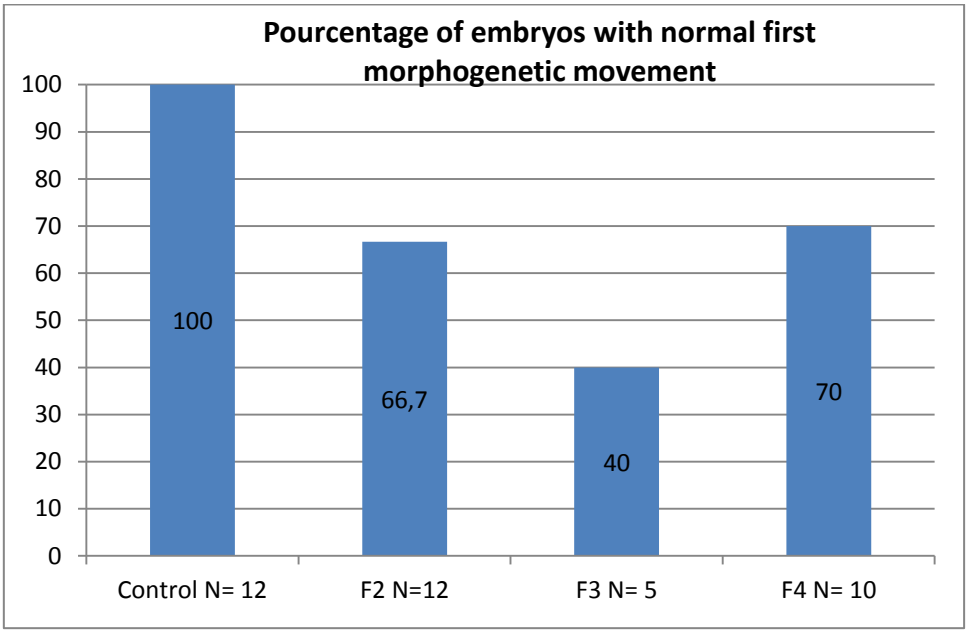

Figure 86: Video analysis of embryo with no development problems around gastrulation. These videos were taken between cellularisation and germ band extension under microscope.

In some cases, germ band started to extend along a random axis, before to come back to the right direction and extend correctly. In some other cases, it didn't extend fully and the embryo died. We also often noticed problems in dorso-ventral polarities, with germ-band extending fully along lateral or ventral axis with regard to the vitelline membrane orientation (Figure 85). We checked that none of the control embryo (N=14) showed anomaly during their development (Figure 85, Figure 86). In the progeny of indented embryos, only at least 2/3 of the embryos showed a normal germ band extension.

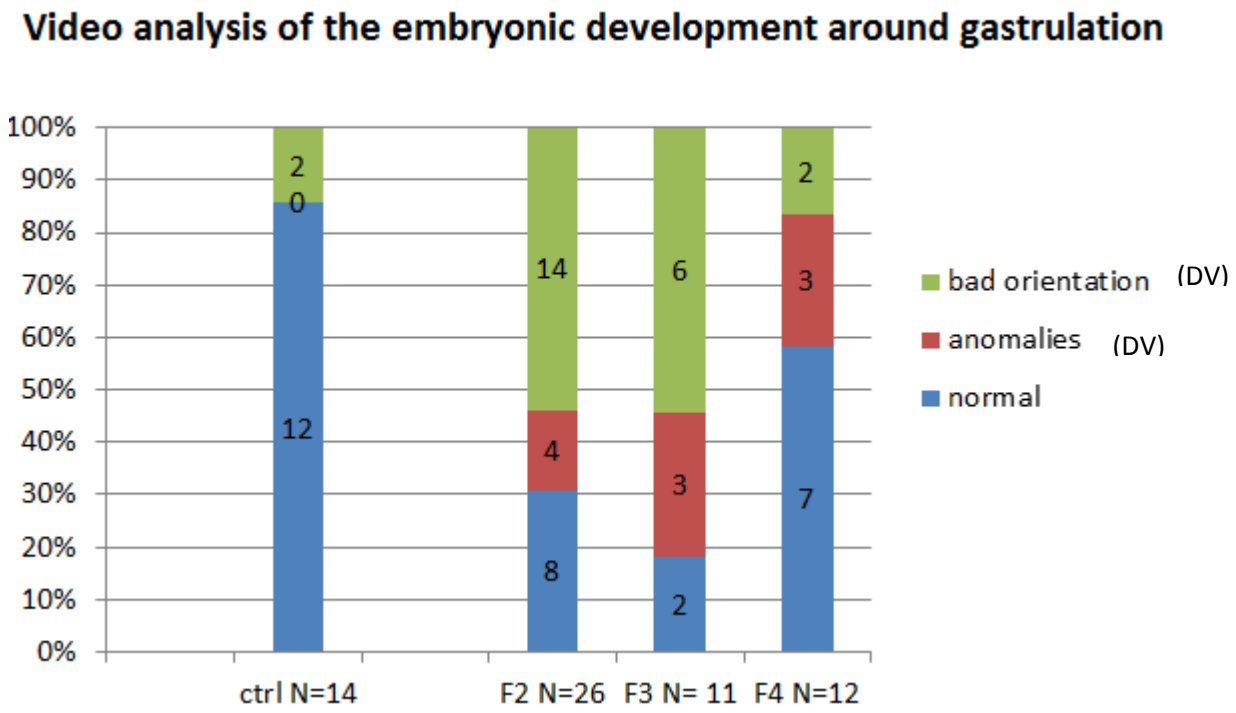

Figure 87: Video analysis of the embryonic development. Anomalies in germ band extension or mesoderm invagination and orientation problems are much important in indented lineage than in control one.

Note that the orientation of the embryo is indeed an important parameter to control, because if the embryo is not correctly sagitally positioned one cannot see clearly the invagination, letting us ignoring if it happened correctly. Indeed, because indented progeny's embryos have dorso-ventral polarity anomalies, mesoderm invagination of these anomalously orientated embryos occurred out of the ventral pole of the embryos (as define by the viteline membrane shape), which made impossible its visualization (Figure 87). In some cases, dorso-ventral polarity appeared to be maintained with correctly orientated germ-band extension, but with strong defects in mesoderm invagination. These cases were included with anomalous GBE in the statistics of the red parts of Figure 87 histogram.

3- Hypothesis: the mechanically induced dorsalised phenotype as induced by checkpoint activation

As we saw in the introduction, there exists a check point checking for DNA damages after meiosis. In case this checkpoint is activated, the egg develops dorso-ventral polarity anomalies, thereby susceptible to show dorsalised phenotypes at embryonic stages, due to Check-2 activation from damaged DNA.

a- Dorsalized ventro-dorsal gradient of Dorsal nuclear translocation

To check for the molecular origins of dorsalised phenotypes, we realized quantitative analyses of the nuclear localization of the *Drosophila* embryo Dorso-Ventral morphogen "Dorsal" (180 St Johntson et al. 1992). Indeed, maternal signals in oogenesis activate the nuclear translocation of the Dorsal transcription factor on the ventral pole of the early embryo only, leading to the expression of the ventral genes *snail* and *twist* (Roth.s in St Johntson 1992). Dorsalisation should thus lead to a lack of nuclear translocation. We thus let indented lines reproduce until generation F1 and F2, and fixed their embryos for Dorsal labelling with antibodies. These analyses consisted in labelling both Dorsal and Snail proteins in stage 5.

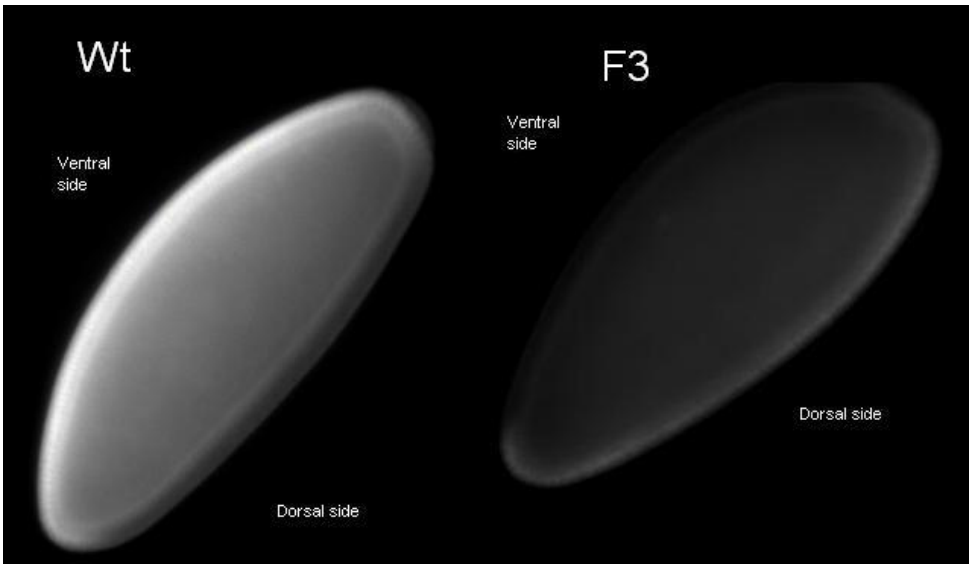

Figure 88: Lateral view of Dorsal labelling of a wild type and a F3 embryo. Dorsal protein is mainly expressed in ventral side in the wild type embryo.

Our first results showed Dorsal nuclear translocation defects, and inversions of polarities. In a first experiment, we observed 4 embryos on 11 showing dorsal deficiency in expression or location of Dorsal (Figure 88) whereas none of the 8 controls did.

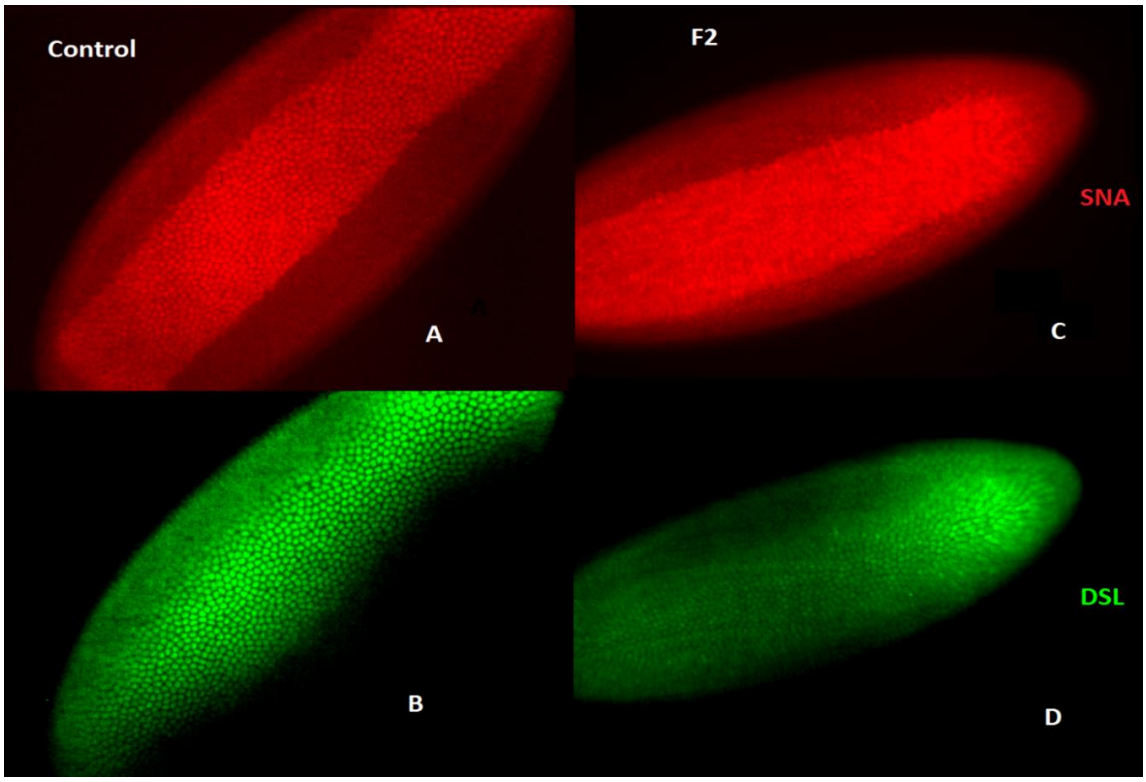

Figure 89: Perturbed expression of DSL expression in F2 embryo. (A ,C) Expression of Sna is restricted to the ventral side of the embryo.(B) Strong dorsal expression in ventral side. (D) Strong defect in Dorsal nuclear translocation in the snail expressing mesoderm

In a second set of experiments, we double labelled the embryos with both Snail and Dorsal. Snail expression was evaluated and was also used (Figure 89) to facilitate the orientation of embryos, because lack of Dorsal was often strong. This was a major point because in F2 16 embryos over 23 showed abnormal expression or localization of the Dorsal protein (Figure 89), preventing correct orientation without double labelling.

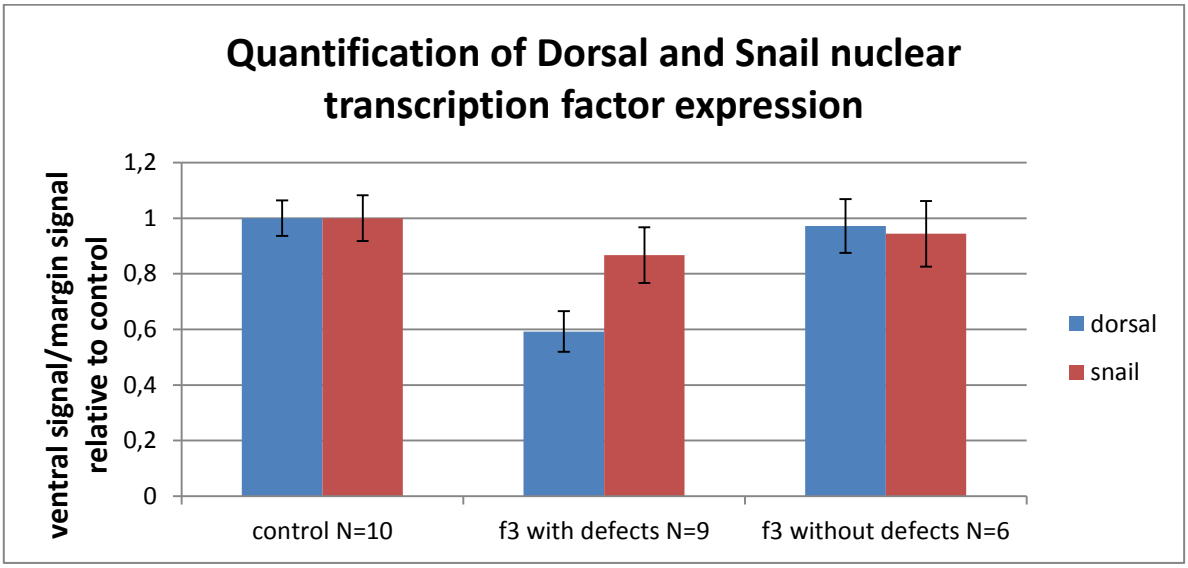

Figure 90: Quantification of nuclear Dorsal and Snail in the ventral side compared to dorsal side signals. The signal is normalized to control's level. p<0.0001 and the experiment has been replicated at least 4 time. Tthis is the result of only one experiment.

We observed two populations of embryos, one with defects in the Dorsal nuclear accumulation at the ventral pole, and the other with a normal pattern. We systematically analyzed the level of Dorsal nuclear accumulation and of Snail expression (Figure 90).

This quantification was realized by measuring the ratio between the levels of expression in the ventral cells with dorsal cells. Quantification revealed important differences in Dorsal nuclear translocation in F3, with a slight but statistically significant difference in Snail expression.

Quantified labelling thus confirmed that the generations produced by the indented G0 are characterized by strong defects in the dorso-ventral polarity biochemical patterning establishment at embryonic stages 5. The question is now: are these anomalies produced by checkpoint activation during meiosis.

b- Testing the inhibition of the check point phenotype by indenting p53 and Check-2 mutants

The mutants of Check2 and p53 are characterized by a defect in the activation of the meiotic checkpoints (Abdu 2002) and are thus unable to activate the DNA reparation neither to start apoptosis. The objective was thus here to indent these 2 mutants and to observe the subsequent effects on their progeny. If the dorsalisation phenotype we observe in the progeny of the indented is associated to DNA damages activating DNA repair through Check-2 and p53 activation, we should observe a higher death rate in the embryo progeny (no more DNA repair) with a lost of their dorsalised phenotype (no more activation of DNA repair).

In Check-2 mutants indented F2 lineage, we found a death rate twice higher than in WT, with 34% of early death compare to 15% in non-indented progeny. This death rate is much higher than in WT which death rate was of 7% in non-indented and increased to 11.7% in F2 indented progeny. Experiments are in progress to study dorsalisation by immuno-labelling.

In p53 mutants, G0 indented embryos were not able to give birth to living flies. Most of their eggs didn't give larvae and the few larvae alive couldn't reach the adult stage. This point is important to notice because the flies were not sterile in a sense that they couldn't produce eggs. They were sterile, in a sense that they couldn't give birth to other living flies. This experiment had been replicated at least 4 times, every time with the same conclusion.

This very strong phenotype gives us the opportunity to test efficiently different control on the importance of the location of the indent on germ cells by produce the perturbed phenotype. After an indent on the lateral side at stage 5, the flies gave birth to viable a progeny. Indent on the head of the embryos still need to be realized. They will give us information on the specific requirement of the application of the strain on germ cell to induce the perturbed phenotype. Until now p53 embryos do not survive to the indent on the head leading to the impossibility to test this hypothesis. Note that even without indentation the high majority of controlled embryos with the same treatment as the indented one (dechorionation, glue, transfer to a new tube) die.

Our first result thus tend to prove that mechanical deformations of germ cells cause genomic perturbations that will be repaired during DNA replication. The most plausible explanation would be the mechanically induced generation of double strand breaks. However, the underlying molecular mechanism involved can either be genetic or epigenetic. Our two main hypotheses are:

- Genetic hypothesis: the DNA of the indented germ cells has been broke as a consequence of the mechanical perturbation. During meiosis, these breaks were detected at the different checkpoints and the DNA was repaired.

- Epigenetic hypothesis: the dorsalised phenotypes could also be due to a modification of the pi-RNA pathway. The indentations overactivating the Check-2 and p53 pathways could inhibit the expression of the pi-RNA which regulates the transposons. As a consequence, transposons would be activated and free to replicate and invade the genome leading to DNA damage.

A first experiment is in progress to give clues on these two hypotheses. Using p53, we took advantage of a very strong phenotype helping us to realize experiments with a very sensitive. The objective was to cross individual couples, one individual with a non-indented and to study their progeny. At the moment, we crossed 4 indented virgin females with non-indented males, which couldn't give birth to any new fly. We have not been able yet to cross a p53 indented male with a virgin female (experiment still processing). However a cross has been made between non-virgin females and p53 indented males, and females produced flies during the 2 weeks after the cross. Because females are known to produce eggs fertilized by the last male they mate with at 98% (181 C Bloch Qazia), this indicates that the cross between p53 indented male and a virgin female might give birth to living flies. However, we need to confirm the result of the experiment by crossing virgin females with indented males.

The result of this experiment may give us a first important clue of evaluation of our main hypothesis. Effectively, if indented female crossed by non indented males are sterile and the reverse is not true, the underlying mechanism of inheritance has more chance to be epigenetic, because in *Drosophila,* epigenetic perturbations are mainly transmitted by females and not by males. Indeed a pi-RNA dependent epigenetic heritable transmission of the perturbation should be transmitted by the mother only. In contrast if a male indented crossed with a virgin non-indented is sterile the mechanism has more chance to be genetic, genetic transmission being a sex-insensitive mode of transmission.

4- Testing the transposon activation hypothesis

a- Candidate approach

One of our hypothesis concerning the checkpoint activation is the accumulation of errors in the DNA caused by the insertion and accumulation of transposon in the coding sequence. Normally, transposons are silenced by pi-RNAs. We hypothesized that one way or another, the indent affects pi-RNA transposon silencing efficiency. To test this hypothesis, we followed a candidate approach by testing the involvement of the usual transposon elements regulated by pi-RNA silencing.

First, we realized indents on the Singed Weak p lineage, to test the involvement on the "p" element. In this strain, the gene *singed* contains a transposable element that is defective for the transposition and can be reactivated by different bio mechanism (182 Laski 1986). The activation of p, in this strain, leads to a curly silk phenotype. In our case, we wished to check the induction of the transposition of the p-element by indentation. We never observed the curly silk phenotype after the first type of indentation, stage 5. We are currently performing the same manipulation, with the early indentation at stage 3.

We also tested the BX2* strain developed in Stéphane Ronsseray's lab (Vanssay et al 2012). The specificity of this strain consists in its possibility to maintain pi-RNA production ovaries based on the pi-RNA produced in early germ cells. We anticipated that the indentation could inhibit pi-RNA production at a given generation and at a given stage of development, with this inhibition maintained in the ovaries of the indented flies progeny with a lack Z reporter of the locus p1039 reporter for the repression of BX2*. However, the indentation at stage 5 didn't produce an observable effect in the LacZ expression. Indentation at stage 3 will be performed soon on this lineage, to analyze if the impact will be different.

We also realized QPCR analysis on ovaries of F2 indented wild type, to test the expression of several canonical transposons. In case of piRNA activity would decrease, the transposon should show their activity increased. We tested 3 different reporters have been taken:

- Het-A, a telomeric transposon playing a role in structure and function of telomere and healing broken chromosomes

- Roo, a somatic transposon

- Burdock, a germinal transposon

No modification of the activity was observed in each of the transposons tested (Figure 91).

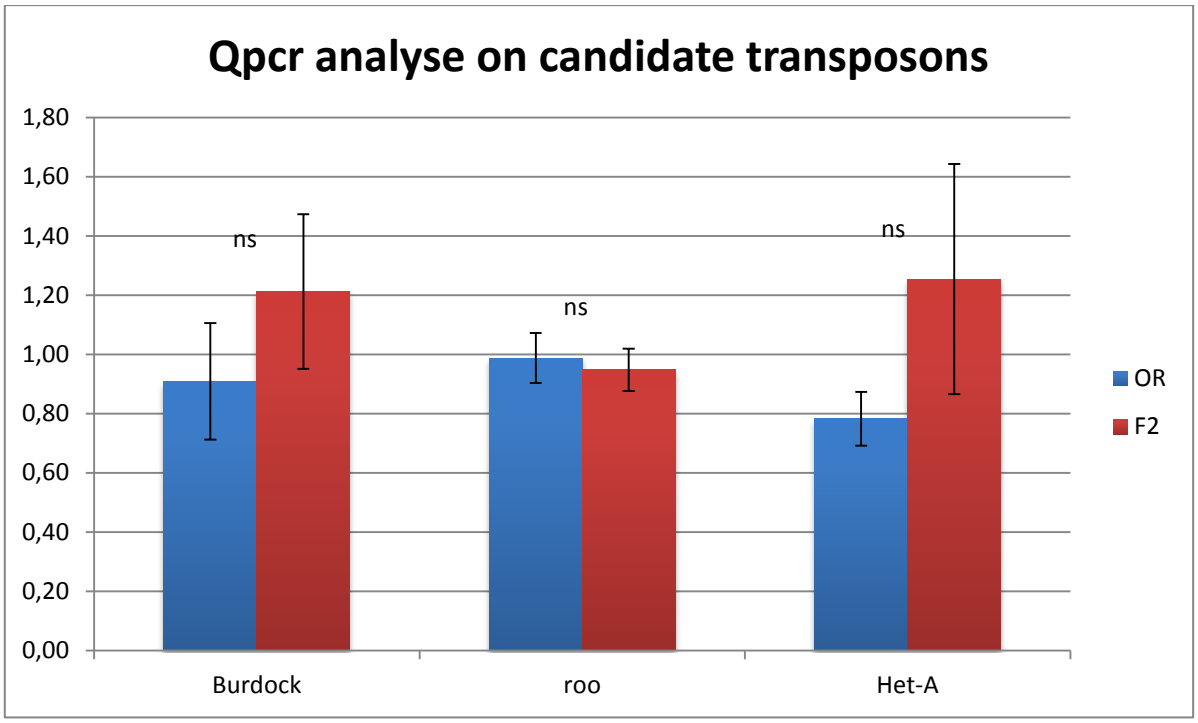

Figure 91: QPCR analyses on WT and indented F2 WT ovaries showing no effect of the indent on transposons expression.

None of our approaches revealed pi-RNA related positive results so far. New type of indention will be realized at stage 3, which can be more sensitive. However, our read outs were up to day associated to the adult stage, which does not exclude the existence of earlier heritable stages transient effects of transposon repression. Other approaches will thus be used to test if transient effects exist during development. For instance, we will use fluorescent genetic strains in which we will be able to quantify the expression of transposons in real time, like Idefix GFP strain (183 Dufourt 2013).

b- Non-candidate screening approach

- Genome sequencing.

In the perspective for searching for more clues on the genetic parameters potentially involved in the underlying mechanism of the dorsalised phenotype induced by generation after generation, we are realizing the sequencing of *Drosophila* progeny genome of the indented lineage compared to control. Indeed transposon activation could lead, as discuss before, to genome perturbations. We will thus compare the DNA sequence of the 30 wild type flies control and 30 flies progeny from indented embryos, to check for differences in the genome sequence.

- Pi-RNA: deep sequencing.

Deep sequencing is a technique allowing measuring and quantifying the existence of pi-RNA present in our sample. In my thesis, I first checked for small RNA present in the ovaries of the F2 indented strain. Would the

number of pi-RNA be reduced by the indented strain, this would give us a first clue on the underlying molecular mechanism. We are at that time expecting the results of the analysis.

The major limitation of this technique is the impossibility to fix an event that would inhibit pi-RNA (and activate transposon) transiently at a specific point of the individual development, and that would not been seen at other stages, including at adult stages in the ovaries. To avoid this limitation, we will project to develop a new technique, in collaboration with Stephane Ronsseray and Antoine Boivin, to fix gene activity pi-RNA dependent transient event. This experiment is developed in the perspectives.

5- Conclusion

Here we demonstrated the induction of heritable dorsalised phenotypes after indentation of the embryonic germ cells. The heritable effects have been characterised: high embryonic lethality, the phenotypic and molecular dorsalisation of the embryo. This description now needs to be completed by the finding of both the underlying molecular mechanism of transmission and the initiation of such process.

However the key features indicative of putative epigenetic underlying mechanisms have been established through the possible activation of the G2 checkpoint.

Based on the current data, two genetic and 2 epigenetic hypotheses can be postulated.

a- Genetic transmission

In this hypothesis, the genomic DNA sequence is modified, and the transmission occurs through classical chromosomal genetic transmission. This could be mediated via various mechanisms. Interestingly, we have identified genomic modifications associated to dorsalised phenotypes. Indeed, important genomic stresses result in chromosome mis-recombination during completion of meiosis at the onset of development. This is known to over-activate the check-points detector of genomic defects. This over-triggers the DNA-repair machinery, which leads to dorsalisation defects, as a side effect. We are generating mechanical cues in Drosophila mutant lines for candidate genes involved in check-points and are testing for the suppression of transmission of deleterious phenotypes. We are currently sequencing the genome of the progeny (F1 and F2).

- The genome can be modified “directly” by double strain brakes: we will thus check for the repression of the expression of chromatin scaffold proteins, like APC, known to be required for the stability of the genome, using immunofluorescence of qPCR.

- Alternatively, the genome can be modified by the activation of transposons. Transposons are repetitive mobile DNA sequences whose mobilization can create some genome instability. Transposons activation can be induced by the inhibition of the production of small non-coding RNAs including the recently discovered RNAs associated to Piwi proteins, called Piwi-interacting RNAs (piRNAs). We will test if a mechanical indent can induce activation of GFP-tagged transposons, thanks to the GFP expression transgenic reporters available in the community.

Some of our results however, suggest that this hypothesis may not be the correct one. Our first results on fertility of the couple with male indented p53 and female non-indented, and the non-fertility of indented females cross with non-indented males tends to prove that another mechanism should be at work (a genetically transmitted dominant effect should be sex insensitive). We also observed that dorsalised phenotypes caused by checkpoint activation are still present in F3 generation (Figure 88, Figure 90). We can think that if a mutation is created in G0 and repaired in F1 we should not see any activation of a repair process leading to dorsalisation

defects in F3. These points favour epigenetic processes as the process underlying the heritable dorsalisation phenotype induced by indent at G0.

b- Epigenetic transmission

- piRNAs pattern defects could induce transposons activation not only in F0 but also in further generations. The involvement of inherited piRNA in our *trans*-generational phenomenon will be analyzed by deep sequencing analysis of 20-30nt transposons homologous small RNAs in the ovaries of the perturbed progeny.

- piRNA pattern defects transmitted over generations could also play a specific role in the developmental regulation of dorso-ventral gene expression during early development, independently from activation of the transposons (184 Joly 2013). Ovarian piRNAs homologous to candidate genetic sequences will be analysed in the perturbed progeny.

Such hypotheses are more probable given our results, because, an epigenetic mechanism should be visible generation after generation based on transposable element activation. Effectively, if the indent creates perturbations in the level of expression of pi-RNA such dysregulation can be transmitted from one generation to the other and trigger the activation of transposons and associated dorsalisation phenotypes in the embryo generation after generation. At each new generation, the lack of pi-RNA will allow the propagation of new transposon that will invade the DNA leading to DNA damages activation the repair machinery and therefore the dorsalisation phenotype as side effect.

6- Perspectives

a- Transposon activation

To learn more about the mechanism of this transposon activation, we anticipated with A.Boivin and Stéphane Ronseray, the elaboration of a system to fix in the genome any putative pi-RNA inhibition transient events. The proposed system consists in 2 transgenics. In the first transgenic chromosome we propose to insert an ubiquitous gene coding for GFP with a stop codon between them. So the GFP could not be expressed (Figure 92). The stop codon is surrounded by two FRT, a flipase that will be expressed in another chromosome to remove the stop codon. The flipase will be under the control of a candidate transposon sequence and a germinal promoter. The activity of piRNA will prevent the transposon activation, and thus the flipase to be transcript. If piRNA activity is repressed, this repression will allow the transcription of the flipase. The flipase will delete the sequence between the 2 FRT including the codon stop and the cell will start produce GFP. The activation of the FRT will additionally be checked by a RFP tag. This system will allow us to fix in the genome and observe the effect of a transient event in specific transposon activation. The creation of this tool required the pre-identification of activated transposons and could additionally take time. We can of course think about ways to observe transient transposon using several fluorescent strains like Idefix-GFP and UAS-TE-GFP.

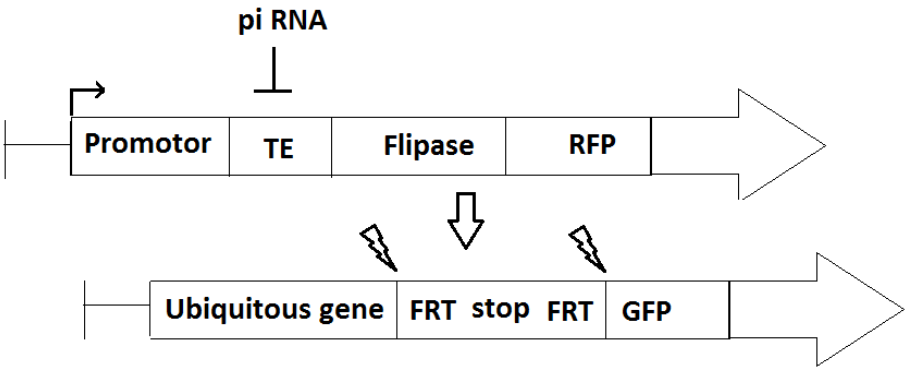

Figure 92: By modification on 2 genes we can have a tool that will fix in the genome transitory events.If the piRNA is inactive the flipase will be expressed removing the stop codon in the other gene. Then GFP could be produced.

b- Individual flies sequencing

We will realize a second set of experiment by trying to establish indented lines with the same stable genetic background. To do so, we first isogenize the flies by systematically crossing brothers with sisters. After 5 generations one can consider that the genome is the same for all embryos. Using this couple, we will generate two new generations of *Drosophila* strains, one indented and one control. After 2 generations, we will sequence the genome of each one. This sequencing will be done on sample of 1 fly and not a group of 30, so we will be able to compare precisely how close the difference between the two genomes is. Based on this experiment, we

should be able to identify for example the invasion of the genome by transposons, because they will change the sequence. The indented genome should diverge from the control one. We can hope to stabilize the transmitted effect on more than 3 generations this way.

c- Physical characterization of the underlying mechanotransductive process

Experiments should be done to get a better understanding of the effect of indent. The first experiment would be to follow the germ cells just after the indent. We anticipate to first use a Vasa-GFP strain allowing us to see the formation of the germ cells inside the piRNA machinery cloud of granule elements. This would give us first cues on the structural perturbation of the cloud complex.

As an underlying mechanism, a mechanically induced change in the 3D architecture of the genome could for instance move the piRNA producing loci far from nucleus pores, at which their production is normally regulated. Modulation of the 3D physical chromatin structures will thus be checked in response to indents (coll. with Edith Heard, Institut Curie-UPMC). In parallel, we will refine our tools of mechanical perturbation by injecting magnetic liposomes inside the targeted tissue to quantitatively evaluate the force involved, instead of perturbing mechanically directly the tissue with a direct mechanical device.

Mechanical deformations have a specific status by the fact that the embryo itself can generate stresses through the development of its genetically regulated morphogenetic movements. This makes the shape of some specific stages of development of the embryo itself a potential motor of mechanically induced heritable modulation of the developmental program. Finally, we will thus experimentally test if this could importantly make genetic or mechanical accidents in the embryonic development leading to morphogenetic movement modifications susceptible to lead to inheritable developmental consequences. Which we should be able to test combining genetically induced defects in morphogenetic movements with magnetically induced rescue.

d- Putative speciation process

During my PhD I was also interested in possible mechanically induced processes of speciation of the indented progeny. The idea consists in crossing F3 adults with none indented adults and see if they are able to reproduce. A first analyze showed a decrease of fertility when F3 females were crossed with WT male compared to F3 females with F3 males. Indeed a cross between F3 indented females and non-indented males produces around 40% to 60% only of the flies produces by a wild type couple, whereas, a cross between F3 indented couples produces around 80% of the amount of flies produce by a wild type couples. More investigations is required to progress on this aspect.

General conclusion

The work realized during my PhD consisted in raising the question of the role of mechanotransduction in developmental biology and its putative implication in evolution.

In part I, I established *in silico* the plausibility of mechanotransduction as a process activating the very first morphogenetic movement of the *Drosophila* embryo mesoderm invagination.

In part II, I first investigated the putative involvement of mechanotransductive processes in evolution, upstream of a major transition in species patterning. I found the involvement of the β-cat mechanotransductive pathway in the activation of the differentiation of the mesoderm in response to the first morphogenetic movement of embryogenesis, in both the early zebrafish and *Drosophila* embryos. I found a common underlying mechanotransductive pathway in this process in both an arthropod and a vertebrate specie. This allowed to propose that the Y654 β-cat mechanically induced phosphorylation could be at the origin of mesoderm emergence in the last common ancestor of bilaterians. The emergence of mesoderm is a major transition in species evolution, which origin is not fully understood and which we thus propose to have been induced by mechanotransduction event in response to the very first morphogenetic movements of embryogenesis.

In part III, I showed that a mechanical input on germ cells can create perturbations in an embryo, and affect the development of its progeny along generations. One can speculate that several of these induced perturbations could randomly give benefit to a few individuals and to their lineage, possibly giving rise to advantageous speciation.

Mechanotransduction is emerging as a key process with implications in development, cells specification, and cancer. During my PhD, I suggested for the first time to my knowledge first evidences of a role of mechanotransductive processes in organisms evolution.

References

ntroduction

1. *Gospodarowicz, D., Greenburg, G. & Birdwell, C. R. 1978 Determination of cellular shape by the extracellular matrix and its correlation with the control of cellular growth. Cancer Res 38, 4155-4171*

2. *Resnick, N. et al. 1993 Platelet-derived growth factor B chain promoter contains a cis-acting fluid shear-stress-responsive element. Proc Natl Acad Sci U S A 90, 4591-4595.*

3. *Ghajar, C. M. & Bissell, M. J. 2008 Extracellular matrix control of mammary gland morphogenesis and tumorigenesis: insights from imaging. Histochem Cell Biol 130, 1105-1118, doi:10.1007/s00418-008-0537-1*

4. *Farge E 2011 Mechanotransduction in development.. Curr Top Dev Biol.;95:243-65.*

5. *Mammoto T1, Ingber DE 2010 . Mechanical control of tissue and organ development. Development. 137(9):1407-20Zhou J, Yao J, Joshi H. 2002. "Attachment and tension in the spindle assembly checkpoint". Journal of Cell Science 115 Pt 18: 3547–.doi:10.1242/jcs.00029. PMID 12186941.*

6. *Zhou J, Yao J, Joshi H. 2002. "Attachment and tension in the spindle assembly checkpoint". Journal of Cell Science 115 Pt 18: 3547–.doi:10.1242/jcs.00029. PMID 12186941.*

7. *Janet M. Tse et all 2002 Mechanical compression drives cancer cells toward invasive phenotype PNAS vol. 109 no. 3, 911-916*

8. *le Noble, F., Moyon, D., Pardanaud, L., Yuan, L., Djonov, V., Matthijsen, R.,Breant, C., Fleury, V. and Eichmann, A. 2004. Flow regulates arterial-venousdifferentiation in the chick embryo yolk sac. Development 131, 361-375.*

9. *Adamo, L., Naveiras, O., Wenzel, P. L., McKinney-Freeman, S., Mack, P. J.,Gracia-Sancho, J., Suchy-Dicey, A., Yoshimoto, M., Lensch, M. W., Yoder,M. C. et al. 2009. Biomechanical forces promote embryonic haematopoiesis.Nature 459, 1131-1135.*

10. *Horner, V. L. and Wolfner, M. F. 2008. Transitioning from egg to embryo: triggers and mechanisms of egg activation. Dev. Dyn. 237, 527-544.*

11. *Foty, R. A. and Steinberg, M. S. 2005. The differential adhesion hypothesis: a direct evaluation. Dev. Biol. 278, 255-263.*

12. *Krieg, M., Arboleda-Estudillo, Y., Puech, P. H., Kafer, J., Graner, F., Muller, D. J. and Heisenberg, C. P. 2008. Tensile forces govern germ-layer organization in zebrafish. Nat. Cell Biol. 10, 429-436.*

13. *Allen MJ, Rudd RE, McElfresh MW, Balhorn R. 2010. Time-dependent measure of a nanoscale force-pulse driven by the axonemal dynein motors in individual live sperm cells. Nanomedicine 6:510–15*

14. *Brokaw CJ. 1989. Direct measurements of sliding between outer doublet microtubules in swimming sperm flagella. Science 243:1593–96*

15. *Acheson, D.J. 1990, Elementary Fluid Dynamics, book*

16. *Boccaccio A, Frassanito MC, Lamberti L, Brunelli R, Maulucci G, et al. 2012. Nanoscale characterization of the biomechanical hardening of bovine zona pellucida. J. R. Soc. Interface 9:2871–82*

17. *Reinsch S, Gonczy P. 1998. Mechanisms of nuclear positioning. J. Cell Sci. 111Pt. 16:2283–95*

18. *Desai A, Mitchison TJ. 1997. Microtubule polymerization dynamics. Annu. Rev. Cell Dev. Biol. 13:83–117*

19. *Papalopulu 2012 Dev Cell. 2012 Apr 17;224:775-87. doi: 10.1016/j.devcel.2012.01.002. Epub 2012 Mar 8.Spindle position in symmetric cell divisions during epiboly is controlled by opposing and dynamic apicobasal forces.*

20. *Kozlowski, C., Srayko, M. and Nedelec, F. 2007. Cortical microtubule contactsposition the spindle in C. elegans embryos. Cell 129, 499-510.*

21. Wang, Y. & Riechmann, V. 2007 The role of the actomyosin cytoskeleton in coordination of tissue growth during Drosophila oogenesis. *Curr Biol* **17**, 1349-1355

22. *Nonaka, S., Shiratori, H., Saijoh, Y. and Hamada, H. 2002. Determination of left-right patterning of the mouse embryo by artificial nodal flow. Nature 418, 96-99.*

23. *Tanaka, Y., Okada, Y. and Hirokawa, N. 2005. FGF-induced vesicular release of Sonic hedgehog and retinoic acid in leftward nodal flow is critical for left-right determination. Nature 435, 172-177.*

24. *Costa M, Sweeton D, Wieschaus E. 1993Gastrulation in Drosophila: cellular mechanisms of morphogenetic movements. In: Bate M, Martinez-Arias A, editors. The Development of Drosophila. New York: Cold Spring Harbor Laboratories Press;. pp. 425–465.*

25. *Colas J-F, Schoenwolf GC. 2001. Towards a cellular and molecular understanding of neurulation. Dev. Dyn.221:117–45 Development 137, 1407-1420*

26. *Jacinto, A., Wood, W., Woolner, S., Hiley, C., Turner, L., Wilson, C., Martinez-Arias, A. and Martin, P. 2002. Dynamic analysis of actin cable function during Drosophila dorsal closure. Curr. Biol. 12, 1245-1250*

27. *Gospodarowicz, D., G. Greenburg, et al. 1978. Determination of cellular shape by the extracellular matrix and its correlation with the control of cellular growth. Cancer Res 38, 4155-4171.*

28. *Nakache, M. and H. E. Gaub 1988. "Hydrodynamic hyperpolarization of endothelial cells." Proc Natl Acad Sci U S A 856: 1841-1843.*

29. *Bershadsky, A. D., Balaban, N. Q., and Geiger, B. 2003. Adhesion-dependent cell mechanosensitivity. Annu Rev Cell Dev Biol 19, 677-695.*

30. *Dike, L. E., Chen, C. S., Mrksich, M., Tien, J., Whitesides, G. M., and Ingber, D. E. 1999. Geometric control of switching between growth, apoptosis, and differentiation during angiogenesis using micropatterned substrates. In Vitro Cell Dev Biol Anim 35, 441-448.*

31. *Ghajar CM, Bissell MJ. 2008 Extracellular matrix control of mammary gland morphogenesis and tumorigenesis: insights from imaging. Histochem Cell Biol. 2008 Dec;130(6):1105-18.*

32. *Mitrossilis D, Fouchard J, Pereira D, Postic F, Richert A, Saint-Jean M, Asnacios A. 2010 Real-time single-cell response to stiffness. Sep 21;10738:16518-23.*

33. *Saez A, Ghibaudo M, Buguin A, Silberzan P, Ladoux B. 2007 Rigidity-driven growth and migration of epithelial cells on microstructured anisotropic substrates. 10420:8281-6.*

34. *Fink J, Carpi N, Betz T, Bétard A, Chebah M, Azioune A, Bornens M, Sykes C, Fetler L, Cuvelier D, Piel M. . 2011 External forces control mitotic spindle positioning. Nat Cell Bio 137:771-8*

35. *Tseng Q, Duchemin-Pelletier E, Deshiere A, Balland M, Guillou H, Filhol O, Théry M. 2012 Spatial organization of the extracellular matrix regulates cell-cell junction positioning. Proc Natl Acad Sci 1095:1506-11.*

36. *Rauch, C., Brunet, A. C., Deleule, J., and Farge, E. 2002. C2C12 myoblast/osteoblast transdifferentiation steps enhanced by epigenetic inhibition of BMP2 endocytosis. Am J Physiol Cell Physiol 283, C235-243.*

37. *Engler, A. J., Sen, S., Sweeney, H. L., and Discher, D. E. 2006. Matrix elasticity directs stem cell lineage specification. Cell 126, 677-689.*

38. *McBeath R, Pirone DM, Nelson CM, Bhadriraju K, Chen CS. 2004. Cell shape, cytoskeletal tension, and RhoA regulate stem cell lineage commitment. Dev Cell 6, 483-95.*

39. *Buxboim, A., Ivanovska, I. L., and Discher, D. E. 2010. Matrix elasticity, cytoskeletal forces and physics of the nucleus: how deeply do cells 'feel' outside and in? J Cell Sci 123, 297-308.*

40. *Shivashankar, G. V. 2011. Mechanosignaling to the cell nucleus and gene regulation. Annu Rev Biophys 40, 361-378.*

41. *Simon, D. N., and Wilson, K. L. 2011. The nucleoskeleton as a genome-associated dynamic 'network of networks'. Nat Rev Mol Cell Biol 12, 695-708.*

42. *Wang, N., Tytell, J. D., and Ingber, D. E. 2009. Mechanotransduction at a distance: mechanically coupling the extracellular matrix with the nucleus. Nat Rev Mol Cell Biol 10, 75-82*

43. Wang, Y. & Riechmann, V. 2007 The role of the actomyosin cytoskeleton in coordination of tissue growth during Drosophila oogenesis. *Curr Biol* **17**, 1349-1355

44. *Nelson, C. M. et al. 2005.Emergent patterns of growth controlled by multicellular form and mechanics. Proc. Natl Acad. Sci. USA 102, 11594–11599*

45. *Pouille PA, Ahmadi P, Brunet AC, Farge E. 2009 Mechanical signals trigger Myosin II redistribution and mesoderm invagination in Drosophila embryos. Sci Signal. 2009 Apr 14;2(66)*

46. *Fernandez-Gonzalez R[1], Simoes Sde M, Röper JC, Eaton S, Zallen JA. 2009. Myosin II dynamics are regulated by tension in intercalating cells. Dev Cell. 17(5):736-43.*

47. *Kimmel ,Willan w.Ballard, Seth R.Kimmel 1995 Stages of Embryonic Development of the Zebrafish. Developmental dynamics*

48. *Hove, J. R., Koster, R. W., Forouhar, A. S., Acevedo-Bolton, G., Fraser, S. E. and Gharib, M. 2003. Intracardiac fluid forces are an essential epigenetic factor for embryonic cardiogenesis. Nature 421, 172-177*

49. *Voronov, D. A., Alford, P. W., Xu, G. and Taber, L. A. 2004. The role of mechanical forces in dextral rotation during cardiac looping in the chick embryo. Dev. Biol. 272, 339-350*

50. *Chen Q, Jiang L, Li C, Hu D, Bu JW, et al. 2012. Haemodynamics-driven developmental pruning of brain vasculature in zebrafish. PLoS Biol. 10:e1001374*

51. *Kahn J, Shwartz Y, Blitz E, Krief S, Sharir A, Breitel DA, Rattenbach R, Relaix F, Maire P, Rountree RB, Kingsley DM, Zelzer E. 2009 Muscle contraction is necessary to maintain joint progenitor cell fate. Dev Cell. 16(5):734-43. doi: 10.1016/j.devcel.2009.04.013.*

Mechanotransduction in Drosophila embryo mesoderm invagination: transition from individual pulsating to collective constriction behaviour

52. *Driquez B1, Bouclet A, Farge E.2011 Mechanotransduction in mechanically coupled pulsating cells: transition to collective constriction and mesoderm invagination simulation. Phys Biol. 2011 Dec;8(6):066007. doi: 10.1088/1478-3975/8/6/066007.*

53. *Costa M, Wilson E T and Wieschaus E 1994 A putative cell signal encoded by the folded gastrulation gene coordinates cell shape changes during Drosophila gastrulation Cell 76 1075–89*

54. *Seher T C, Narasimha M, Vogelsang E and Leptin M 2007 Analysis and reconstitution of the genetic cascade controlling early mesoderm morphogenesis in the Drosophila embryo Mech. Dev 124 167–79*

55. *Sweeton D, Parks S, Costa M and Wieschaus E 1991 Gastrulation in Drosophila: the formation of the ventral furrow and posterior midgut invaginations Development 112 775–89*

56. *Martin A C, Kaschube M and Wieschaus E F 2009 Pulsed contractions of an actin-myosin network drive apical constriction Nature 457 495–9*

57. *Pouille P A, Ahmadi P, Brunet A C and Farge E 2009 Mechanical signals trigger Myosin ii redistribution and mesoderm invagination in Drosophila embryos Sci. Signal. 2 ra16*

58. *Koehl MAR. 1990 Biomechanical approaches to morphogenesis. Sem Dev Biol.; 1:367–378.*

59. *Taber LA. 1995 Biomechanics of growth, remodeling, and morphogenesis. Appl Mech Rev. 1995; 48:48*

60. *Farge E. .2003 Mechanical induction of twist in the Drosophila foregut/stomodeal primordium. Curr Biol; 13:1365–1377.*

61. *Vogel V, Sheetz M. 2006; Local force and geometry sensing regulate cell functions. Nat Rev Mol Cell Bio. 7:265–275.*

62. *Wozniak MA, Chen CS. 2009 Mechanotransduction in development: a growing role for contractility. NatRev Mol Cell Bio.; 10:34–43*

63. *Mammoto T, Ingber DE. 2010 Mechanical control of tissue and organ development. Development.;137:1407–1420.*

64. *Odell, G. M., G. Oster, ., B. Burnside. 1981. The mechanical basis of morphogenesis. I. Epithelial folding and invagination. Dev. Biol.*

65. *Sherrard, K., Robin, F., Lemaire, P. & Munro, 2010 E. Sequential activation of apical and basolateral contractility drives ascidian endoderm invagination. Curr Biol 20, 1499-1510,*

66. Davidson, L. A., Koehl, M. A., Keller, R. & Oster, G. F. 1995 How do sea urchins invaginate? Using biomechanics to distinguish between mechanisms of primary invagination.*Development* 121, 2005-2018.

67. *Munoz, J. J., K. Barrett, and M. Miodownik. 2007. A deformation gradient decomposition method for the analysis of the mechanics of morphogenesis. J. Biomech. 40:1372–1380.*

68. *Conte, V., J. J. Mun˜oz, and M. Miodownik. 2008. A 3D finite element model of ventral furrow invagination in the Drosophila melanogaster embryo. J. Mech. Behav. Biomed. Mater. 1:188–198.*

69. *Pouille P A and Farge E 2008 Hydrodynamic simulation of multicellular embryo invagination Phys. Biol. 5 15005*

70. *Conte, V., J. J. Mun˜oz, ., M. Miodownik. 2009. Robust mechanisms of ventral furrow invagination require the combination of cellular shape changes. Phys. Biol. 6:016010*

71. *Conte, V., F. Ulrich, ., M. Miodownik. 2012. A biomechanical analysis of ventral furrow formation in the Drosophila melanogasterembryo. PLoS ONE. 7:e34473.*

72. *Brodland, G. W., V. Conte, ., M. Miodownik. 2010. Video force microscopy reveals the mechanics of ventral furrow invagination in Drosophila. Proc. Natl. Acad. Sci. USA. 107:22111–22116.*

73. *Ho_cevar Brezav_s_cek, A., M. Rauzi, ., P. Ziherl. 2012. A model of epithelial invagination driven by collective mechanics of identical cells. Biophys. J. 103:1069–1077.*

74. *Alberga A, Boulay J L, Kempe E, Dennefeld C and Haenlin M 1991The snail gene required for mesoderm formation in Drosophila is expressed dynamically in derivatives of all three germ layers Development 111 983–92*

75. *Martin A C 2009 Pulsation and stabilization: contractile forces that underlie morphogenesis Dev. Biol. 341 114–25*

76. *Kam Z, Minden J S, Agard D A, Sedat J W and Leptin M 1991 Drosophila gastrulation: analysis of cell shape changes in living embryos by three-dimensional fluorescence microscopy Development 112 365–70*

77. *Martin A C, Gelbart M, Fernandez-Gonzalez R, Kaschube M and Wieschaus E F 2010 Integration of contractile forces during tissue invagination J. Cell Biol. 188 735–49*

78. *Solon J, Kaya-Copur A, Colombelli J and Brunner D 2009 Pulsed forces timed by a ratchet-like mechanism drive directed tissue movement during dorsal closure Cell 137 1331–42*

79. *Dawes-Hoang R E, Parmar K M, Christiansen A E, Phelps C B, Brand A H and Wieschaus E F 2005 Folded gastrulation, cell shape change and the control of myosin localization Development 132 4165–787*

80. *Sawyer J K, Harris N J, Slep K C, Gaul U and Peifer M 2009 The Drosophila afadin homologue Canoe regulates linkage of the actin cytoskeleton to adherens junctions during apical constriction J. Cell Biol. 186 57–73*

Evolutionary conservation of early mesoderm specification by mechanotransduction in Bilateria

81. *Brunet T1, Bouclet A, Ahmadi P, Mitrossilis D, Driquez B, Brunet AC, Henry L, Serman F, Béalle G, Ménager C, Dumas-Bouchiat F, Givord D,Yanicostas C, Le-Roy D, Dempsey NM, Plessis A, Farge E. 2013. Evolutionary conservation of early mesoderm specification by mechanotransduction in Bilateria. Nat Commun. 2013;4:2821. doi: 10.1038*

82. *Farge, E. 2003 Mechanical induction of twist in the Drosophila foregut/stomodeal primordium. Curr Biol 13, 1365-1377*

83. *Desprat, N., Supatto, W., Pouille, P. A., Beaurepaire, E. & Farge, E.2008 Tissue deformation modulates twist expression to determine anterior midgut differentiation in Drosophila embryos. Dev Cell 15, 470-477,*

84. *Norvell SM[1], Alvarez M, Bidwell JP, Pavalko FM. 2004 Fluid shear stress induces beta-catenin signaling in osteoblasts. Calcif Tissue Int. 2004 Nov;75(5):396-404*

85. *Kahn J, Shwartz Y, Blitz E, Krief S, Sharir A, Breitel DA, Rattenbach R, Relaix F, Maire P, Rountree RB, Kingsley DM, Zelzer E. 2009 Muscle contraction is necessary to maintain joint progenitor cell fate. Dev Cell. 16(5):734-43.*

86. *Whitehead, J. et al.2008 Mechanical factors activate beta-catenin-dependent oncogene expression in APC mouse colon. HFSP J 2, 286-294*

87. *Samuel, M. S. et al. 2011 Actomyosin-mediated cellular tension drives increased tissue stiffness and beta-catenin activation to induce epidermal hyperplasia and tumor growth. Cancer Cell 19, 776–791 .*

88. *Kimmel ,Willan w.Ballard, Seth R.Kimmel 1995 Stages of Embryonic Development of the Zebrafish. Developmental dynamics*

89. *Kimmel, C.B., and Law, R.D. 1985a Cell lineage of zebrafish blastomeres.. Cleavage pattern and cytoplasmic bridges between cells.Dev. Biol. 10878-85.*

90. *Kane, D.A., Warga, R.A., and Kimmel, C.B. 1992 Mitotic domains inthe early embryo of the zebrafish. Nature 360:735-737.*

91. *Trinkaus, J.P. 1992 The midblastula transition, the YSL transition and the onset of gastrulation in Fundulus. Development 75-80.*

92. *Solnica-Krezel, L., and Driever, W. 1994 Microtubule arrays of the zebrafish yolk cell: organization and function during epiboly. Development 120:2443-2455.*

93. *Wood, A., and Timmermans, L.P.M. 1988 Teleost epiboly: reassessment of deep cell movement in the germ ring. Development 102: 575-585.*

94. *Hanneman, E., and Westerfield, M. 1989 Early expression of acetylcholine-sterase activity in functionally distinct neurons of the zebrafish.. Comp. Neurol. 284:350-361*

95. *Thisse, C., Thisse, B., Schilling, T.F., and Postlethwait, J.H. 1993 Structure of the zebrafish snail1 gene and its expression in wildtype, spadetail and no tail mutant embryos. Development 119: 1203-1215*

96. *Antoine Agathon, Christine Thisse & Bernard Thisse 2003 The molecular nature of the zebrafish tail organizer Nature 424, 448-452*

97. *Ballard, W.W. 1981 Morphogenetic movements and fate maps of vertebrates. Am. Zool. 21:391-399.*

98. *Gould, S.J. 1977 "Ontogeny and Phylogeny." Cambridge: Harvard Univ. Press. Book*

99. *Reib, J.P. 1973 La circulation sanguine chez l'embryon de Bruchyd a n ~ ore rio. Ann. Embryol. Morphol. 6:43-54.*

100. *Milos, N., and Dingle, A.D. 1978 Dynamics of pigment formation in the zebrafish, Brachydunio rerio. I. Establishment and regulation of the lateral line melanophore stripe during the first eight days of development. J. Exp. Zool. 205:205-216.*

101. *Schneider, S., Steinbeisser, H., Warga, R. M. & Hausen, 1996. P. Beta-catenin translocation into nuclei demarcates the dorsalizing centers in frog and fish embryos. Mech Dev 57, 191-198*

102. *De Robertis, E. M. Evo-devo: variations on ancestral themes.2008 Cell 132, 185-195,*

103. *Stern, C. D.2004 Gastrulation: From Cells to Embryo Cold Spring Harbor Laboratory Press, .*

104. *Schohl, A. & Fagotto, F. 2003.A role for maternal beta-catenin in early mesoderm induction in Xenopus. Embo J 22, 3303-3313*

105. *Valenta, T. et al. 2011. Probing transcription-specific outputs of beta-catenin in vivo. Genes Dev 25, 2631-2643,*

106. *Lewis, J. L. et al.2004 Reiterated Wnt signaling during zebrafish neural crest development. Development 131, 1299-1308*

107. *Ueno, S. et al.2007 Biphasic role for Wnt/beta-catenin signaling in cardiac specification in zebrafish and embryonic stem cells. Proc Natl Acad Sci U S A 104, 9685-9690*

108. *Kahn, J. et al.2009 Muscle contraction is necessary to maintain joint progenitor cell fate. Dev Cell 16, 734-743,*

109. *Sen, B. et al. 2008 Mechanical strain inhibits adipogenesis in mesenchymal stem cells by stimulating a durable beta-catenin signal. Endocrinology 149, 6065-6075*

110. *Fukazawa, C. et al. 2010 .Poky/chuk/ikk1 is required for differentiation of the zebrafish embryonic epidermis. Dev. Biol. 346, 272–283*

111. *Limouze, J., Straight, A. F., Mitchison, T. & Sellers, J. R.2004. Specificity of Blebbistatin, an inhibitor of myosin II. Journal of muscle research and cell motility 25, 337-341,*

112. *Solnica-Krezel, L. & Driever, W.1994 Microtubule arrays of the zebrafish yolk cell: organization and function during epiboly.. Development 120, 2443-2455*

113. *Schulte-Merker, S. et al. 1994 Expression of zebrafish goosecoid and no tail gene products in wild-type and mutant no tail embryos. Development 120, 843–852 Stachel 1995*

114. *Stachel, S. E., Grunwald, D. J. & Myers, P. Z. 1993 Lithium perturbation and goosecoid expression identify a dorsal specification pathway in the pregastrula zebrafish. Development 117, 1261–1274 ().*

115. *De Robertis, E. M. 1995 Developmental biology. Dismantling the organizer. Nature 374, 407–408.*

116. *Dempsey, N. M. et al. High performance hard magnetic NdFeB thick films for integration into micro-electro-mechanical-systems. Appl. Phys. Lett. 90, 092509-1–092509-3 (2007). Dempsey 2007*

117. *Bealle, G. et al 2012. Ultra magnetic liposomes for mr imaging, targeting, and hyperthermia. Langmuir 28, 11834–11842*

118. *Rebagliati, M. R., Toyama, R., Fricke, C., Haffter, P. & Dawid, I. B. 1998 Zebrafish nodal-related genes are implicated in axial patterning and establishing left-right asymmetry. Dev. Biol. 199, 261–272*

119. *Feldman, B. et al. 1998 Zebrafish organizer development and germ-layer formation require nodal-related signals. Nature 395, 181–185 Hargos 2007*

120. *Hagos, E. G. & Dougan, S.2007 . Time-dependent patterning of the mesoderm and endoderm by Nodal signals in zebrafish. BMC Dev. Biol. 7, 1–22*

121. *Christine Thisse and Bernard Thisse 1999 DEV2332 Antivin, a novel and divergent member of the TGFβ superfamily, negatively regulates mesoderm induction Development 126, 229-240*

122. *van Veelen, W. et al. 2011 beta-catenin tyrosine 654 phosphorylation increases Wnt signalling and intestinal tumorigenesis. Gut 60, 1204-1212,*

123. *Leptin M. 1991. twist and snail as positive and negative regulators during Drosophila mesoderm development. Genes Dev. 1568-76*

124. *Brouzés E1, Farge E 2004 Interplay of mechanical deformation and patterned gene expression in developing embryos.. Curr Opin Genet Dev. ;14(4):367-74.*

125. *Leptin Leptin, M. & Grunewald, B. Cell shape changes during gastrulation in Drosophila. Development 110, 73–84 1990*

126. *Peifer, M., Sweeton, D., Casey, M. & Wieschaus, E. 1994 Wingless signal and Zestewhite 3 kinase trigger opposing changes in the intracellular distribution of Armadillo. Development 120, 369–380*

127. *Takahashi, M., Takahashi, F., Ui-Tei, K., Kojima, T. & Saigo, K. 2005 Requirements of genetic interactions between Src42A, armadillo and shotgun, a gene encoding E- cadherin, for normal development in Drosophila. Development 132, 2547-2559*

128. *Arendt, D. In Gastrulation. 2004 ed Stern, C. D. Ch. 51, 679–693 University College London .*

129. *Martindale, M. Q., Pang, K. & Finnerty, J. R. 2004 Investigating the origins of triploblasty: 'mesodermal' gene expression in a diploblastic animal, the sea anemone Nematostella vectensis phylum, Cnidaria; class, Anthozoa. Development 131, 2463–2474 .*

130. *Schohl, A. & Fagotto, F. 2003 A role for maternal beta-catenin in early mesoderm induction in Xenopus. EMBO J. 22, 3303–3313 .*

131. *Harvey S. A., Tumpel, S., Dubrulle, J., Schier, A. F. & Smith, J. C. no tail integrates two modes of mesoderm induction. Development 137, 1127-1135, doi:10.1242/dev.046318 (2010)*

132. *Keller, R. E. 1980 The cellular basis of epiboly: an SEM study of deep-cell rearrangement during gastrulation in Xenopus laevis. J. Embryol. Exp. Morphol. 60, 201–234 .*

133. *Kornikova, E. S., Troshina, T. G., Kremnyov, S. V. & Beloussov, L. V. 2010 Neuro-mesodermal patterns in artificially deformed embryonic explants: a role for mechano-geometry in tissue differentiation. Dev. Dyn. 239, 885–896 .*

134. *Gross, J. M. & McClay, D. R. 2001 The role of Brachyury T during gastrulationmovements in the sea urchin Lytechinus variegatus. Dev. Biol. 239, 132–147.*

135. *Stern, C. D. 2004 Gastrulation: From Cells to Embryo Cold Spring Harbor Laboratory Press,.*

136. *Valenta, T. et al. 2011 Probing transcription-specific outputs of beta-catenin in vivo. Genes Dev. 25, 2631–2643*

137. *Sharma, M., Jamieson, C., Johnson, M., Molloy, M. P. & Henderson, B. R. 2012 Specific armadillo repeat sequences facilitate beta-catenin nuclear transport in live cells via direct binding to nucleoporins Nup62, Nup153, and RanBP2/ Nup358. J. Biol. Chem. 287, 819–831 .*

138. Polakis, P. 2012 Wnt signaling in cancer. Cold Spring Harb. Perspect. Biol. 4, 1–13 .

139. Tamada, M., Farrell, D. L. & Zallen, J. A. 2012 Abl regulates planar polarized junctional dynamics through beta-catenin tyrosine phosphorylation. Dev. Cell 22, 309–319 .

140. Samuel, M. S. et al. 2011 Actomyosin-mediated cellular tension drives increased tissue stiffness and beta-catenin activation to induce epidermal hyperplasia and tumor growth. Cancer Cell 19, 776–791 .

141. Schweizer, L., Nellen, D. & Basler, K. 2003 Requirement for Pangolin/dTCF in Drosophila wingless signaling. Proc. Natl Acad. Sci. USA 100, 5846–5851 .

142. Arendt, D. & Nu¨bler-Jung, K. 1997 Dorsal or ventral: similarities in fate maps and gastrulation patterns in annelids, arthropods and chordates. Mech. Dev. 61, 7–21 .

143. Dickinson, D. J., Nelson, W. J. & Weis, W. I. 2011 A polarized epithelium organized by beta- and alpha-catenin predates cadherin and metazoan origins. Science 331, 1336–1339 .

144. Roth, S. 2004 In Gastrulation. From cells to Embryo. ed Stern, C. D. Ch. 8, 105–121 University College London .

145. Shen, M. M. 2007 Nodal signaling: developmental roles and regulation. Development 134, 1023–1034

146. Lynch, J. A. & Roth, S. 2011 The evolution of dorsal-ventral patterning mechanisms in insects. Genes Dev. 25, 107–118 .

147. Douzery, E. J., Snell, E. A., Bapteste, E., Delsuc, F. & Philippe, H. 2004 The timing of eukaryotic evolution: does a relaxed molecular clock reconcile proteins and fossils? Proc. Natl Acad. Sci. USA 101, 15386–15391

148. Peterson, K. J. et al. 2004 Estimating metazoan divergence times with a molecular clock. Proc. Natl Acad. Sci. USA 101, 6536–6541 .

Mechanically Induced Heritable Modulation of Developmental Biochemical Regulation

149. Rutherford SL[1], Lindquist S. 1998 Hsp90 as a capacitor for morphological evolution Nature 396(6709):336-42

150. Walsl Cristopher 2006 chapter 5 protein mehylation

151. Grewal, S. I.; Rice, J. C. (2004)). "Regulation of heterochromatin by histone methylation and small RNAs" Current Opinion in Cell Biology 16 (3): 230–238.).

152. Carroll, Sean B; Wessler, Susan R; Griffiths, Anthony J. F; Lewontin, Richard C (2008). Introduction to genetic analysis (9th ed.). New York: W.H. Freeman and CO. p. 403).

153. Sato K, Siomi MC. 2013. Piwi-interacting RNAs: biological functions and biogenesis. Essays Biochem. ;54:39-52.

154. Augustin de Vanssay, Anne-Laure Bougé, Antoine Boivin, Catherine Hermant, Laure Teysset, Valérie Delmarre, Christophe Antoniewski & Stéphane Ronsseray Affiliations 2012. Paramutation in Drosophila linked to emergence of a piRNA-producing locus Contributions Corresponding authors Nature 490, 112–115

155. Biemont, C., and Vieira, C. 2006 Genetics: junk DNA as an evolutionary force. Nature 443, 521–524.

156. Lander, E. S., Linton, L.M., Birren, B., Nusbaum, C., Zody, M. C., Baldwin, J., Devon, K., Dewar, K., Doyle, M., FitzHugh, W., et al. 2001 Initial sequencing and analysis of the human genome. Nature 409, 860–921.

157. Finnegan, D. J. 2012 Retrotransposons. Curr. Biol. 22, R432–R437.

158. Gogvadze, E., and Buzdin, A. 2009 Retroelements and their impact on genome evolution and functioning. Cell. Mol. Life Sci. 66, 3727–3742.

159. Callinan, P. A., and Batzer, M. A. 2006 Retrotransposable elements and human disease. Genome Dyn. 1, 104–115.

160. Brennecke, J. et al. Discrete small RNA-generating loci as master regulators of transposon activity in Drosophila. Cell 128, 1089–1103 (2007).

161. Mikiko C. Siomi Kaoru Sato Dubravka Pezic Alexei A. Aravin 2011 PIWI-interacting small RNAs: the vanguard of genome defence Nature Reviews Molecular Cell Biology 12, 246-258

162. Gunawardane, L. S. et al. A slicer-mediated mechanism for repeat-associated siRNA 5′ end formation in Drosophila. Science 315, 1587–1590 (2007).

163. Masrouha N, Yang L, Hijal S, Larochelle S, Suter B. 2003; The Drosophila chk2 gene loki is essential for embryonic DNA double-strand-break checkpoints induced in S phase or G2. Genetics 163:973–982.

164. Masahiro Yamaguchi , Noriko Fujimori-Tonou, Yukihiro Yoshimura Tsutomu Kishi, Hitoshi Okamoto and Ichiro Masai 2008 Mutation of DNA primase causes extensive apoptosis of retinal neurons through the activation of DNA damage checkpoint and tumor suppressor p53 Development135, 1247-1257.

165. Takanami ,T., Sato, S., Ishihara, T., Katsura, I., Takahashi, H., and Higashitani, A. 1998. Characterization of a Caenorhabditis elegans recA-like gene Ce-rdh-1 involved in meiotic recombina- DNA Res. 5, 373–377

166. . Gartner , A., Milstein, S., Ahmed, S., Hodgkin, J., and Hengartner, M.O. 2000. A conserved checkpoint pathway mediates DNA damage-induced apoptosis and cell cycle arrest in C. elegans. Mol. Cell 5, 435–443.

167. Edelman W., Cohen, P.E., Kane, M., Lau, K., Morrow, B., Ben- nett, S., Umar, A., Kunkel, T., Cattoretti, G., Chaganti, R., et al. 1996. Meiotic pachytene arrest in MLH1-deficient mice. . 85, 1125–1134. 145

168. Pittman D.L., Cobb, J., Schimenti, K.J., Wilson, L.A., Cooper, D.M., Brignull, E., Handel,M.A., and Schimenti, J.C. 1998.Meiotic prophase arrest with failure of chromosome synapsis in mice deficient for Dmc1, a germline-specific RecA homolog. Mol. Cell 1, 697–705.

169. Brodsky MH, Nordstrom W, Tsang G, Kwan E, Rubin GM, Abrams JM. 2000; Drosophila p53 binds a damage response element at the reaper locus. Cell 101:103–113. [PubMed: 10778860]

170. Ollmann M, Young LM, Di Como CJ, Karim F, Belvin M, Robertson S, et al. 2000; Drosophila p53 is a structural and functional homolog of the tumor suppressor p53. Cell 101:91–101. [PubMed: 10778859].

171. Titen SW, Lin HC, Bhandari J, Golic KG.2014 Chk2 and p53 regulate the transmission of healed chromosomes in the Drosophila male germline. PLoS Genet. ;10(2):e1004130

172. Klattenhoff C, Bratu DP, McGinnis-Schultz N, Koppetsch BS, Cook HA, Theurkauf WE 2007. Drosophila rasiRNA pathway mutations disrupt embryonic axis specification through activation of an ATR/Chk2 DNA damage response. Dev Cell;12:45–55. [PubMed: 17199040]

173. Chen Y, Pane A, Schüpbach T. 2007. cutoff and aubergine mutations result in retrotransposon upregulation and checkpoint Activation in Drosophila. Current Biology;17:1–6. [PubMed: 17208179]

174. Pane A, Wehr K, Schüpbach T. 2007 zucchini and squash encode two putative nucleases required for rasiRNA production in the Drosophila germline. Dev Cell;12:851–862. [PubMed: 17543859] 16.

175. Fichelson P, Jagut M, Lepanse S, Lepesant JA, Huynh JR. 2010 lethal giant larvae is required with the par genes for the early polarization of the Drosophila oocyte. Development. 137(5):815-24.

176. Karen Olsen, K Tracy Reynolds and Ary A Hoffmann 2001 A field cage test of the effects of the endosymbiont-Wolbachia on Drosophila melanogaster Heredity 86, 731–737;

177. Wieschaus E, Marsh J, Gehring W. fs(1) K10, a germ-line dependent female ste- rile mutation causling abnormal chorion morphology in Drosophila melanogaster. Arch Dev Biol 1 978 ; 1 84 : 75-82.

178. *Abdu U1, Brodsky M, 2002 Activation of a meiotic checkpoint during Drosophila oogenesis regulates the translation of Gurken through Chk2/Mnk. Schüpbach T. Curr Biol. 1;12(19):1645-51.*

179. *St Johnston, D. and Nusslein-Volhard, C. 1992. The origin of pattern andpolarity in the Drosophila embryo. Cell 68, 201-219.*

180. *Margaret C Bloch Qazia, Yael Heifetza, b, Mariana F Wolfnera, 2003 The developments between gametogenesis and fertilization: ovulation and female sperm storage in Drosophila melanogaster Developmental Biology Volume 256, Issue 2, 15 Pages 195–211*

181. *FA Laski, DC Rio, GM Rubin 1986 Tissue specificity of Drosophila P element transposition is regulated at the level of mRNA splicing- Cel*

182. *Augustin de Vanssay, Anne-Laure Bougé, Antoine Boivin, Catherine Hermant, Laure Teysset, Valérie Delmarre, Christophe Antoniewski & Stéphane Ronsseray Affiliations 2012. Paramutation in Drosophila linked to emergence of a piRNA-producing locus Contributions Corresponding authors Nature 490, 112–115*

183. *Dufourt 2013 Spatio-temporal requirements for transposable element piRNA-mediated silencing during Drosophila oogenesis*

184. *Joly W, Chartier A, Rojas-Rios P, Busseau I, Simonelig M. 2013 Stem Cell Reports. Nov 7;1(5):411-24*